MECHANISM OF CHROMOSOME ALIGNMENT BY MICROTUBULE OVERLAPDEPENDENT FORCES AND ITS RELEVANCE FOR CHROMOSOME SEGREGATION ERRORS

Risteski, Patrik

Doctoral thesis / Disertacija

2022

Degree Grantor / Ustanova koja je dodijelila akademski / stručni stupanj: **University of Zagreb, Faculty of Science / Sveučilište u Zagrebu, Prirodoslovno-matematički fakultet**

Permanent link / Trajna poveznica: https://urn.nsk.hr/urn:nbn:hr:217:637095

Rights / Prava: In copyright / Zaštićeno autorskim pravom.

Download date / Datum preuzimanja: **2024-03-28**

Repository / Repozitorij:

Repository of the Faculty of Science - University of Zagreb

University of Zagreb
FACULTY OF SCIENCE
DEPARTMENT OF BIOLOGY

Patrik Risteski

MECHANISM OF CHROMOSOME ALIGNMENT BY MICROTUBULE OVERLAP-DEPENDENT FORCES AND ITS RELEVANCE FOR CHROMOSOME SEGREGATION ERRORS

DOCTORAL THESIS

Zagreb, 2022.

Sveučilište u Zagrebu

PRIRODOSLOVNO-MATEMATIČKI FAKULTET

BIOLOŠKI ODSJEK

Patrik Risteski

MEHANIZAM PORAVNANJA KROMOSOMA SILAMA KOJE OVISE O PREKLAPANJU MIKROTUBULA I NJEGOV UTJECAJ NA POGREŠKE U RAZDVAJANJU KROMOSOMA

DOKTORSKI RAD

Zagreb, 2022.

This work was done in the Laboratory of Cell Biophysics at Ruđer Bošković Institute, Zagreb, under supervision of Iva M. Tolić, PhD, Senior Research Group Leader. As a part of Postgraduate doctoral programme of Biology, this thesis is submitted for review to Department of Biology at Faculty of Science, University of Zagreb in order to achieve the academic degree Doctor of Biology.

Supervisor Biography

Prof Iva M. Tolić was born in Zagreb, Croatia. She graduated in Molecular biology from the Faculty of Science, University of Zagreb, Croatia in 1996. During graduate studies, Prof Tolić worked as a research assistant in the group of Prof Nenad Trinajstić at Ruđer Bošković Institute. Her PhD work was done with Prof Ning Wang at Harvard School of Public Health, Boston, MA, USA. She achieved the academic degree of Doctor of Biology at the University of Zagreb in 2002. After this, she worked as a postdoctoral fellow with Prof Kirstine Berg-Sørensen at Niels Bohr Institute, Copenhagen, Denmark, and later with Prof Francesco Pavone at European Laboratory for Non-Linear Spectroscopy, Florence, Italy. From 2005 to 2014, Prof Tolić worked as a research group leader at Max Planck Institute of Molecular Cell Biology and Genetics in Dresden, Germany. Her research areas are mitosis, mitotic spindle mechanics, microtubules, motor proteins, and aneuploidy. Prof Tolić has received 15 research grants including the prestigious projects funded by the European Research Council (ERC) - Consolidator and Synergy grants. She has published more than 90 papers in peer-reviewed journals including Science, Cell, and Nature Cell Biology, cited more than 4400 times, and served as a reviewer for these and various other journals. She has been elected to EMBO and Academia Europaea membership and received numerous awards such as the Ignaz Lieben Award of the Austrian Academy of Sciences and the European Biophysical Societies Association (EBSA) Young Investigators' Medal and Prize. To this date, she has mentored 11 PhD and 22 Master theses. As an invited speaker, she has participated in more than 100 conferences and research seminars worldwide. She organized several scientific meetings including the EMBO Conference on Meiosis in 2017 and Mitotic spindle: From living and synthetic systems to theory in 2019 and 2021. Currently, Prof Tolić is a Senior Research Group Leader with tenure at Ruđer Bošković Institute in Zagreb.

University of Zagreb
Faculty of Science
Department of Biology

Doctoral thesis

MECHANISM OF CHROMOSOME ALIGNMENT BY MICROTUBULE OVERLAP-DEPENDENT FORCES AND ITS RELEVANCE FOR CHROMOSOME SEGREGATION ERRORS

PATRIK RISTESKI

Ruđer Bošković Institute

Chromosome alignment is a hallmark of mitosis and alignment defects, which persist in anaphase, lead to direct aneuploidy. Alignment at the spindle equator depends on pulling forces exerted at kinetochore fiber tips together with polar ejection forces. However, kinetochore fibers are also subjected to forces that drive their poleward flux. Here I introduce a microtubule flux-driven centering mechanism that relies on flux generated by forces within the overlaps of bridging and kinetochore fibers. This centering mechanism works so that the longer kinetochore fiber fluxes faster than the shorter one, moving the kinetochores towards the center. Kinetochores are better centered when overlaps are shorter and the kinetochore fiber flux is markedly slower than the bridging fiber flux. I identified Kif18A and Kif4A proteins as overlap and flux regulators and NuMA protein as a fiber coupler. Thus, I propose that length-dependent sliding forces exerted by the bridging fiber onto kinetochore fibers support chromosome alignment.

(90 pages, 31 figures, 1 table, 238 references, original in English)
Key words: mitotic spindle, chromosome alignment, kinetochores, microtubule poleward flux, speckle microscopy, chromosome segregation errors
Supervisor: Iva M. Tolić, PhD, Full Professor and Senior Research Group Leader
Reviewers: Vedrana Filić Mileta, PhD, Senior Research Associate
Biljana Balen, PhD, Full Professor
Andrew D. McAinsh, PhD, Professor and Senior Investigator

Sveučilište u Zagrebu
Prirodoslovno-matematički fakultet
Biološki odsjek

Doktorski rad

MEHANIZAM PORAVNANJA KROMOSOMA SILAMA KOJE OVISE O PREKLAPANJU MIKROTUBULA I NJEGOV UTJECAJ NA POGREŠKE U RAZDVAJANJU KROMOSOMA

PATRIK RISTESKI

Institut Ruđer Bošković

Poravnanje kromosoma je jedno od obilježja mitoze i problemi u poravnavanju, koji opstaju u anafazi, vode izravnoj aneuploidiji. Poravnanje na ekvatoru vretena ovisi o silama vučenja koje djeluju na vrhove kinetohornih vlakana zajedno sa silama izbacivanja s pola. Međutim, kinetohorna vlakna također su podvrgnuta silama koje pokreću njihov tok prema polu. U ovom radu predstavljam mehanizam za centriranje vođen tokom mikrotubula koji se oslanja na tok generiran silama unutar preklopa između premošćujućih i kinetohornih vlakana. Ovaj mehanizam centriranja radi tako da duže kinetohorno vlakno teče brže od kraćeg, što pomiče kinetohore prema centru. Kinetohore su bolje centrirane kada su preklapanja kraća i tok kinetohornih vlakana izrazito sporiji od toka premošćujućih vlakana. Identificirao sam proteine Kif18A i Kif4A kao regulatore preklapanja i toka mikrotubula i protein NuMA kao spojnicu vlakana. Stoga predlažem da sile klizanja koje su ovisne o duljini, a koje premošćujuće vlakno prenosi na kinetohorna vlakna, podržavaju poravnanje kromosoma.

(90 stranica, 31 slika, 1 tablica, 238 literaturnih navoda, jezik izvornika engleski)
Ključne riječi words: diobeno vreteno, poravnanje kromosoma, kinetohore, tok mikrotubula prema polu, *speckle* mikroskopija, pogreške u podjeli kromosoma
Mentor: prof.dr.sc. Iva M. Tolić, Znanstveni savjetnik u trajnom zvanju
Ocjenjivači: dr.sc. Vedrana Filić Mileta, Viši znanstveni suradnik
prof.dr.sc. Biljana Balen, Redoviti profesor
prof.dr.sc. Andrew D. McAinsh, Redoviti profesor

Table of Contents

1. INTRODUCTION 1

2. RESEARCH OVERVIEW 3

2.1. Mitotic spindle and chromosome movements during mitosis 5

2.2. Physical mechanisms that underly chromosome alignment 7

2.2.1. Microtubule length-dependent pushing forces 8

2.2.2. Microtubule length-dependent pulling forces 9

2.2.3. Microtubule length-dependent regulation of microtubule dynamics 11

2.3. Molecular mechanisms that generate and regulate pulling forces on kinetochores 12

2.3.1. Kinetochore microtubules pull on kinetochores 12

2.3.2. Molecular mechanisms that regulate the dynamics and length of kinetochore microtubules 13

2.4. Polar ejection forces act on chromosome arms 17

2.5. Forces originating from mechanical coupling of k-fibers and bridging fibers 18

2.6. Chromosome segregation errors and aneuploidy 21

2.6.1. Erroneous kinetochore-microtubule attachments 21

2.6.2. Link between chromosome segregation errors and genomic instability 24

2.6.3. Consequences of aneuploidy on cell proliferation 25

2.8.4. Chromosome misalignment in cancer 26

3. MATERIALS AND METHODS 28

3.1. Cell culture 28

3.2. RNA interference and transfection 29

3.3. Speckle microscopy 29

3.4. Cell-micropatterning 30

3.5. Immunostaining 30

3.5. Photoactivation assay 32

3.6. Long-term imaging for chromosome segregation error assessment 32

3.7. Image analysis 32

4. RESULTS 34

4.1. Speckle microscopy assay to follow the movement of individual microtubules within the spindle 34

4.2. Longer kinetochore fiber undergoes flux at a higher velocity than the shorter one 37

4.3. Bridging microtubules undergo poleward flux at a higher velocity than kinetochore microtubules 39

4.4. Kinetochore centering efficiency depends on the flux velocity of k-fibers 46

4.5. Longer overlaps of antiparallel microtubules lead to an increase in the k-fiber flux velocity to the bridging fiber flux velocity 48

4.6. The difference in the flux of bridging and k-fibers increases for smaller concentrations of passive crosslinkers 51

4.7. Comparison with the model 52

4.8. Aneuploidy can occur due to persistent chromosome alignment defects in metaphase 55

5. DISCUSSION 62
5.1. Flux-driven centering model explains kinetochore alignment at the equatorial plane 62
5.2. Kinetochore fiber flux is driven by interactions with the bridging fiber 63
5.3. Chromosome alignment depends on the overlap length of bridging microtubules 66
5.4. Chromosome alignment defect leads to aneuploidy 67
6. CONCLUSION 69
7. REFERENCES 70
8. AUTHOR BIOGRAPHY 90

1. INTRODUCTION

Metaphase chromosome alignment at the spindle equator is a hallmark of mitosis and is important for proper completion of mitosis (Fonseca et al., 2019; Maiato et al., 2017). Chromosome movements on the spindle that lead to their alignment are driven by pulling forces exerted by kinetochore microtubules that pull the kinetochores poleward and polar ejection forces exerted by non-kinetochore microtubules that push the chromosome arms away from the pole (Rieder and Salmon, 1994). The role of these forces in chromosome movements and alignment were explored in theoretical studies (Joglekar and Hunt, 2002; Civelekoglu-Scholey et al., 2006, 2013; Armond et al., 2015). The main mechanism of chromosome alignment in these models relies on polar ejection forces, which have a centering effect on chromosomes because these forces decrease away from the spindle pole (Ke et al., 2009).

Similar to the polar ejection forces, pulling force generated by kinetochore microtubules can have a centering effect on chromosomes even though forces generated at the microtubule plus end do not depend on microtubule length (Grishchuk et al., 2005; Koshland et al., 1988). The centering effect arises due to motor proteins such as kinesin-8, which measure microtubule length by binding along the microtubule lattice and walking all the way to the microtubule plus end, where they make microtubule dynamics length-dependent (Varga et al., 2006). Indeed, kinesin-8 is required for chromosome alignment at the spindle center (Mayr et al., 2007; Stumpff et al., 2008, 2012; West et al., 2002). Theoretical studies have shown that length-dependent microtubule catastrophe induced by kinesins or length-depending pulling forces can center kinetochores in yeast cells (Gardner et al., 2008; Mary et al., 2015; Gergely et al., 2016; Klemm et al., 2018). Thus, in addition to polar ejection forces, measuring of microtubule length by kinesins has an important contribution to chromosome centering.

However, this is not a complete picture of the forces that act on chromosomes. Kinetochore fibers (k-fibers) are also subjected to forces that drive their poleward flux (Forer, 1965; Hamaguchi et al., 1987; Hiramoto and Izutsu, 1977; Mitchison, 1989). This movement can be imagined as a conveyor belt-like transport where the whole k-fiber is being shifted towards the pole, while its minus ends depolymerize and plus ends polymerize. This complex process is driven and regulated by multiple motor proteins (Miyamoto et al., 2004; Ganem et al., 2005; Rogers et al., 2004; Steblyanko et al., 2020). It has been proposed that poleward flux of k-fibers is generated by motor-driven sliding of k-fibers with respect to interpolar microtubules (Mitchison, 2005), inspired by electron microscopy images of *Xenopus* extract

spindles (Ohi et al., 2003). The mechanical interaction between k-fibers and the associated interpolar bundles called bridging fibers has been demonstrated by laser cutting of these fibers in human cells (Kajtez et al., 2016). It is known that kinesin-5 activity contributes to the poleward flux of k-fibers and interpolar microtubules in *Drosophila* syncytial embryo mitosis (Brust-Mascher et al., 2009) and *Xenopus laevis* egg extract spindles (Miyamoto et al., 2004). However, inhibition of kinesin-5 activity in mammalian cells only slightly reduces poleward flux rates (Cameron et al., 2006), suggesting a coordinated action of multiple players (Steblyanko et al., 2020). How poleward flux of interpolar microtubules transmitted to k-fibers regulates forces acting on kinetochores has been explored in a theoretical model, which suggests that flux promotes tension uniformity on kinetochores, in agreement with experiments showing large variability in kinetochore tension in cells with abolished microtubule flux (Matos et al., 2009). Interestingly, physical coupling between k-fibers and the associated interpolar bundles, i.e. bridging fibers, is important not only for tension but also for chromosome alignment, given that optogenetic perturbation of bridging fibers leads to chromosome misalignment (Jagrić et al., 2021). In these experiments, chromosome misalignment was accompanied by elongation of bridging microtubule overlaps. These recent findings, together with the idea that poleward flux is generated within bridging fibers and transmitted to k-fibers, open an interesting possibility that chromosome alignment, bridging microtubule overlaps and poleward flux are mutually related. Thus, the mechanism of chromosome alignment on the spindle is incompletely understood.

In this thesis, I hypothesize that poleward flux drives chromosome centering and propose a flux-driven centering mechanism that relies on the interaction between bridging and k-fibers. The centering mechanism is based on length-dependent pulling forces exerted by k-fibers onto the kinetochores. These forces increase with the overlap length between bridging and k-fibers and with the velocity difference between the fibers. To test this mechanism, I developed a speckle microscopy assay on spindles of human cells and measured the flux of individual bridging and kinetochore microtubules. I found that when kinetochores are displaced, the longer k-fiber undergoes flux at a higher velocity than the shorter one, which is at the core of the flux-driven centering because in this mechanism the faster flux of the longer k-fiber pulls the kinetochores in the direction of this fiber, i.e. towards the spindle center. Experiments, in which a set of depletions of spindle proteins were performed, indicate that kinetochores are better centered when the overlaps between bridging and k-fibers are shorter and the kinetochore fiber flux markedly slower than the bridging fiber flux. Forces from the bridging fiber are transmitted to the k-fiber in a manner dependent on the coupling between

bridging and k-fibers. Furthermore, k-fibers flux slower after depletion of NuMA (nuclear mitotic apparatus protein), which is a passive cross-linker of parallel microtubules, indicating that NuMA couples the fibers. Moreover, k-fibers flux faster after depletion of plus-end directed molecular motors, specifically Kif18A (Kinesin Family Member 18A; kinesin-8 motor protein family) and/or Kif4A (Kinesin Family Member 4A; kinesin-4 motor protein family), which results in longer overlaps implying stronger coupling. Results in this thesis suggest that lateral length-dependent sliding forces that the bridging fiber exerts onto k-fibers promote the movement of kinetochores towards the spindle center.

Additionally, by quantitatively assessing chromosome segregation errors in healthy and tumor cell lines, I tested the relevance of chromosome misalignment for inheritance fidelity. Here, chromosome misalignment defects are a distinctive feature of mitosis in tumor cell lines as cervical carcinoma (HeLa) and osteosarcoma (U2OS) cells exhibit persistently misaligned chromosomes which end up in the same daughter cells and cause aneuploidy. I found this rate to be 3-4% in both cancer cell lines. Before anaphase, the frequency of misaligned chromosomes was roughly 2x higher in U2OS than in HeLa cells. In U2OS cells, I found a 60-minute delay in anaphase entry during which most of the misaligned chromosomes were resolved. Here, results suggest that misaligned chromosomes can lead to aneuploidy, presumably due to spindle assembly checkpoint override, and indicate that multiple errors per cell are due to defects in the mitotic machinery.

2. RESEARCH OVERVIEW

During a lifetime cells divide, which is essentially a duplication process as it produces two genetically identical cells from a single one. In order to divide, a cell must undergo several key events that precede the cell division, i.e. cell growth, replication and physical segregation of the genetic material. These events are organized into temporally distinct phases that form the cell cycle (Alberts et al., 2002). Replication of the genetic material is limited to S (synthesis) phase, whilst segregation occurs in M (mitotic) phase. The periods that separate S from M phase are named G (gap) phases and serve as key periods for cell cycle regulation; cell cycle entry during G1 and initiation of processes that lead to segregation of genetic material during G2. As the most eventful phase of the cell cycle, M phase involves a major rearrangement of almost all cell components, including nuclear and cytoplasmic division known as mitosis and cytokinesis, respectively.

Mitosis, which is the focus of this thesis, consists of five stages: prophase, prometaphase, metaphase, anaphase, and telophase (**Figure 1**) (Alberts et al., 2002). Amid mitosis, the duplicated genetic material condenses, the nuclear envelope breaks down and the interphase cytoskeleton network reorganizes into the mitotic spindle that separates duplicated genetic material into daughter cells.

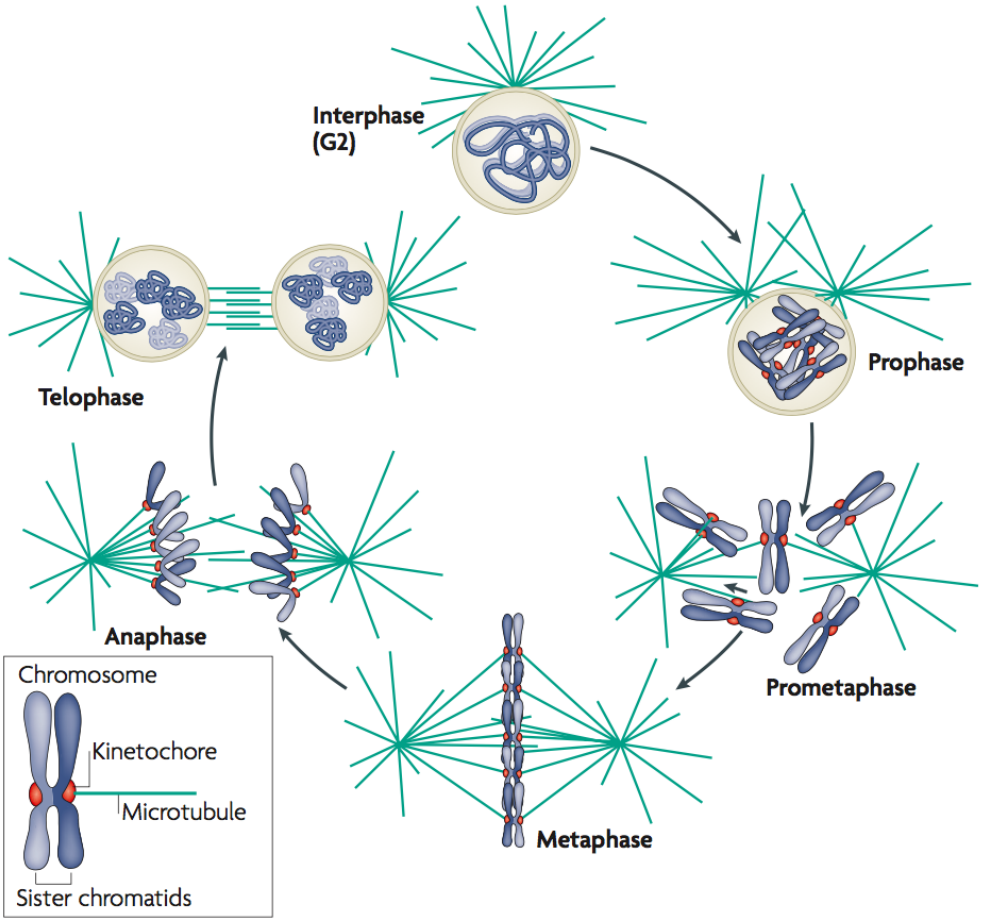


Figure 1. The stages of the M phase. The major phases of the cell cycle are the interphase and M phase. Interphase consists of the S phase, during which DNA replication occurs, and the G1 and G2 phases which serve as decision windows between S and M phases. In the M phase, first the nucleus and then the cytoplasm segregate. Mitosis starts with prophase when duplicated chromosomes condense, after which microtubules incorporate chromosomes into a mitotic spindle. In prometaphase, chromosomes congress to the spindle equator, whilst metaphase is evident by the chromosome alignment at the metaphase plate. In anaphase, chromatids separate to the opposite spindle poles. Mitosis finishes with chromosome decondensation and nuclei reformation in telophase, after which daughter cells separate during cytokinesis. Illustration from Cheeseman and Desai, (2008).

2.1. Mitotic spindle and chromosome movements during mitosis

Essential to reliable genome inheritance is the mitotic spindle, which mediates the physical separation of a complete set of genetic material into each daughter cell. Structurally, this self-assembled macromolecular machine is built from microtubules and microtubule-associated proteins (Pavin and Tolić, 2016; Petry, 2016; Prosser and Pelletier, 2017). To illustrate its importance, proteome analysis of the human mitotic spindle identified over 800 proteins associated with this structure (Sauer et al., 2005). Genetic material, in the form of distinct chromosomes, is incorporated into the mitotic spindle via microtubule attachments to kinetochores, complex protein-based structures associated with chromosome's centromere (McIntosh et al., 2002; Cheeseman and Desai, 2008).

Central to chromosome movements within the spindle are microtubules, polar polymeric structures whose plus ends are more dynamic and undergo dynamic instability characterized by persistent periods of growth and shrinkage (Desai and Mitchison, 1997; Howard and Hyman, 2003). *In vitro* experiments have demonstrated that growing or shrinking microtubules can generate pushing or pulling forces, respectively (Dogterom and Yurke, 1997; Grishchuk et al., 2005), suggesting that these forces drive movements within cells including chromosome positioning on the spindle (Tolić-Nørrelykke, 2008).

Microtubules within the spindle can be divided into three main groups based on their position and function (**Figure 2**). Kinetochore microtubules bind the kinetochore and form a k-fiber. Overlap microtubules grow from the opposite spindle halves and overlap in the central part of the spindle. In numerous cell types and organisms, overlap microtubules laterally link sister k-fibers like a bridge, thus being called bridging fibers (Pavin and Tolić, 2016; Tolić, 2018). Astral microtubules extend from the spindle pole towards the cell periphery and contact the cell cortex.

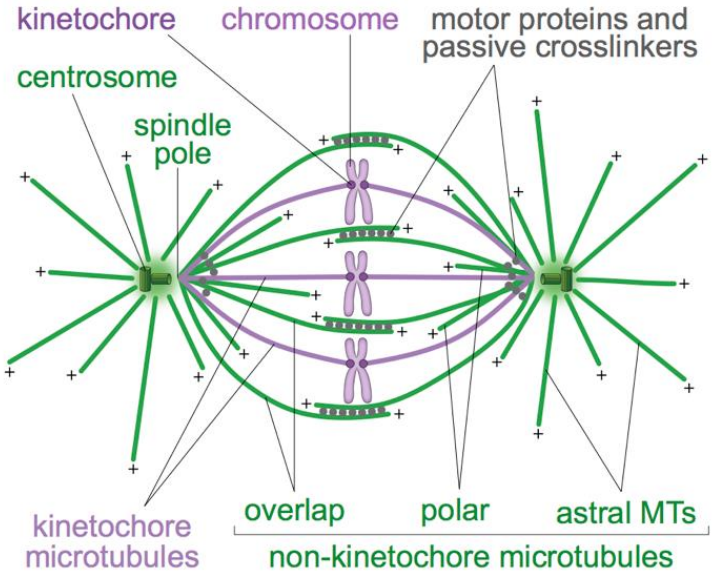


Figure 2. Microtubule classes within the mitotic spindle. Microtubules within the mitotic spindle can be divided into kinetochore microtubules (magenta) that attach to chromosomes via kinetochores and non-kinetochore microtubules (green) that do not. Non-kinetochore microtubules can be divided into polar, overlap, and astral microtubules. Astral microtubules emanate from spindle poles and grow toward the cell cortex. Polar microtubules emanate from spindle poles and grow toward the center of the spindle. Overlap microtubules emanate from opposing spindle poles and form antiparallel regions in the center of the spindle. Illustration from Tolić, (2018).

Before chromosome segregation in anaphase, evident by sister chromatid separation towards the opposite spindle poles, chromosomes align at the spindle equator, a position equidistant from spindle poles (Walczak et al., 2010). In this process, termed chromosome congression (**Figure 3A**), chromosomes undertake different pathways to get positioned at the spindle equator (Pavin and Tolić, 2016; Maiato et al., 2017). Chromosome congression is coupled closely in time with chromosome biorientation (**Figure 3A**), i.e., the formation of stable attachments of sister kinetochores to microtubules that emanate from the opposite spindle poles. The establishment of proper kinetochore-microtubule attachments, which will be discussed later, and the alignment of chromosomes at the spindle equator are a prerequisite for synchronous poleward movement of chromosomes in anaphase (**Figure 3B**), and therefore chromosome inheritance fidelity (Walczak et al., 2010; Maiato et al., 2017; Fonseca et al., 2019).

To discern between terms of chromosome congression (**Figure 4A**), centering (**Figure 4B**), and alignment (**Figure 4C**) that I will use throughout the thesis, I will refer to processes of prometaphase chromosomes being aligned at the spindle equator, bioriented metaphase chromosomes being centered towards the spindle equator during their oscillatory movements in the metaphase plate, and the metaphase position of chromosomes at the spindle equator, respectively.

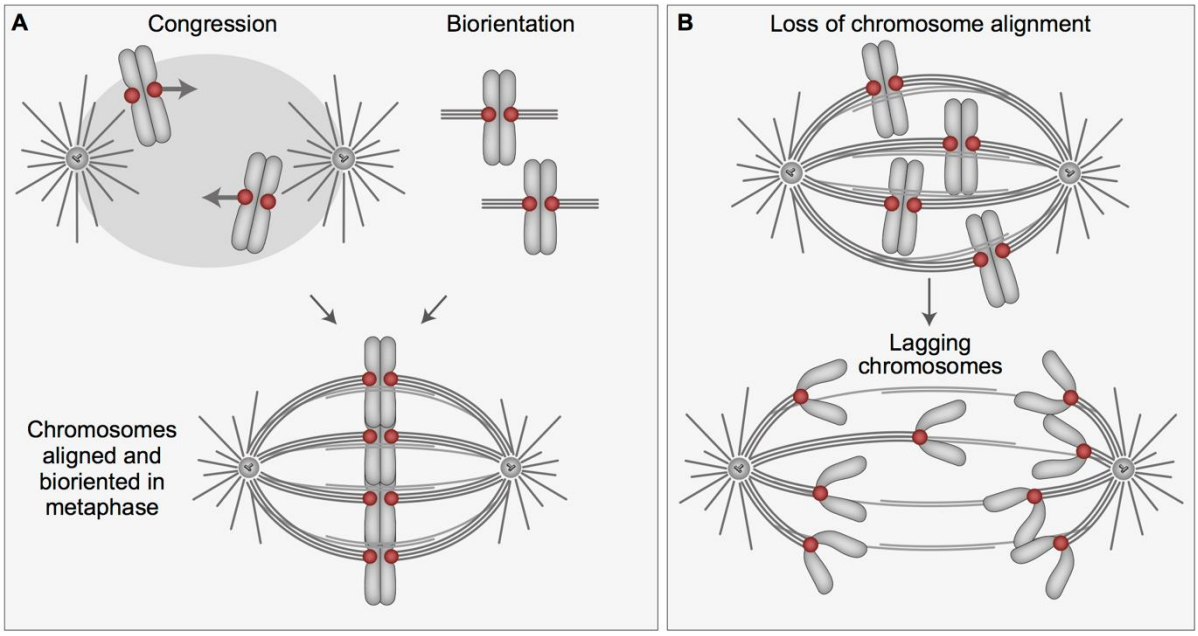


Figure 3. Metaphase chromosome alignment and its biological relevance. (**A**) During spindle assembly chromosomes congress to the spindle equator and become bioriented, i.e. their kinetochores (red) are attached to microtubules (grey lines) extending from the opposite spindle poles (grey spheres). (**B**) Loss of chromosome alignment leads to asynchronous poleward movements of chromatids in anaphase and chromosome segregation errors. Adapted from Risteski et al., (2021b).

2.2. Physical mechanisms that underly chromosome alignment

In order to position chromosomes at its equator, the mitotic spindle needs a mechanism that measures length. There are three classes of mechanisms that are involved in spindle length sensing, based on microtubule length-dependent pushing forces, pulling forces and microtubule dynamics (Risteski et al., 2021b).

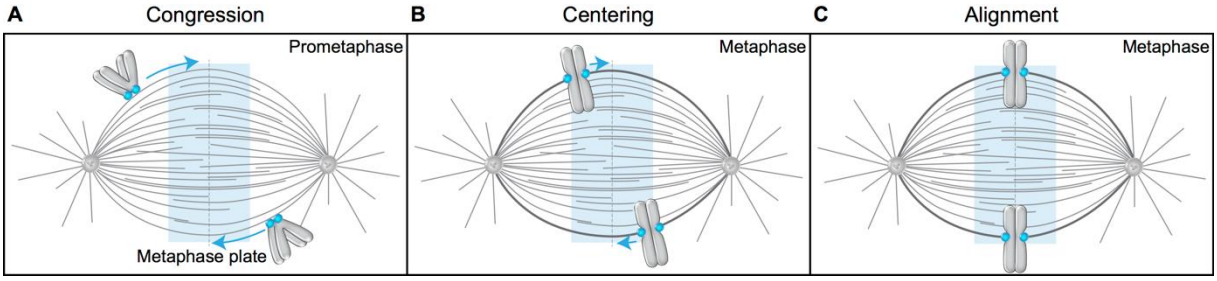


Figure 4. Schematics of chromosome congression, centering, and alignment. Chromosome movements toward the spindle equator involve (**A**) chromosome congression and (**B**) centering that underly (**C**) chromosome alignment. Blue circles; kinetochores. Thick grey lines; k-fibers.

2.2.1. Microtubule length-dependent pushing forces

In 1937, the idea that chromosomes experience pushing forces within the mitotic spindle emerged as Darlington hypothesized that chromosomes move towards the spindle equator by being repelled by the poles due to electric charges (Darlington, 1937). Darlington's initial idea about the existence of repulsive forces and their ability to help center the chromosomes on the spindle was correct, though the origin of forces was later shown to be mechanical and microtubule-dependent (Rieder et al., 1986). Microtubule pushing forces, as discussed here, depend on the distance from the centrosome for three reasons.

First, the density of microtubules that are nucleated at the centrosome is high close to the centrosome, and many of them reach a unit area situated close to the centrosome, producing a high pushing force (**Figure 5A**). Far away from the pole, microtubules are rare and few of them reach large distances, generating a smaller pushing force per unit area. In mathematical terms, microtubule density decreases with the distance from the centrosome, d, as $1/d^2$ for an ideal isotropic aster (Campàs and Sens, 2006) (**Figure 5A**). Note that an isotropic distribution is a mathematical idealization of a microtubule aster, whereas in spindles of human cells microtubules are nucleated not only at the centrosome but also along existing microtubules by the augmin complex, leading to a weaker reduction of microtubule density with distance than for centrosomal nucleation alone (David et al., 2019).

Second, the length distribution of microtubules is roughly exponential, with many short microtubules and few long ones (**Figure 5A**). Such a distribution is a consequence of microtubule dynamic instability (Mitchison and Kirschner, 1984; Dogterom and Leibler, 1993) and has been observed in electron tomography images of spindles in *Caenorhabditis elegans* embryos (Redemann et al., 2017). The exponential length distribution amplifies the microtubule

density effect, resulting in an even larger difference in the number of microtubules reaching shorter and longer distances.

The third effect is based on microtubule buckling (**Figure 5A**). If the pushing force exerted by a growing microtubule exceeds a critical force, the microtubule buckles under its own compression. The critical force for buckling, also called the Euler force, depends on microtubule length, L, as $1/L^2$ (**Figure 5A**) (Howard, 2001). Therefore, a shorter microtubule has a larger Euler force and thus produces a stronger push than a long one. When all three effects are put together, a chromosome that is displaced towards one spindle pole has more microtubules extending from the nearer than the farther pole, pushing it away. Moreover, the Euler force of the microtubules extending from the nearer pole is higher. Due to the higher number of microtubules and their higher force, the chromosome will be pushed away from the nearer pole towards the spindle center (**Figure 5A**).

2.2.2. Microtubule length-dependent pulling forces

In contrast to the microtubule pushing forces within the spindle, which are widely accepted to depend on microtubule length and the distance from the centrosome, the length-dependence of the pulling forces is controversial. In pioneering work on spindle forces, Östergren proposed that a longer traction fiber of a displaced chromosome generates a stronger pulling force toward the more remote pole, causing the stabilization of chromosome positioning at the equatorial plate (Östergren, 1950). However, at that time microtubules had not yet been discovered, and these concepts were not developed further.

Östergren's hypothesis was tested three decades later by elegant experiments in which multivalent chromosomes with three or four kinetochore fibers were created by γ-irradiation in grasshopper spermatocytes (Hays et al., 1982). These chromosomes shifted closer to the pole to which the greater number of kinetochore fibers were attached, and the analysis of the stable asymmetric positions of the chromosomes supported Östergren's hypothesis that the magnitude of poleward force along a kinetochore fiber is proportional to the length of the fiber. Similarly, analysis of chromosome positions following partial reduction of kinetochore microtubule number confirmed the length-dependence of the poleward force (Hays and Salmon, 1990).

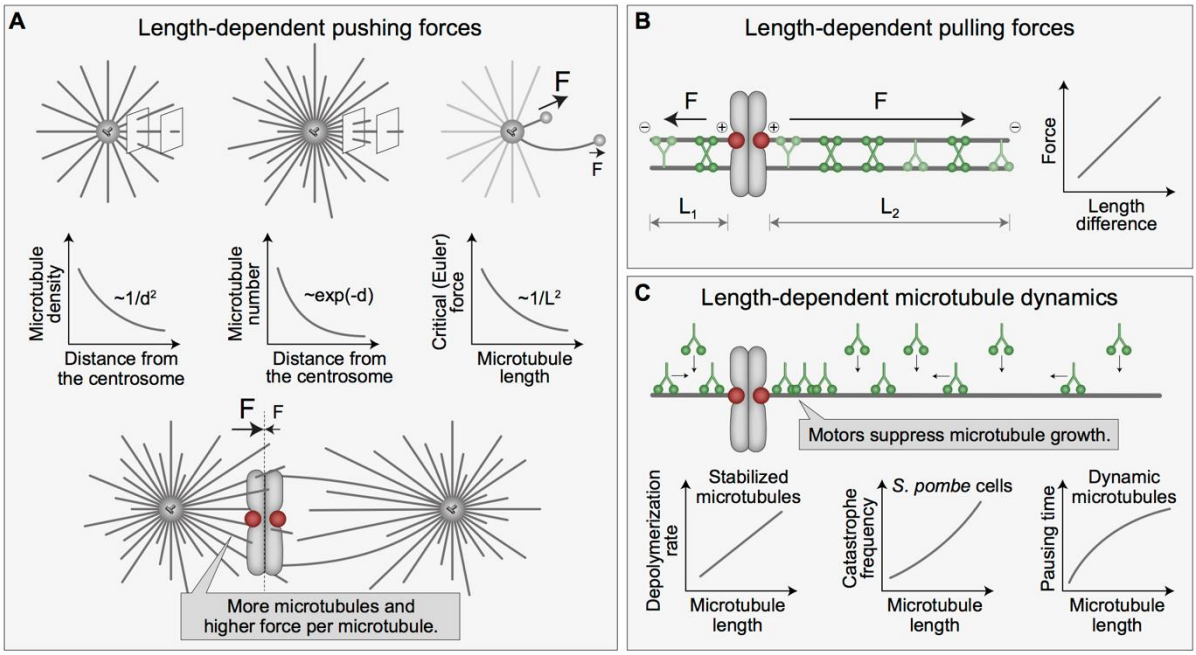


Figure 5. Principles of length measurements within the spindle. (**A**) Pushing forces exerted by growing microtubules decrease with an increasing distance from the centrosome because microtubule density decreases due to aster geometry (left aster and graph), a roughly exponential distribution of microtubule lengths due to microtubule dynamics (middle aster and graph), and a decreasing critical (Euler) force, *F*, at which the microtubule buckles (right aster and graph). A displaced chromosome is contacted by more microtubules from the nearer pole, and they can exert a higher force per microtubule than the long ones extending from the other spindle half, resulting in a net force towards the spindle center (bottom). (**B**) Pulling forces, *F*, exerted by motor proteins (tetrameric, dark green and/or dimeric, light green) attached along the k-fibers depend on the length of the overlap between the k-fiber and non-kinetochore microtubules, *L*. The net force is proportional to the difference in the overlap length on either side (graph at the right). (**C**) Motor proteins (green) that walk towards the microtubule plus end with a low detachment rate accumulate there in a microtubule length-dependent manner. If these motors are modulators of microtubule dynamics, then microtubule depolymerization rate, catastrophe frequency, or the fraction of time that the microtubule spends in a pausing state depend on the microtubule length (graphs). Illustration from Risteski et al., (2021b).

As discussed in Maiato et al., (2017), some studies have observed that after laser cutting of k-fibers, chromosomes exhibit minor movements towards the pole of the unperturbed k-fiber, thereby showing evidence against the length-dependent nature of the k-fiber derived forces. However, this could depend on the time scale of response, as the movement of the

chromosomes towards the attached pole does not occur immediately after cutting (Czaban et al., 1993), or the position of the cut with respect to the kinetochores (Vukušić et al., 2017). Additionally, after severing, in the majority of the cells, the k-fiber stub is pulled back toward the spindle pole and reintegrated into the spindle (Vukušić et al., 2017).

The discovery of the dynamic instability of microtubules led to the idea that the events on the plus and minus ends of kinetochore microtubules regulate the pulling forces on the kinetochore (Mitchison et al., 1986; Mitchison and Salmon, 1992). Thus, the field shifted its focus towards the forces generated at microtubule ends, whereas pulling forces exerted along the length of the microtubule were largely neglected.

Kinetochore microtubules are not isolated within the spindle but are laterally attached to non-kinetochore microtubules (Kajtez et al., 2016; O'Toole et al., 2020). As recently proposed (Jagrić et al., 2021), motor proteins may bind within the overlaps of kinetochore and non-kinetochore microtubules and longer overlaps accumulate more motors, consequently exerting larger forces (**Figure 5B**). The total force on the chromosome is then directed towards the spindle center and proportional to the difference in the length of the overlap on either side (**Figure 5B**).

2.2.3. Microtubule length-dependent regulation of microtubule dynamics

The pulling force generated by the depolymerizing plus end of a microtubule does not depend on microtubule length (Grishchuk et al., 2005; Koshland et al., 1988) and thus cannot center the chromosome, but some motor proteins can measure microtubule length and make microtubule dynamics length-dependent (**Figure 5C**). Such length-dependent mechanisms are achieved by the motors that bind along the microtubule lattice and walk all the way to the microtubule plus end. Thus, the longer the microtubule, the more motors accumulate at its plus end. This effect, known as the antenna model, has been shown for kinesin-8 (Varga et al., 2006, 2009; Mayr et al., 2007) and kinesin-4 (Bieling et al., 2010). For the antenna model to be functional, the motors must be highly processive, i.e. walk for a large distance along the microtubule without detachment and must walk faster than the microtubule grows in order to reach the plus end. If the motors showing this behavior are regulators of microtubule dynamics, then the dynamics will be regulated in a length-dependent manner. For example, due to the kinesin-8 Kip3 from budding yeast, long, stabilized microtubules *in vitro* depolymerize faster than short microtubules (**Figure 5C**) (Varga et al., 2006). Similarly, in the fission yeast *Schizosaccharomyces pombe*, the dynamics of the longest microtubule in an interphase bundle

is regulated in a length-dependent manner, although a different feature is affected, namely the catastrophe rate of longer microtubules is higher than that of shorter ones (**Figure 5C**) (Tischer et al., 2009). Finally, *in vitro*, dynamic microtubules become less dynamic and spend more time in a pausing state when the human kinesin-8 Kif18A accumulates at their plus end (Stumpff et al., 2012; Du et al., 2010) (**Figure 5C**).

2.3. Molecular mechanisms that generate and regulate pulling forces on kinetochores

2.3.1. Kinetochore microtubules pull on kinetochores

Back in the 1980s, laser ablation experiments on prometaphase or metaphase mitotic spindles revealed the existence of poleward pulling force on chromosomes exerted by k-fibers. Ablation of one of the two sister kinetochores led to the movement of the whole chromosome towards the spindle pole to which the non-ablated kinetochore was oriented (McNeill and Berns, 1981). Similarly, ablation of chromosome arms of mono-oriented chromosomes, in which only one sister kinetochore is attached to microtubules emanating from the spindle pole, caused the kinetochores to move towards the attached spindle pole (Rieder et al., 1986). In these experiments, chromosome cutting was done to reduce outward, i.e. polar ejection forces, which I will discuss later. Ablation of the region between sister kinetochores resulted in the movement of each kinetochore towards the pole it was attached to (Khodjakov and Rieder, 1996). These experiments have demonstrated that k-fibers exert pulling forces on kinetochores.

Mitotic chromosomes are elastic and upon biorientation, their centromeres become stretched by kinetochore microtubules pulling on both sister kinetochores (Claussen et al., 1994; Pickett-Heaps et al., 1982). This pulling generates opposing forces that tend to return the centromere to its non-stretched configuration. In line with this, the inter-kinetochore distance between bioriented sister kinetochores is larger than that of mono-oriented kinetochores, suggesting increased tension when both sister kinetochores are attached to opposing spindle poles (Waters et al., 1996). Even though attached to kinetochores, kinetochore microtubule plus-ends remain dynamic, yet with slower tubulin turnover compared to non-kinetochore microtubules (Zhai et al., 1995). Due to the mechanical coupling between kinetochore microtubules and kinetochores, the dynamic instability of kinetochore microtubules contributes to the oscillatory motion of the kinetochores along the spindle axis (Skibbens et al., 1993; Rieder and Salmon, 1994). These abrupt changes between the poleward and anti-poleward movement of kinetochores, termed directional instability, are less prominent during

chromosome congression in prometaphase when chromosomes have directional persistence towards the spindle equator due to differences in the durations but not in the velocities of movements towards and away from the equator (Skibbens et al., 1993). Once aligned close to the equator, sister kinetochores move in a coordinated manner within a narrow region in the central part of the spindle.

2.3.2. Molecular mechanisms that regulate the dynamics and length of kinetochore microtubules

How are the length-measurement mechanisms and the forces that control chromosome alignment implemented in cells at the molecular level? Motor proteins can make microtubule dynamics length-dependent, which has a centering effect on chromosomes, the principles of which are described above (**Figure 5C**). This centering mechanism works well due to the precise regulation of microtubule dynamics achieved by a large number of motor proteins and other microtubule-associated proteins.

Microtubule plus ends, responsible for pulling forces on kinetochores, are a hub for multiple microtubule regulators (**Figure 6A**). One of the most important regulators is kinesin-8, which promotes microtubule catastrophe in budding yeast (Gupta et al., 2006), increases catastrophe frequency in fission yeast (Tischer et al., 2009; West et al., 2001), and promotes microtubule destabilization in *Drosophila* (Goshima and Vale, 2003). Similar activity was observed for the human homolog Kif18A (Mayr et al., 2007), although more recent studies indicate that it suppresses microtubule dynamics rather than induces microtubule depolymerization (Stumpff et al., 2012; Du et al., 2010). Accordingly, depletion of Kif18A results in increased spindle length and loss of inter-kinetochore tension (Mayr et al., 2007; Stumpff et al., 2008; Janssen et al., 2018). With its role at kinetochore microtubule plus ends, kinesin-8 is required for proper mitotic chromosome movement and alignment (Mayr et al., 2007; Stumpff et al., 2012; Goshima and Vale, 2003; Stumpff et al., 2008; West et al., 2002; Garcia et al., 2002; Gandhi et al., 2004; Zhu et al., 2005; Klemm et al., 2018; Wargacki et al., 2010). Quantitative tracking of kinetochore positioning upon Kif18A depletion indicated that Kif18A limits kinetochore movements around the spindle equator by affecting the frequency of kinetochore directional switches and by decreasing the velocity of kinetochore movements (Stumpff et al., 2008; Armond et al., 2015; Jaqaman et al., 2010), although another study reported the opposite effect on kinetochore velocity, possibly due to a lower time resolution of imaging (Mayr et al., 2007).

Several plus end-tracking proteins have been implicated in kinetochore alignment. MCAK/Kif2C (Mitotic Centromere-Associated Kinesin/Kinesin Family Member 2C; kinesin-13 motor protein family) is a microtubule depolymerase that localizes on centromeres and kinetochores and is thus a strong candidate for force generation involved in chromosome movements and positioning (Wordeman and Mitchison, 1995; Hunter et al., 2003) (**Figure 6A**). MCAK is a motor that diffuses along the microtubule lattice without directional bias, i.e. it targets and destabilizes both microtubule ends *in vitro* (Helenius et al., 2006). Depletion of MCAK leads to chromosome alignment defects, a decrease in chromosome oscillation speed and directional coordination between sister kinetochores, without affecting the period of oscillations (Kline-Smith et al., 2004; Wordeman et al., 2007; Jaqaman et al., 2010). Based on these results and the observation that MCAK preferentially accumulates on the leading sister kinetochore of a congressing chromosome (Kline-Smith et al., 2004) – the one moving towards its associated pole and towards spindle equator – it was suggested that MCAK sets the velocity of chromosome oscillations together with Kif18A. In this model, MCAK depolymerizes microtubules within the k-fiber of the leading kinetochore, whereas Kif18A suppresses dynamics at the trailing kinetochore – the one moving away from its associated pole – thereby providing resistance to sister pair movement (Kline-Smith et al., 2004; Jaqaman et al., 2010).

Upon microtubule attachment, CLASPs (Cytoplasmic Linker-Associated Proteins) remain localized at the kinetochore-microtubule interface (Maiato et al., 2003; Mimori-Kiyosue et al., 2006; Pereira et al., 2006) (**Figure 6A**). With their redundant roles in promoting microtubule rescue and suppressing microtubule catastrophe, without affecting the overall microtubule polymerization rate, CLASPs act as microtubule stabilizers (Al-Bassam et al., 2010; Al-Bassam and Chang, 2011). By stabilizing kinetochore microtubules, CLASPs increase tension on kinetochores and decrease both oscillations and microtubule growth (Mimori-Kiyosue et al., 2006). Thus, CLASPs help keep the kinetochores in tight alignment at the spindle equator.

Contrary to the highly dynamic plus ends that interact with kinetochores, minus ends are mostly anchored at the microtubule nucleation sites, i.e. centrosomes or microtubule lattice in the case of augmin-dependent microtubule nucleation (Akhmanova and Steinmetz, 2019). The key player involved in the minus end dynamics is Kif2A (Kinesin Family Member 2A; kinesin-13 motor protein family), which depolymerizes microtubules (Rogers et al., 2004; Ganem et al., 2005) (**Figure 6B**), though other proteins are likely also involved as Kif2A antibody injection does not completely eliminate depolymerization (Civelekoglu-Scholey et al., 2013).

Dynamics at the microtubule ends underlie a process termed poleward flux, defined as a continuous translocation of tubulin subunits in the direction of the minus end (Mitchison, 1989). Even though the molecular mechanisms responsible for this process are not yet fully elucidated, two main models have been suggested. One model proposes that flux is driven by kinesin-13-mediated depolymerization at spindle poles with simultaneous CLASP-mediated polymerization at kinetochore microtubule plus-ends (Ganem et al., 2005; Maiato et al., 2005; Girão et al., 2020). A different model explains the origin of poleward flux as a response to the sliding of antiparallel interpolar microtubules, which is transmitted to kinetochore microtubules due to their coupling mediated by different crosslinking molecules (Miyamoto et al., 2004; Brust-Mascher et al., 2009). As suggested, this sliding may be coupled to plus end dynamic instability and minus end disassembly as k-fiber is displaced poleward. Recently, it was proposed that poleward flux is driven by Kif4A/kinesin-4 on chromosome arms and that the distribution of poleward flux across the spindle is achieved by coupling of non-kinetochore and kinetochore microtubules (Steblyanko et al., 2020). Microtubule-sliding motors in this model, i.e. Eg5/Kif11 (Kinesin Family Member 11; kinesin-5 motor protein family) and Kif15 (Kinesin Family Member 15; kinesin-12 motor protein family), collaboratively act on interpolar microtubules, assisted by CENP-E/Kif10 (Centromere Protein E/Kinesin Family Member 10; kinesin-7 motor protein family) at kinetochores in prometaphase and Kif4A on chromosome arms in metaphase, where Kif4A generates microtubule fluxing force toward the poles (Steblyanko et al., 2020). Microtubule flux has been implicated in the regulation of spindle length, correction of erroneous kinetochore-microtubule attachments, and equalization of forces at kinetochores prior to segregation (Matos et al., 2009; Rogers et al., 2004; Ganem et al., 2005).

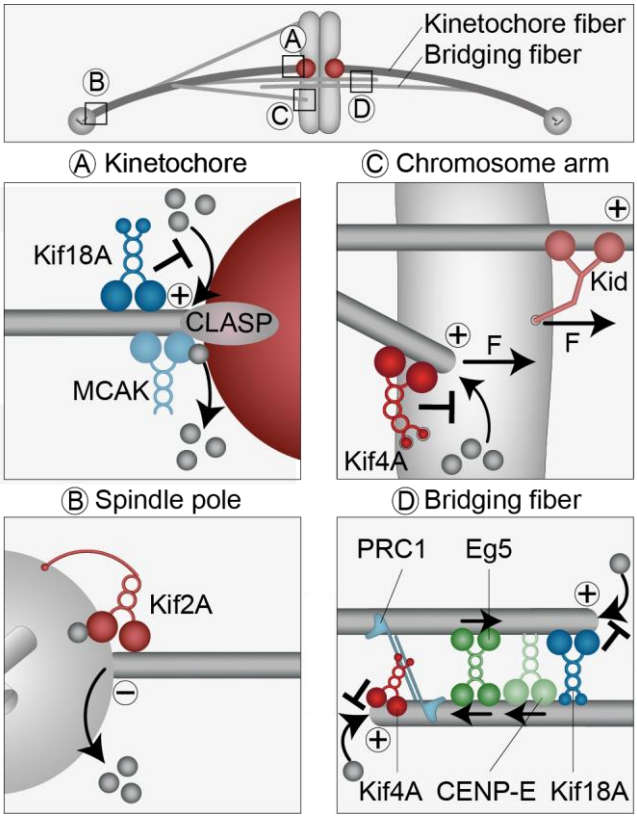


Figure 6. Molecular players involved in chromosome alignment. A chromosome with k-fibers (dark grey) and non-kinetochore microtubules (bridging microtubules overlapping in the middle and other microtubules interacting with chromosome arms, all in light grey) is sketched at the top with boxes marking the enlarged areas shown below. (**A**) At the kinetochore, Kif18A suppresses microtubule dynamics, CLASP promotes microtubule polymerization and MCAK promotes depolymerization. (**B**) At the spindle pole, Kif2A promotes microtubule depolymerization. (**C**) At the chromosome arm, chromokinesins generate polar ejection forces. Kid/Kif22 (Kinesin-like DNA-binding Protein/Kinesin Family Member 22; kinesin-10 motor protein family) moves the chromosome along the microtubule and Kif4A suppresses microtubule dynamics. Growing microtubules also generate polar ejection forces as they push into the chromosome. (**D**) Within the bridging fiber, Eg5 and CENP-E are involved in the sliding antiparallel microtubules apart. Kif18A and Kif4A, which interacts with the crosslinker PRC1 (Protein Regulator of Cytokinesis 1), suppress the dynamics of microtubule plus ends, thereby controlling the length of antiparallel overlaps. Illustration from Risteski et al., (2021b).

2.4. Polar ejection forces act on chromosome arms

The existence of polar ejection forces, generated by microtubules that push the chromosomes away from the pole, was first demonstrated by laser ablation of chromosome arms on chromosomes in monopolar and bipolar spindles, which resulted in the transport of the created acentric chromosome fragments away from the pole (Rieder et al., 1986; Rieder and Salmon, 1994). Polar ejection forces originate from interactions between non-kinetochore microtubules and chromosome arms, with anti-poleward forces being generated by microtubule polymerization against chromosome arms, or by the activity of chromokinesins, proteins that bind to both microtubules and chromosomes (Rieder et al., 1986; McIntosh et al., 2002; Bajer et al., 1982; Ault et al., 1991; Brouhard and Hunt, 2005) (**Figure 6C**). It was shown that polar ejection forces exerted by individual microtubules on metaphase chromosomes are consistent with forces generated by polymerizing microtubules pushing against chromosomes or by individual kinesin motors (Marshall et al., 2001). However, chromokinesins contribute to polar ejection forces to a larger extent than the pushing forces of polymerizing microtubules, given that a larger fraction of acentric chromosome fragments is able to congress to the spindle equator when chromokinesins are present (Barisic et al., 2014).

Among chromokinesins, the generation of polar ejection forces primarily depends on the activity of Kid to move chromosomes toward the microtubule plus ends. This conclusion is based on the experiments showing that Kid is involved in chromosome alignment (Funabiki and Murray, 2000; Antonio et al., 2000), chromosome oscillations, and chromosome arm orientation (Levesque and Compton, 2001; Wandke et al., 2012). By directly suppressing dynamics of microtubule plus ends, chromokinesin Kif4A independently contributes to polar ejection force modulation (Stumpff et al., 2012; Levesque and Compton, 2001; Wandke et al., 2012) (**Figure 6C**).

Within the spindle, polar ejection forces are proportional to the size of chromosome arms since the larger surface area of chromosome arms is available for interaction with microtubules (Ke et al., 2009). Laser ablation experiments have shown that cutting a larger portion of a chromosome arm allows the kinetochore-containing chromosome fragment to move further away from the equator, evident in the increase of its oscillation amplitude (Ke et al., 2009). This is due to the reduction of polar ejection forces that push chromosomes towards the spindle center. Similarly, stronger polar ejection forces acting on peripheral chromosomes due to their large size in comparison with central chromosomes were proposed to cause the

more extensive oscillations of central versus peripheral chromosomes (Civelekoglu-Scholey et al., 2013).

Furthermore, polar ejection forces were hypothesized to depend on microtubule density, meaning that polar ejection forces should increase towards the spindle pole due to an increase in microtubule density (**Figure 5A**). The precise spatial distribution of polar ejection forces across the spindle was determined experimentally based on the relationship between reduction in chromosome size after laser ablation and increased oscillation amplitude, yielding a force map in which polar ejection forces increase most rapidly near the equator and flatten towards the poles (Ke et al., 2009). These experiments led to a model in which polar ejection forces limit the extent of oscillations by exerting tension on the leading kinetochore during its movement away from the equator, thus inducing microtubule rescue and chromosome reversal (Ke et al., 2009). Accordingly, elevated polar ejection forces achieved by overexpression of Kid stabilized synthetic kinetochore-microtubule attachments, whereby both sister kinetochores are attached to microtubules from the same spindle pole, through higher tension exerted on kinetochores and by preventing chromosomes from moving closer to the poles where error correction takes place (Cane et al., 2013). Altogether, by operating in concert with the mechanisms of length-dependent modulation of microtubule dynamics, polar ejection forces contribute to the positioning of chromosomes at the spindle equator by promoting reversal in their movement as the chromosomes approach the pole.

2.5. Forces originating from mechanical coupling of k-fibers and bridging fibers

Initial electron microscopy studies of the mitotic spindle in PtK1 cells and grasshopper cells proposed that interpolar microtubules contribute to the structural integrity of the spindle and provide mechanical support for the forces exerted on chromosomes (Nicklas et al., 1982; McDonald et al., 1992; Mastronarde et al., 1993). Indeed, recent findings show that sister k-fibers are physically linked with an antiparallel interpolar microtubule bundle, termed the bridging fiber (Tolić, 2018; Kajtez et al., 2016) (**Figure 7A**). These fibers have been observed also in electron microscopy images of human and other mammalian spindles (O'Toole et al., 2020; Nixon et al., 2017; Yu et al., 2019) (**Figure 7B,C**). Electron tomography reconstructions of spindles in human RPE1 cells revealed that the minus ends of bridging microtubules are typically found near the wall of a kinetochore microtubule (O'Toole et al., 2020). In the vicinity of the kinetochore, the bridging fiber consists of 10–15 microtubules and lies next to the k-fiber, which also consists of 10–15 microtubules. As the bridging microtubules pass the

kinetochores, roughly half of them interact with the sister k-fiber while others fan out and comingle with nearby k-fibers. Most bridging microtubules from one side of the spindle also interact with those extending from the other side (O'Toole et al., 2020).

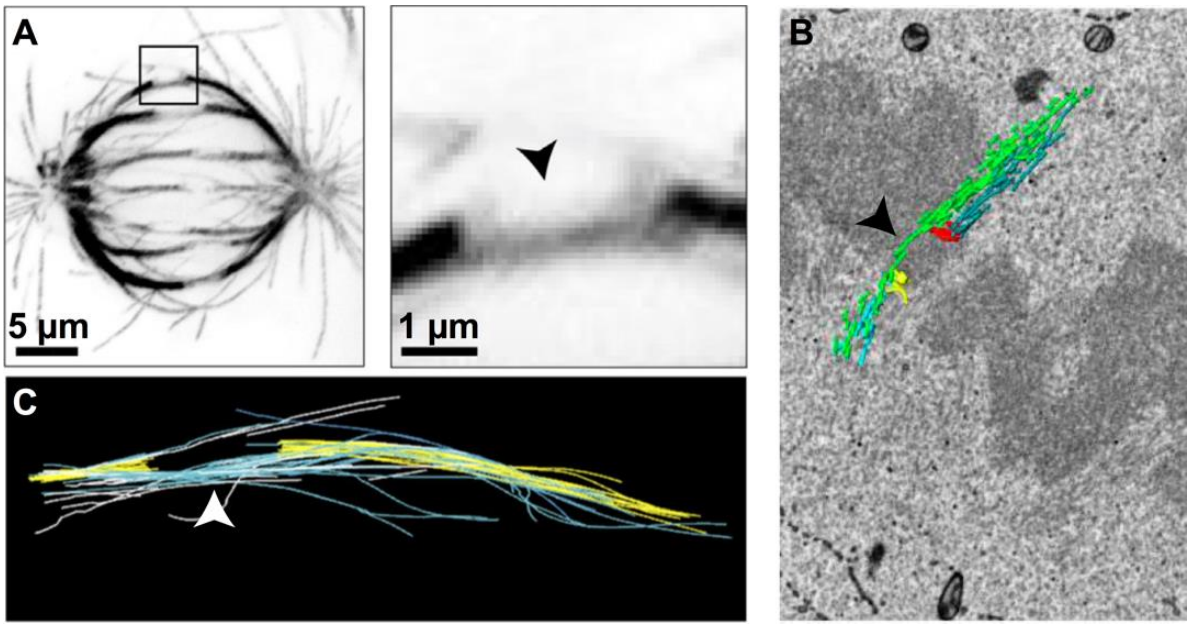


Figure 7. Bridging fibers are laterally associated with k-fibers.
(**A**) Physically expanded RPE1 cell immunostained for anti-α-tubulin. Image from Ponjavić et al., (2021). (**B**) A single serial block face scanning electron microscopy image of a HeLa cell spindle area with a 3D model of microtubules and kinetochores. Sister kinetochores (red and yellow); microtubules (blue and green). Image from Nixon et al., (2017). (**C**) Modeled k-fibers (yellow) and midzone-crossing microtubules (blue) extracted from PtK2 cell image data, retrieved by electron tomography. Image from O'Toole et al., (2020). Arrows show bridging fibers passing the region between sister k-fibers.

Bridging microtubules are mainly centrosome-independent and are nucleated from pre-existing microtubules, through augmin, an eight-subunit protein complex that recruits the γ-tubulin ring complex (Manenica et al., 2020), in agreement with the localization of bridging microtubule minus ends along kinetochore microtubules (O'Toole et al., 2020). Crosslinking of parallel overlap regions between bridging and kinetochore microtubules could be mediated by NuMA (Elting et al., 2017), whereas antiparallel overlaps within bridging fibers are linked together by PRC1. Several motor proteins that slide microtubules or regulate microtubule dynamics are also found within the bridging fiber (**Figure 6D**), including Eg5 (Kajtez et al., 2016; Mann and Wadsworth, 2018), CENP-E (Steblyanko et al., 2020), Kif4A, Kif18A, and

MKLP1/Kif23 (Mitotic Linesin-Like Protein 1/Kinesin Family Member 23; kinesin-6 motor protein family) (Jagrić et al., 2021). Eg5 is likely the main microtubule slider as its inactivation during metaphase results in spindle shortening and collapse in RPE1 cells (Gayek and Ohi, 2014). Note that in U2OS and HeLa cells, depletion of Kif15 is needed together with inhibition of Eg5 to cause spindle collapse. The overlap length of the antiparallel overlaps within the bridging fiber is regulated by Kif4A and Kif18A (Jagrić et al., 2021).

By spanning the gap and acting as a bridge between sister k-fibers, bridging fibers balance the tensile forces at kinetochores (Kajtez et al., 2016) and restrict extensive stretching of the centromere (Suresh et al., 2020). This mechanical support for k-fibers extends up to ~2 μm laterally from each sister kinetochore (Kajtez et al., 2016; Suresh et al., 2020) and is defined as an overlap region selectively marked by the microtubule crosslinker PRC1 (Kajtez et al., 2016; Polak et al., 2017).

As PRC1-labeled bridging fibers show one-to-one association with a pair of sister k-fibers (Polak et al., 2017), this could give rise to flux-dependent equalization of tension at kinetochores (Matos et al., 2009) and a closed-loop force network independent of centrosomes, which is required to move chromosomes, and absence of which would cause the k-fibers to move towards the chromosomes (Pereira and Maiato, 2012). Indeed, it was shown that bridging microtubules slide apart and serve as a platform for force generation that underlies spindle elongation in anaphase (Vukušić et al., 2021). This sliding opens a new perspective on the physical mechanisms that could drive chromosome positioning in metaphase, where forces are generated within the overlaps between bridging and k-fibers. Such forces belong to the class of length-dependent pulling forces, which have a centering effect as described above (**Figure 5B**).

The typical amplitude of chromosome oscillations in human cells is about 1.2 μm (Stumpff et al., 2008), which lies within the PRC1-labeled overlap region. Interestingly, upon acute PRC1 removal by an optogenetic approach, kinetochores are found to extrude out of the narrow region in the central part of the spindle, suggesting that bridging fibers have a role in buffering chromosome movements within this region. As PRC1 removal results in elongated overlaps of antiparallel microtubules and kinetochores moving further away from the spindle midplane in metaphase, these results suggest that chromosome centering is achieved by overlap length-dependent forces transmitted to the associated k-fibers (Jagrić et al., 2021).

2.6. Chromosome segregation errors and aneuploidy

Chromosome segregation errors cause aneuploidy, i.e. occurrence of one or more extra or missing chromosomes, which leads to an unbalanced karyotype. This unbalanced karyotype characterizes a major source of spontaneous abortions, mental retardation, and is strongly associated with cancer (Santaguida and Amon, 2015; Ben-David and Amon, 2020). The mitotic defects that underly unfaithful chromosome segregation can be classified as erroneous kinetochore-microtubule attachments (Gregan et al., 2011), spindle assembly checkpoint deficiencies (Foley and Kapoor, 2013; Sacristan and Kops, 2015), mitotic spindle aberrations (Godinho and Pellman, 2014), cohesion defects (Barber et al., 2008) and chromosome misalignment (Fonseca et al., 2019). However, here I will discuss the occurrence of lagging chromosomes as a direct consequence of improper kinetochore-microtubule attachments and chromosome misalignment defects, and the consequences of chromosome missegregation on genomic stability and cell fitness.

2.6.1. Erroneous kinetochore-microtubule attachments

Chromosome segregation during cell division is carefully choreographed to ensure the equal partition of the duplicated genetic material. Proper chromosome segregation requires that individual chromosomes simultaneously attach to and orient toward the poles of the forming mitotic spindle, i.e. bi-orient, so that sister chromatids move into opposite directions during anaphase (Rieder and Salmon, 1998). Since kinetochores reside on the opposite sides of the chromosome's centromere, this back-to-back geometry favors amphitelic configuration (**Figure 8A**) (Loncarek et al., 2007; Paul et al., 2009). However, sister kinetochores rarely attach to microtubules simultaneously (Roos, 1976) due to the stochastic nature of the search-and-capture mechanism of the spindle formation resulting in kinetochore-microtubule attachment being an error-prone process (Mitchison and Kirschner, 1984; Hayden et al., 1990; Rieder and Alexander, 1990). These random encounters generate erroneous kinetochore attachments which may, if they persist through anaphase, generate aneuploid cells.

During the early stages of cell division, only the kinetochore proximal to and facing a pole may attach to spindle microtubules. As a result of this attachment, chromosome mono-orients, undergoes poleward movements, and shifts towards the connected pole (Rieder and Alexander, 1990). The majority of the mono-oriented chromosomes congress to the spindle equator within minutes after nuclear envelope breakdown and can move toward the spindle

equator alongside neighboring kinetochore fibers of already bioriented chromosomes (Kapoor et al., 2006). However, mono-oriented chromosomes are seen remaining in the proximity of the pole for variable times (Roos, 1976; Rieder et al., 1994, 1995). This temporal variability could depend on establishing biorientation, meaning that the unattached sister kinetochore must attach to microtubules from the distal pole, or resolving erroneous attachments made during initial encounters.

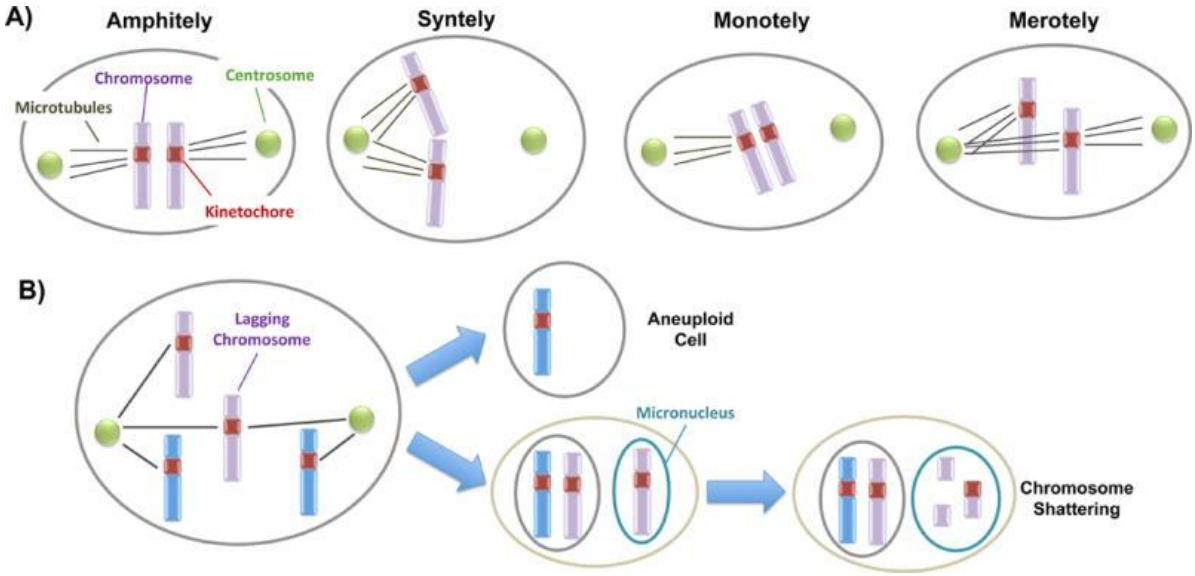


Figure 8. Kinetochore-microtubule configurations and effects of chromosome segregation errors. (**A**) Proper, i.e., amphitelic, and improper, i.e., syntelic, monotelic, and merotelic kinetochore-microtubule attachments (from left to right). (**B**) A lagging chromosome may lead to the formation of micronuclei and/or aneuploid daughter cells. The chromosome that ends up in micronuclei is prone to chromosome shattering. Illustration from Rosenkrantz and Carbone, (2017).

Mono-oriented chromosomes are referred to as monotelic or syntelic (**Figure 8A**). In monotelic configuration, as only one sister kinetochore is attached to spindle microtubules, the unattached kinetochore is positioned on the opposite side of the centromere and its unoccupied microtubule-attachment sites accumulate spindle assembly checkpoint proteins that keep the spindle assembly checkpoint active so that anaphase onset is prevented (Rieder et al., 1995). This happens even if only one unattached kinetochore is present (Rieder et al., 1994, 1995). It is thought that monotelic configuration is an intermediate state that precedes proper amphitelic configuration (Gregan et al., 2011). In contrast, syntelic configuration arises when both sister

kinetochores attach to microtubules emanating from the same spindle pole and consequently sister kinetochores shift toward one side of the centromere, proximal to the connected pole (Ault and Nicklas, 1989; Cimini and Degrassi, 2005). It was debated whether syntelic configurations are sensed by the spindle assembly checkpoint as they experience lower tension (Zhou et al., 2002; Rieder and Maiato, 2004), however, syntelic attachments did not prevent mitotic exit (Loncarek et al., 2007) as the spindle assembly checkpoint in mammals is satisfied in the absence of tension, as long as all kinetochores are attached to microtubules (Rieder et al., 1995; Waters et al., 1998). Syntelic attachments are usually modified into amphitelic attachments through shrinking and severing of the syntelic fibers and later proper attachment of other microtubules at the kinetochores (Lampson et al., 2004). If the above-mentioned mono-oriented chromosomes persist at the anaphase onset, both sister kinetochores, which are in syntelic configuration, are actively pulled towards the same pole (Cimini, 2003). Similarly, the unattached kinetochore of a monotelic chromosome remains in a position that is in the proximity of the pole and is therefore included in the daughter nucleus, together with its sister that is actively pulled, or undergoes attachment to microtubules emanating from the same pole and establishes syntelic configuration (Cimini, 2003).

Erroneous bi-oriented chromosomes have merotelic configuration and occur when a single kinetochore becomes attached to microtubules emanating from both spindle poles (**Figure 8A**). This configuration is frequent in the early stages of cell division due to mammalian kinetochores naturally having 15-30 microtubule attachment sites (Cimini, 2003; Cimini et al., 2004). Like amphitelic attachments, merotelic attachments generate tension across sister kinetochores and do not trigger mitotic arrest as both kinetochores are attached to microtubules (Cimini et al., 2001, 2004; Khodjakov et al., 1997). Even though mechanisms that correct merotelic kinetochore attachments operate during cell division, depending on the ratio of microtubules from each spindle pole, merotely may induce anaphase lagging chromosomes, i.e. chromosomes that remain at the spindle equator with the kinetochore stretched laterally by microtubule connections to opposite spindle pole (**Figure 8B**) (Cimini et al., 2001). During cytokinesis, the lagging chromosome is included in one of the two daughter cells, depending on the cleavage furrow positioning (Cimini et al., 2004). Lagging chromosomes may become micronuclei if chromosomes are not incorporated into one of the daughter nuclei during telophase (**Figure 8B**) (Cimini et al., 2002).

Frequency-wise, lagging chromosomes have been observed in 1-5% of anaphases in untreated human and other mammalian tissue cells in culture: 2.43% (Ford et al., 1988) and 5.13% (Catalán et al., 2000) in human lymphocytes, and 1.16% (Cimini et al., 2001) and 1.1%

(Cimini, 2003) in PtK1 cells. Lagging chromosomes are individual sister chromatids (Cimini et al., 2001) and the frequency of single chromatid loss, i.e. chromatid left behind at the cell equator, is approximately 7 times higher than the loss of paired sister chromatids (Cimini et al., 2002). Taken together, these results are in favour of merotelic attachments being a major mechanism for aneuploidy (Cimini et al., 2001).

For comparison, cancer cell lines, both live and fixed, showed that the occurrence of lagging chromosomes in anaphase can exceed 50% which reflects an elevated frequency of erroneous attachments in cancer cells: 19.0% (Thompson and Compton, 2008) in HT29, 66% (Thompson and Compton, 2008) in Caco2, 50% (Thompson and Compton, 2008) in MCF-7, 13% (Janssen et al., 2009) and 21.7% (Thompson and Compton, 2011) in U2OS, and 25% (Janssen et al., 2009) in HeLa cells. Moreover, live imaging of human U2OS osteosarcoma cells showed that 78% of anaphase cells with lagging chromosomes resulted in at least one daughter cell with a micronucleus, indicating a strong correlation between lagging chromosomes and micronuclei (Thompson and Compton, 2011). However, it was shown that the micronucleus with the marked chromosome was nearly 10 times more likely to reside in the correct daughter cell in an untransformed cell line, which would not alter its karyotype (Cimini et al., 2004; Janicke et al., 2007; Torosantucci et al., 2009; Thompson and Compton, 2011). Thus, when normal segregations into micronuclei are excluded, chromosome missegregation is a rare event occurring in 0.3% of the untreated cells (Thompson and Compton, 2011). This indicates that under normal conditions sister chromatids also missegregate to the same daughter cell without lagging (Thompson and Compton, 2011).

Due to the rare, yet significant occurrence of erroneous attachments that persist through anaphase, it is difficult to study chromosome missegregation rates without introducing large perturbations. These perturbations often include microtubule drugs to elevate rates of erroneous attachments or inactivation of the checkpoint proteins by antibody microinjection. Studies frequently use immunofluorescence microscopy, fixed samples, and fluorescent *in situ* hybridisation techniques, making temporal resolution of erroneous kinetochore-microtubule attachments limited and subject to significant artefacts. Since quantitative information on the mechanism, origin, and propagation of errors is generally lacking, new approaches are needed.

2.6.2. Link between chromosome segregation errors and genomic instability

Chromosome segregation errors that arise during mitosis are thought to cause numerical aneuploidies, which are defined as gains or losses of whole chromosomes. However, chromosome segregation errors are linked to the generation of DNA damage that promotes structural alterations in chromosomes (Levine and Holland, 2018). Here, lagging chromosomes, i.e. chromosomes that lag behind separating chromosome masses in anaphase, besides having a high risk of missegregation, are susceptible to DNA damage acquisition (Levine and Holland, 2018). This can occur by lagging chromosomes becoming trapped in the cleavage furrow during cytokinesis and thus being broken by sheer physical forces (Janssen et al., 2011). Besides being raptured by physical forces, a lagging chromosome may end up in the micronucleus, a small compartment that forms whenever a chromosome or a fragment of a chromosome is not incorporated into one of the main nuclei (**Figure 8B**) (Thompson and Compton, 2011). Micronuclei with missegregated chromatids may produce unbalanced karyotypes in the following cell division (Rizzoni et al., 1989). Studies have shown that micronuclei can be incorporated back into the main nucleus of the daughter cell (Crasta et al., 2012; Soto et al., 2018), which can be critical for triggering genomic instability (Terradas et al., 2016). The reason behind this is that micronuclei are prone to acquire DNA damage and undergo chromosomal rearrangements including chromothripsis, i.e., a chromosome shattering and rejoining phenomenon (Liu et al., 2018; Zhang et al., 2015; Cortés-Ciriano et al., 2020). Besides improperly attached chromosomes ending up in micronuclei, a recent study has shown that loss of chromosome alignment leads to inter-chromosomal compaction defects during anaphase and the formation of micronuclei (Fonseca et al., 2019). In line with this, late-aligning chromosomes were found to exhibit a higher incidence of lagging in anaphase (Kuniyasu et al., 2018). Given that synchronous movement of anaphase chromosomes promotes proper organization of chromosomes into a single nucleus, it is not surprising that correction of erroneous kinetochore-microtubule attachments and chromosome alignment, which is the main focus of this thesis, are involved in ensuring genomic stability.

2.6.3. Consequences of aneuploidy on cell proliferation

An unbalanced organism's karyotype, i.e., the presence of an abnormal number of chromosomes in a cell, affects gene expression at both the transcriptome and proteome levels. Three types of effects observed for gene expression levels in aneuploid cells have been proposed, namely direct dosage effect, secondary effect, and dosage compensation (Birchler and Veitia, 2012). First, expression profiling in yeast showed elevated expression levels for

genes on certain chromosomes to be associated with the increased number of those chromosomes (Hughes et al., 2000). Apart from yeasts (Torres et al., 2007; Rancati et al., 2008; Pavelka et al., 2010), dosage effect on the expression of genes present on aneuploid chromosomes was observed in higher eukaryotes (Williams et al., 2008; Stingele et al., 2012; Hou et al., 2018; Hwang et al., 2021). Furthermore, secondary effects in gene expression arise when expression levels of some genes are affected by gains of chromosomes that do not carry those genes (Rancati et al., 2008; Stingele et al., 2012), e.g. direct gene dosage effects on transcription factors have a secondary effect on their downstream targets. However, the increase in protein abundance does not seem to be universal as subunits of protein complexes and protein kinases are mostly reduced toward diploid levels in cells with aneuploid chromosomes (Stingele et al., 2012; Dephoure et al., 2014). Here, it was proposed that aneuploid cell compensates for changes in chromosome copy number via proteolytic pathways, i.e. by degrading the excess of some proteins (Pfau and Amon, 2012).

Since unbalanced karyotype was shown to affect cellular transcriptome and proteome, it is not surprising that aneuploidy has adverse effects on cell proliferation. In humans, aneuploidy is the leading cause of miscarriage, congenital birth defects, and mental retardation (Hassold and Hunt, 2001). The reason behind this is the lethality of autosomal monosomies and all but three trisomies, specifically, trisomy of chromosomes 13, 18, and 21, which are chromosomes with the lowest gene densities (Hassold and Hunt, 2001; Holland and Cleveland, 2012). Unlike autosomes, aneuploidies of human sex chromosomes are better tolerated. This could be due to low gene density on the Y chromosome and X chromosome inactivation, which equalizes the dosage of gene products regardless of copy number variation (Holland and Cleveland, 2012). Furthermore, experiments on aneuploid yeasts (Torres et al., 2007; Pavelka et al., 2010) and mice (Williams et al., 2008) showed that chromosome gains reduce cell proliferation and alter metabolism, suggesting that the aneuploid state of a cell per se impairs rather than accelerates tumorigenesis (Williams et al., 2008). However, aneuploidy is well-tolerated in cancer cells and ~90% of solid tumors are aneuploid (Ben-David and Amon, 2020). Here, heterogeneity in tumor karyotypes that arises due to chromosome missegregation events is attributed to increased drug resistance in cancers (Ippolito et al., 2021; Lukow et al., 2021).

2.8.4. Chromosome misalignment in cancer

Chromosome alignment defects are observed in human cancer cells and are considered to be one of the numerous origins that could cause chromosomal instability (Thompson et al., 2010; Gordon et al., 2012). Even though aneuploidy due to continuous missegregation events of unaligned chromosomes was shown to promote spontaneous tumorigenesis in mice models (Weaver et al., 2003), the relevance of such observations for tumor development in humans is unclear. However, new studies are shedding light on the effect of continual chromosome misalignment, together with lagging chromosomes and micronuclei formation, on tumor progression through strong selective pressures (Rowald et al., 2016), where the broad distribution of karyotypes would promote gross adaptive leaps (Chen et al., 2012, 2015; Endesfelder et al., 2014).

More than 100 proteins have been implicated in chromosome alignment (Maiato et al., 2017) and the perturbation of the expression levels of these molecules could be directly involved in pathological conditions. Indeed, high-grade serous ovarian carcinoma cells and colorectal cancer cells exhibit pronounced chromosome alignment defects (Ertych et al., 2014; Tamura et al., 2020). In both of these cancer cells, chromosome misalignment phenotype is induced by overexpression of Aurora A, a major mitotic kinase that leads to elevated microtubule dynamics. Furthermore, by inspecting data retrieved from pan-cancer analysis of 2922 cancer genomes, genes that encode proteins involved in chromosome alignment were deleted, amplified, or mutated in the majority of the cancer types (ICGC/TCGA Pan-Cancer Analysis of Whole Genomes Consortium, 2020). Specifically, these genes were altered in ~40-50% of samples of ovarian cancer, melanoma, breast cancer, and esophagogastric cancer (**Figure 9**). Among proteins involved in chromosome alignment, CENP-E (Liu et al., 2009; Kung et al., 2014; Shan et al., 2019), Kif18A (Zhang et al., 2010; Nagahara et al., 2011; Zhong et al., 2019), and Kif4A (Mazumdar et al., 2006; Hou et al., 2017; Gao et al., 2018) are the most studied motor proteins concerning their downregulation or upregulation in cancer.

Chromosome alignment at the metaphase plate is the most eye-catching image of mitosis, with biological relevance for proper chromosome segregation and nuclear reformation. Yet, the mechanisms driving alignment are still under debate due to a large number of players and processes involved.

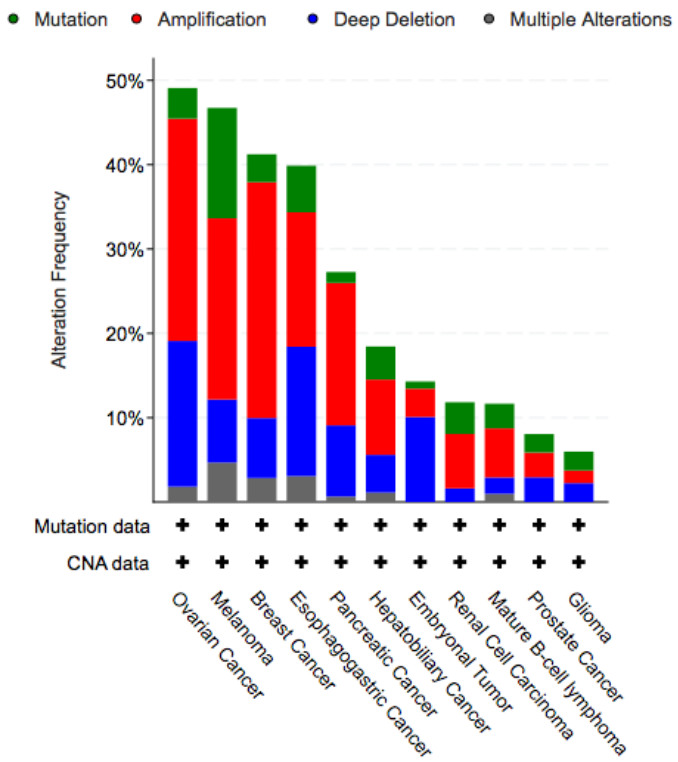


Figure 9. Alteration of chromosome alignment-related genes in different cancers. Pan-cancer analysis study (ICGC/TCGA Pan-Cancer Analysis of Whole Genomes Consortium, 2020) queried by genes involved in chromosome alignment. Genes used are: KIF22, KIF4A, KIF18A, CENPE, KIF2C, KIF2A, KIF11, PRC1, NUMA1, HAUS8 (Maiato et al., 2017; Jagrić et al., 2021). A minimum of 100 total samples per cancer type was used. Data was retrieved from cbioportal.org (Cerami et al., 2012; Gao et al., 2013).

3. MATERIALS AND METHODS

3.1. Cell culture

hTERT-RPE-1 (RPE1) cell line with a stable expression of CENP-A-GFP and centrin1-GFP (Magidson et al., 2011) was a gift from Alexey Khodjakov (Wadsworth Center, New York State Department of Health, Albany, NY, USA). U2OS cell lines stably expressing CENP-A-GFP and photoactivatable PA-GFP-α-tubulin, CENP-A-GFP, and mCherry-α-tubulin (Barisic et al., 2015) were a gift from Marin Barisic (Danish Cancer Society Research Center, Copenhagen, Denmark) and Helder Maiato (Institute for Molecular Cell Biology, University of Porto, Portugal). HeLa cell line with a stable expression of EGFP-CENP-A (Jaqaman et al., 2010) was a gift from Andrew McAinsh (University of Warwick, Coventry, UK). Cells were

maintained in Dulbecco's Modified Eagle's Medium (containing 1 g/L d-glucose, l-glutamine, pyruvate; Lonza) supplemented with 10% Fetal Bovine Serum (Sigma-Aldrich), 100 IU/mL penicillin (Lonza) and 100 mg/mL streptomycin (Lonza). Cells were grown at 37ºC in a Galaxy 170s humidified incubator (Eppendorf) with a 5% CO_2 atmosphere.

3.2. RNA interference and transfection

One day before siRNA transfection, 120 000 RPE1 cells were seeded on 35 mm glass coverslip dishes with 0.17 mm glass thickness (MatTek Corporation). siRNA constructs were diluted in Opti-MEM medium (Life Technologies) and transfection was performed with Lipofectamine RNAiMAX Reagent (Life Technologies) by following the manufacturer's protocol. Constructs and their final concentrations used were: 100 nM Kif18A siRNA (4390825; Ambion), 100 nM Kif4A siRNA (sc-60888; Santa Cruz Biotechnology), 100 nM Kid/Kif22 siRNA (4392420; Ambion), 100 nM CENP-E siRNA (L-003252-000010; Dharmacon), 100 nM MKLP1 siRNA (sc-35936; Santa Cruz Biotechnology), 300 nM PRC1 siRNA (L-019491-00-0010; Dharmacon), 20 nM Haus8 siRNA (L-031247-01-0005; Dharmacon), 100 nM NuMA siRNA (sc-43978; Santa Cruz Biotechnology), and 100 nM Ndc80 siRNA (HA12977117-004; Merck). After 4 h of incubation with the transfection mixture, the medium was replaced with a regular cell culture medium. All experiments on siRNA-treated cells were performed 24 h after transfection, except for Haus8 siRNA-depleted cells, where silencing was done for 48 h. For the experiment with spindles devoid of chromosomes, Ndc80 depleted cells were treated with 3 μM ZM447439 (S1103; Selleckchem) and MG-132 inhibitor (474790; Sigma-Aldrich) 30 min before imaging. All treatments include at least three independent experiments.

3.3. Speckle microscopy

RPE1 cells grown in glass coverslip dishes were stained with 1 nM SiR-tubulin dye (Spirochrome AG). After 15 min of staining, confocal live imaging was performed on a Dragonfly spinning disk confocal microscope system (Andor Technology) using 63x/1.47 HC PL APO glycerol objective (Leica) and Zyla 4.2P scientific complementary metal oxide semiconductor camera (Andor Technology; pixel = 100 nm), and Expert Line easy3D STED microscope system (Abberior Instruments) using 60x/1.2 UPLSAPO 60XW water objective (Olympus) and an avalanche photodiode detector (pixel = 75 nm). Images were acquired using

Fusion software and Imspector software. During imaging, cells were maintained at 37ºC and 5% CO_2 within a heating chamber (Okolab). For live imaging of RPE1 cells expressing CENP-A-GFP and centrin1-GFP, and stained with SiR-tubulin, 488 nm and 640 nm laser lines for the Dragonfly microscope system, and 485 nm and 640 nm for the Expert Line microscope system were used to excitate GFP, and SiR, respectively. In order to visualize SiR-tubulin speckles, images were acquired with 80% laser power and exposure of 1 s. Image acquisition was done on one focal plane every 5 or 10 s. Note that the time frame within which SiR-tubulin, at 1 nM concentration, can be visualized in patches on the mitotic spindle is between 15 and 75 min after SiR-tubulin staining. Cells were imaged for up to 100 s to limit phototoxicity and ensure cell viability.

3.4. Cell-micropatterning

Cell micropatterning was implemented by following a previous protocol (Azioune et al., 2010). 25 mm-round and 0.17 mm-thick glass coverslips were cleaned with absolute acetone and isopropanol. Dry coverslips were exposed to 185 nm high-power UV light in UV Ozone Cleaner (Ossila) for 5 min to oxidize their surface. Activated coverslips were incubated with 100 µL of 0.1 mg/mL poly(l-lysine)-g-poly(ethylene glycol) (PLL-PEG; SuSoS) in 10 mM HEPES (Roth), pH=7.4, for 30 min. Coverslips were washed with 1 mL of 10 mM HEPES and air-dried before putting them on the chrome-printed side of a micropatterning photomask (4DCell). Adhesion was achieved with 5 µL of deionized water. Photomask with coated coverslips was exposed to 185 nm high-power UV light in UV Ozone Cleaner for 15 min to burn PLL-PEG through non-chromed micropatterns on the photomask. Coverslips were detached with deionized water and incubated with 100 µL of 10 µg/mL of fibronectin (#F1141, Sigma-Aldrich) in 100 mM NaHCO3 (Merck), pH=8.4, for 30 min. Finally, coverslips were washed with 1 mL of 100 mM NaHCO3 and used right after or stored in the fridge at 4ºC for future use. Each micropatterned coverslip was placed in a 35 mm glass coverslip dish (MatTek Corporation), and 75 000 U2OS cells expressing CENP-A-GFP were seeded. After visible cell attachment, fresh media was added to the cells before further incubation at 37ºC in a humidified CO_2 incubator.

3.5. Immunostaining

Cells seeded in dishes were fixed in ice-cold methanol for 1 min, except for astrin immunostaining experiment where cells were fixed in 37ºC warm 4% paraformaldehyde for 10 min, and permeabilized for 15 min in 0.5% Triton X-100 in phosphate-buffered saline (PBS). Following permeabilization, cells were blocked with 1% normal goat serum (NGS) in PBS for 1 h and incubated with primary antibodies at 4ºC overnight. Primary antibodies were prepared in 1% NGS in PBS to 1:100 dilution. Following incubation with primary antibodies, cells were incubated with fluorochrome-conjugated secondary antibodies at room temperature for 1 h. Secondary antibodies were prepared in 2% NGS in PBS to 1:250 dilution. To visualize DNA, cells were stained with DAPI (1 mg/ml in PBS) for 10 min. After each step, cells were washed three times in PBS for 5 min. Primary antibodies used were: rabbit anti-Kif18A (A301-080A; Bethyl Laboratories), mouse anti-Kif4A (sc-365144; Santa Cruz Biotechnology), mouse anti-Kid (sc-390640; Santa Cruz Biotechnology), rabbit anti-CENP-E (C7488; Sigma-Aldrich), rabbit anti-MKLP1 (ab174304; Abcam), mouse anti-PRC1 (sc-376983; Santa Cruz Biotechnology), rabbit anti-Haus8 (PA5-21331; Invitrogen), mouse anti-NuMA (sc-365532; Santa Cruz Biotechnology), and mouse anti-astrin (MABN2487; Sigma-Aldrich). Secondary antibodies used were: donkey anti-mouse IgG-Alexa 594 (Abcam), donkey anti-rabbit IgG-Alexa 594 (Abcam), and donkey anti-rabbit IgG-Alexa 647 (Abcam).

For cells seeded on micropatterned coverslips, media was removed 24 h after seeding. After 10-min fixation in paraformaldehyde-glutaraldehyde solution (4% and 0.25%, respectively) heated to 37°C, micropatterns were washed and 15-min incubation at room temperature with 0.5% Triton in PBS was used to permeabilize cell membranes. To block the unspecific binding of antibodies, micropatterns were incubated in 1% NGS in PBS for 1 h, at 4°C. Incubation with rat anti-α-tubulin primary antibody solution (1:300 in 1% NGS in PBS; MA1-80017; Invitrogen) was performed for 1 h, at 4°C. After washing off the primary antibody solution, cells were incubated with donkey anti-rat IgG-Alexa 594 secondary antibody solution (1:1000 in 2% NGS in PBS; Abcam) for 1 h at room temperature. After washing off the secondary antibody, DNA and actin were stained by incubation with DAPI (1 mg/ml in PBS) and SiR-actin (100 nM, Spirochrome AG), respectively. After each incubation step, three 5 min washing steps were carried out in PBS. Finally, micropatterned coverslips were mounted with Abberior Mount Liquid (Abberior) on a glass microscope slide and sealed with clear nail polish.

Immunostained cells were imaged using Bruker Opterra Multipoint Scanning Confocal Microscope (Bruker Nano Surfaces) with a Nikon CFI Plan Apo VC 100x/1.4 numerical aperture oil objective (Nikon). 405/488/561/640 nm laser lights were used with the following emission filters: BL HC 525/30, BL HC 600/37, and BL HC 673/11 (Semrock). Images were

captured with an Evolve 512 Delta Electron Multiplying Charge Coupled Device Camera (Photometrics; pixel = 83 nm) using a 200 ms exposure time for all experiments, except for cell-micropatterning experiments where a 250 ms exposure time was used. Furthermore, images were acquired at 5 focal planes, except for cell-micropatterning experiments where the whole spindle stack was imaged, with 0.5 μm z-spacing.

3.5. Photoactivation assay

For photoactivation experiments, helios one-line 405 nm solid-state laser (Obis lasers, Coherent), mounted on Bruker Opterra Multipoint Scanning Confocal Microscope (Buđa et al., 2017), was used to photoactivate microtubules in U2OS cells with stable co-expression of photoactivatable-GFP-α-tubulin, CENP-A-GFP, and mCherry-α-tubulin. Experiments were performed in *Live/Ablation* mode with 80% laser power by using Prairie View software (Prairie Technologies). In order to visualize GFP and mCherry, 488 nm and 561 nm laser lights were used, respectively, together with a 250 ms exposure time. K-fibers belonging to the same sister kinetochore pairs were sequentially photoactivated when sister kinetochore pairs were displaced from the spindle equator, giving rise to shorter and longer sister k-fibers. Images were acquired at one focal plane with a time interval of 2 s.

3.6. Long-term imaging for chromosome segregation error assessment

To assess the occurrence of chromosome segregation errors, RPE1 cells expressing CENP-A-GFP and centrin1-GFP, U2OS cells expressing photoactivatable PA-GFP-α-tubulin, CENP-A-GFP and mCherry-α-tubulin, and HeLa cells expressing EGFP-CENP-A were imaged by using Bruker Opterra Multipoint Scanning Confocal Microscope, as described above. Image acquisition was performed at 1 min intervals. Z-stacks of 15 slices were acquired at a 1 μm spacing. For U2OS cells, 488 and 561 nm laser lines were used, to image GFP and mCherry, respectively. For RPE1 and HeLa cells, a 561 nm laser line was used to image GFP. *XY Stage* mode was used to film multiple cells at different xyz positions, which underwent mitosis simultaneously. Image acquisition was started at prometaphase and ended after cells entered telophase.

3.7. Image analysis

Measurements were performed in Fiji/ImageJ (National Institutes of Health). Quantification and data analysis were performed in R (R Foundation for Statistical Computing) and MATLAB (MathWorks). Figures and schemes were assembled in Adobe Illustrator CC (Adobe Systems). Statistical analysis was performed using Student's t-test, Mann-Whitney test, and two-proportions z-test.

Upon inspection of tubulin speckle movement within the spindle, speckles that could be followed for at least 30 s were taken into account. For every tubulin speckle position, corresponding CENP-A and centrin1 positions, representing the location of sister kinetochores and spindle poles, respectively, were also tracked. Tracking was done by using the *Multi-point tool*. Speckles that started at a proximal kinetochore and were associated with their proximal pole were categorized as a part of k-fiber, whilst speckles that started between sister kinetochores or proximal to the distal pole and passed through sister kinetochores were categorized as a part of bridging fiber. Note that all kinetochore pairs within each spindle were exhaustively inspected for the occurrence of k-fiber or bridging fiber speckles, thus the ratio of k-fiber speckles and bridging fiber speckles provides information on the relationship of the number of microtubules in these categories. Speckles that could not be unambiguously categorized as a part of k-fiber or bridging fiber were termed “other” and were the most numerous category. These speckles may or may not belong to microtubules that are part of k-fibers or bridging fibers, thus their fraction with respect to k-fiber and bridging fiber speckles in each spindle cannot be used to assess the relative number of different microtubule subgroups in a straightforward manner. Speckle-pole velocity was calculated by fitting linear regression on distances between the tubulin speckle and the associated spindle pole during the first 30 s of its trajectory.

Poleward flux in photoactivation experiments was analyzed by using a 5 pixel-thick segmented line to retrieve pole-to-pole GFP and mCherry intensity profiles during 30 s of photoactivated spot movement. Distance between GFP peaks, which correspond to photoactivated tubulin spots, and mCherry peaks, which correspond to spindle poles, was measured over time. By fitting linear regression on distances over 30 s, poleward velocities of photoactivated spots were calculated.

For kinetochore alignment measurements, the *Multi-point tool* was used to track the positions of sister kinetochore pairs. The equatorial plane was defined with two points placed between the outermost pairs of kinetochores on the opposite sides of the spindle. Kinetochore alignment was calculated as the distance between the midpoint of kinetochore pairs and the equatorial plane.

In cells immunostained for PRC1, a 5 pixel-thick segmented line was used to track the pole-to-pole contour of individual PRC1-labeled overlap regions. The pole-to-pole tracking was performed on single z-planes and the mean value of the cytoplasm was subtracted from the retrieved intensity profiles. The overlap length of individual PRC1-labeled overlap regions was determined as the width of the peak of the signal intensity in the central part of the contour in SciDavis (Free Software Foundation Inc.). The width of the peak was measured at the base of the PRC1 intensity peak where the PRC1 signal is roughly equal to the mean value of the PRC1 signal along the contour on either side of the peak. Similarly, by using the *Line tool* a 100 pixel-thick line was used to retrieve the pole-to-pole profiles of PRC1 intensity within whole spindles. This was done on a sum intensity projection of five z-planes. The overlap length of PRC1-labeled overlap regions within whole spindles was determined as the width of the peak at the half-height of each peak.

To determine the percentage of protein depletion, mean spindle intensity was measured by encompassing the area of the spindle with the *Polygon selection tool*. Mean background intensity in the cytoplasm, measured using a 1x1 μm rectangle, was subtracted from the mean spindle intensity.

For cell-micropatterning experiments, anaphase cells were inspected if the distance between the sister kinetochore groups allowed the assessment of the occurrence of chromosome segregation errors. Here, only cells with horizontal spindles and spindle poles roughly in the same plane were considered. Chromosome segregation error assessment was performed on a maximum-intensity projection of imaging planes in which the mitotic spindle was located.

4. RESULTS

4.1. Speckle microscopy assay to follow the movement of individual microtubules within the spindle

To test whether mechanical coupling between kinetochore and bridging microtubules drives microtubule poleward flux, it is important to measure the poleward flux of different classes of microtubules (kinetochore and bridging), which requires analysis of the movements of individual microtubules. Flux is typically studied by using tubulin photoactivation (Mitchison, 1989), a method in which all the microtubules within the illuminated region are photoactivated, thus the movements of kinetochore and non-kinetochore microtubules cannot be distinguished.

To overcome this issue, I developed an assay based on speckle microscopy (Waterman-Storer et al., 1998) to study microtubules within spindles of the human non-cancer immortalized epithelial cell line hTERT-RPE1 (from here on referred to as RPE1). I used RPE1 cells with a stable expression of CENP-A-GFP (a histone H3 variant found at the centromere) to determine kinetochore positions and centrin1-GFP (a centrosome protein) to determine spindle pole positions. By using a very low concentration (1 nM) of SiR-tubulin (Lukinavičius et al., 2014), I obtained a speckled signal of SiR-tubulin in the spindle (**Figure 10A**), which comes from a few dye molecules within a resolution-limited region (Waterman-Storer and Salmon, 1998).

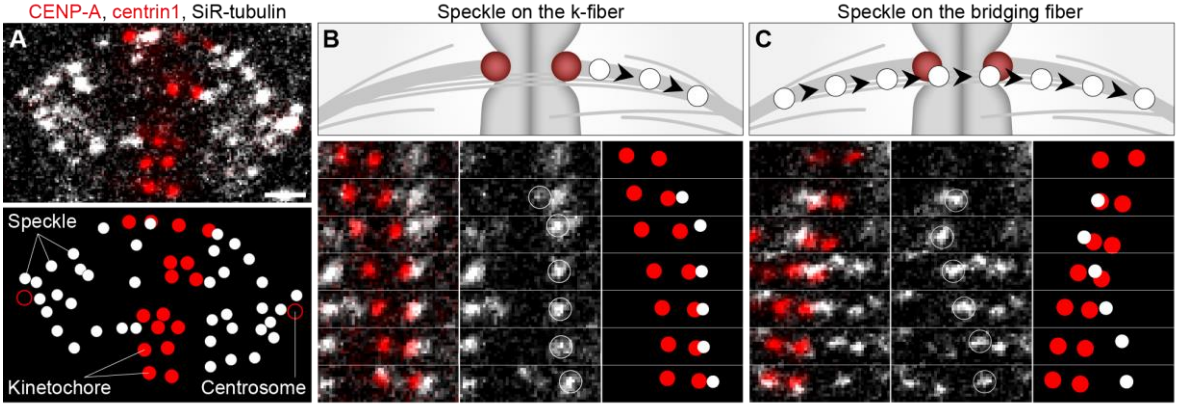


Figure 10. Speckle microscopy assay for measurement of the poleward flux of individual k-fiber and bridging fiber microtubules. (**A**) Spindle in an RPE1 cell stably expressing CENP-A-GFP (red) and centrin1-GFP (red) stained with 1 nM SiR-tubulin dye which appears as distinct speckles marking individual microtubules (grey). (**B**) Scheme of a speckle originating at the kinetochore defined as the one marking a k-fiber microtubule (top). Montage over time demonstrating the movement of the speckle belonging to the k-fiber microtubule (bottom). Left shows merge, middle shows SiR-tubulin channel with encircled speckle, right shows schematic of kinetochores (red) and speckle (white) positions. (**C**) Scheme of a speckle passing the region between sister kinetochores, moving close to the kinetochores, defined as the one marking a microtubule within the bridging fiber (top). Montage over time demonstrating the movement of the speckle belonging to the bridging fiber microtubule (bottom). Legend as in **B**. The time interval between images in **B** and **C** is 10 s. Scale bar: 2 μm.

To identify the speckles that are localized on kinetochore or bridging microtubules, I followed the position of their first appearance and their subsequent movement. The speckles that originate close to a kinetochore, at the pole-facing side, were defined as those on a

kinetochore microtubule (**Figure 10B**). The speckles that appear on one side of a pair of sister kinetochores, pass the region between them, and end up on the other side, were defined as those on a bridging microtubule (**Figure 10C**). All other speckles in the spindle region between the centrosomes, for which I could not determine the type of microtubule they belong to, I refer to as "other" speckles (**Figure 11A,B**). I tracked individual speckles (**Figure 11C**) together with the spindle poles marked by centrioles and calculated poleward flux as the change of the speckle-to-pole distance over the first 30 seconds of their movement (**Table 1**). This assay allowed me to study the movement of kinetochore and bridging microtubules with respect to the poles and to each other.

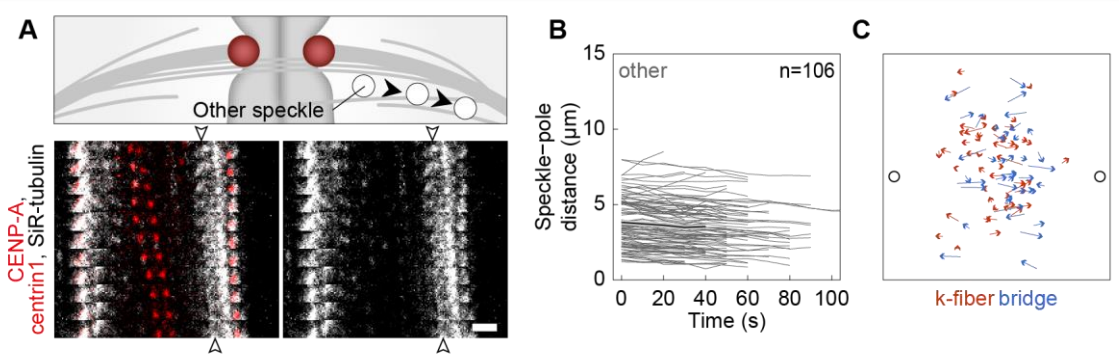


Figure 11. Speckle microscopy assay for measurement of the poleward flux of individual microtubules that cannot be determined, and individual trajectories of speckles found on k-fiber and bridging fiber. (**A**) Scheme of "other" speckles for which it could not be determined the type of microtubule they belong to (top). Montage over time from an RPE1 cell stably expressing CENP-A-GFP (red) and centrin1-GFP (red) stained with 1 nM SiR-tubulin dye (grey) demonstrating the movement of "other" speckles (bottom). Merge (left); tubulin channel only (right). Arrowheads mark starting and ending positions of the tracked speckle. The time interval between images is 10 s. Scale bar: 2 µm. (**B**) Distance of "other" speckles from the pole over time in untreated cells. Grey lines show individual speckles. Black line; mean. Grey area; SEM (standard error of the mean). (**C**) Examples of trajectories of speckles belonging to k-fibers (red) and bridging fibers (blue) within 30 s of their movement. Arrows are pointing towards the corresponding direction. Black circles; spindle poles.

To explore the relevance of microtubule poleward flux to chromosome alignment, I used this assay in unperturbed cells and after a set of perturbations in which I depleted candidate microtubule-associated proteins by corresponding siRNA. I depleted motor proteins that are known to be involved in kinetochore alignment and/or localize to the bridging fiber: Kif18A,

Kif4A, Kid, CENP-E, and MKLP1, and non-motor proteins that are important for k-fiber and bridging fiber integrity and their crosslinking: PRC1, Haus8, and NuMA (Maiato et al., 2017; Tolić and Pavin, 2021). For all these treatments, I analyzed the poleward flux of bridging and k-fibers, kinetochore positions as a read-out of chromosome alignment, and the length of antiparallel overlaps (**Table 1**). Although these treatments most likely also affect other aspects of the spindle architecture and dynamics, I expect to identify general interdependence between flux dynamics and kinetochore centering.

4.2. Longer kinetochore fiber undergoes flux at a higher velocity than the shorter one

To explore the microtubule poleward flux of k-fibers within the spindles, I compared the flux of k-fibers of different lengths by using the speckle microscopy assay developed in this thesis. The speckles on k-fibers, defined as those originating close to a kinetochore, were located at various distances from the pole, which correspond to the k-fiber length.

Strikingly, the k-fiber poleward velocity increased with an increasing k-fiber length in untreated cells ($p = 4e-04$, $n = 164$, **Figure 12A-C**). The same trend was observed when the k-fibers were divided into 3 groups: short, medium, and long, as those with a length smaller than 0.4, between 0.4 and 0.6, and larger than 0.6 of the spindle length, respectively. Short k-fibers had a flux of 0.91 ± 0.08 μm/min ($n = 51$ speckles from 68 cells), whereas the flux of long k-fibers was significantly faster, 1.81 ± 0.34 μm/min ($n = 11$ speckles from 68 cells, $p = 3e-04$), and the flux of medium k-fibers was between these values. The average poleward flux velocity of all speckles on k-fibers was 1.23 ± 0.06 μm/min ($n = 164$ speckles from 68 cells), which is similar to the flux rate previously measured by tubulin photoactivation on kinetochore fibers in RPE1 cells expressing photoactivatable-GFP-α-tubulin (Dudka et al., 2018), supporting criteria for identification of speckles on k-fibers.

To test the difference in flux between short and long k-fibers by an independent method, I used a photoactivation assay on U2OS cells with stable expression of photoactivatable-GFP-α-tubulin (**Figure 12D**, **Figure 13A**). By sequentially photoactivating sister k-fibers of an individual kinetochore pair found outside the metaphase plate during its oscillations, I found that the longer sister k-fiber fluxes faster than the corresponding shorter sister k-fiber (**Figure 12E,F**). Interestingly, the difference between long and short sister k-fiber is relative to a kinetochore as the speed of a long and short k-fiber flux from different kinetochores can have the same rate. This could be due to the length of sister k-fibers being dependent on the position of kinetochores within the spindle, i.e. sister k-fibers are longer towards the spindle periphery

than in the spindle center. Overall, the poleward flux increased with an increasing k-fiber length (**Figure 13B**). Additionally, I tested whether this length-dependence is related to the k-fiber state, i.e. whether it is growing (associated with trailing kinetochore) or shrinking (associated with leading kinetochore), and found that speckles on both growing and shrinking k-fibers flux at similar velocities (**Figure 13C**). Thus, experiments based on two independent methods, speckles and photoactivation, reveal that longer k-fibers flux faster than shorter ones (**Figure 12G**).

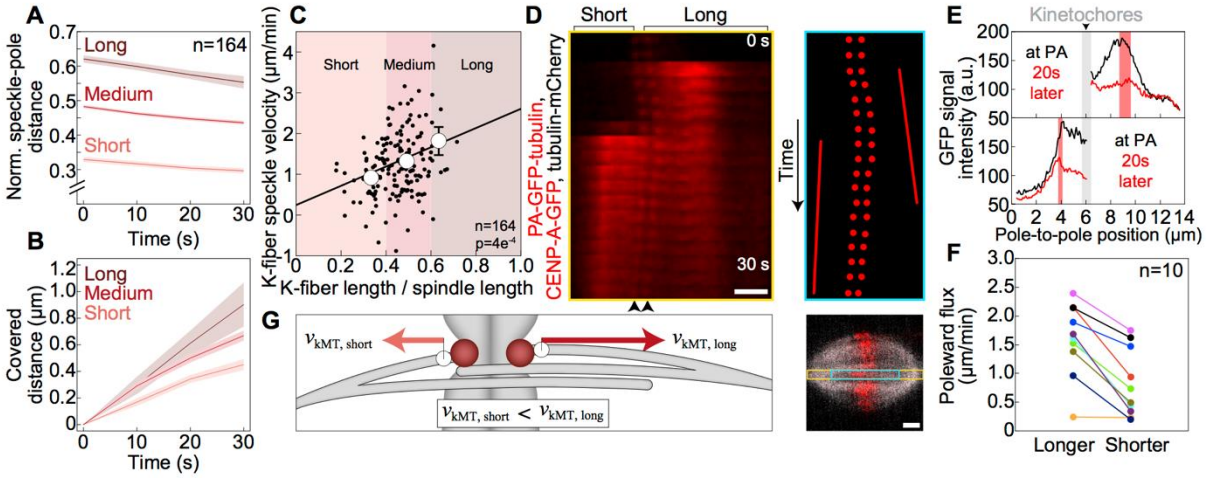


Figure 12. Longer kinetochore fiber exhibits higher poleward flux rates than the shorter one. (**A**) The speckle-pole distance over time divided by spindle length for k-fibers classified as short, medium, and long, according to the k-fiber length being smaller than 0.4, between 0.4 and 0.6, and larger than 0.6 of the spindle length, respectively. (**B**) Change in the speckle-pole distance over time for speckles within groups as in **A**. (**C**) The poleward velocity of k-fiber speckles within groups as in **A** depending on its relative starting speckle-pole distance. (**D**) Montage over time (left) and scheme (right) of a photoactivated region in U2OS cell (bottom) stably co-expressing PA-GFP-α-tubulin (red), CENP-A-GFP (red), and mCherry-α-tubulin (grey). The time interval is 2 s. Shorter and longer sister k-fiber and kinetochore positions (black arrows) are shown. In scheme (right), lines highlight the poleward motion of the photoactivated regions. (**E**) Graphs show pole-to-kinetochore profile intensities of GFP signal for longer (top) and shorter (bottom) k-fiber from the spindle in **G** at the time of photoactivation (black line) and 20 s later (red line). Red shaded areas; the covered distance of photoactivated regions. Grey shaded areas; kinetochore positions. (**F**) The poleward flux of longer and shorter sister k-fiber retrieved from photoactivation assay in U2OS cells and color-coded for each pair. (**G**) Scheme of speckles on longer and shorter k-fiber, where the speckle on the longer k-fiber fluxes faster than the speckle on the shorter k-fiber. Scale bars: 2 µm.

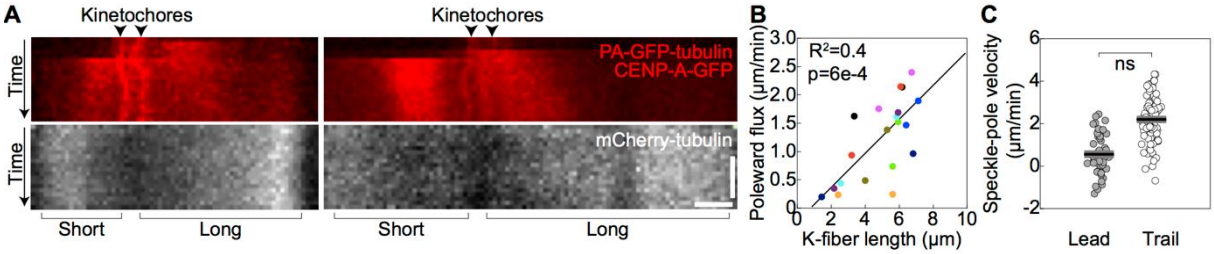


Figure 13. The poleward flux of sister k-fibers increases with an increasing k-fiber length. (**A**) Kymographs retrieved by pole-to-pole segmented lines in U2OS cells stably co-expressing PA-GFP-α-tubulin (red), CENP-A-GFP (red), and mCherry-α-tubulin (grey) during poleward motion of the photoactivated spots on shorter and longer sister k-fibers. Horizontal scale bar, 2 μm; vertical scale bar, 20 s. (**B**) Graph shows the poleward flux of photoactivated spots in U2OS cells with respect to their corresponding k-fiber length, color-coded for each sister k-fiber pair as in **Figure 12F**. (**C**) Poleward velocity of the k-fibers associated with leading (lead) and trailing (trail) kinetochores. Each dot corresponds to an individual speckle. Black line; mean. Grey area; SEM. Statistical analysis, t-test. p-value: ≥ 0.05 (ns).

4.3. Bridging microtubules undergo poleward flux at a higher velocity than kinetochore microtubules

If motors within the bridging fiber drive the flux of bridging microtubules and the interaction between the bridging and k-fibers generates the flux of k-fibers, the tension between sister kinetochores would opposes the flux of k-fibers, making it slower than the flux of the bridging fiber. Can the same feature also be observed in experiments?

Remarkably, speckles on the bridging microtubules moved poleward at a velocity of 2.07 ± 0.11 μm/min in untreated cells (n = 101 speckles from 68 cells), which is significantly faster than for the speckles on kinetochore microtubules (p = 1e-10) (**Figure 14A–D** and **Table 1**). In contrast to k-fibers, bridging fiber flux did not depend on the position of the associated kinetochores along the spindle axis (**Figure 15A**), additionally supporting the result that this dependence is k-fiber specific.

Because these experiments provide the first measurement of the poleward flux of bridging microtubules in human spindles, I decided to validate this method of identification of speckles in the bridging fiber. First, the distance between these speckles and the kinetochore-kinetochore axis of the associated k-fibers was 0.15 ± 0.01 μm, which was similar to the previously measured bridge-kinetochore distance (Kajtez et al., 2016; Polak et al., 2017) and significantly smaller than the distance to the kinetochore-kinetochore axis of their nearest

neighbors, 0.89 ± 0.04 μm (n = 101, p = 2e-16; **Figure 15B**). Furthermore, I used PRC1 siRNA, which is known to specifically reduce the number of bridging microtubules to ~50% of the original number (Jagrić et al., 2021; Polak et al., 2017). In agreement with this, cells treated with PRC1 siRNA had a roughly 2-fold smaller ratio of bridging to kinetochore microtubule speckles in comparison with untreated cells, providing support for the described method of identifications of speckles on bridging fibers (0.37 ± 0.05 vs. 0.62 ± 0.04, **Figure 15C**).

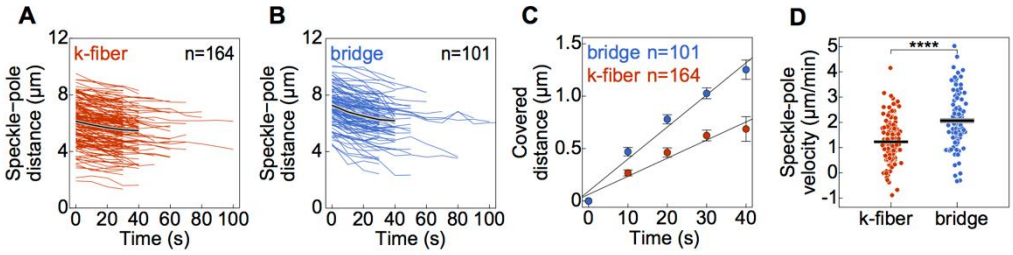


Figure 14. Bridging microtubules flux faster than kinetochore microtubules. Distance between k-fiber (**A**) and bridging fiber (**B**) speckles from the corresponding pole over time in untreated cells. Colored lines show individual speckles. Black line; mean. Grey area; SEM. (**C**) Change in the speckle-pole distance over time for speckles within k-fibers and bridging fibers in untreated cells. (**D**) The poleward velocity of the k-fiber and bridging fiber speckles. Each dot corresponds to an individual speckle. Black line; mean. Grey area; SEM. Statistical analysis, t-test. p-value legend: < 0.0001 (****), 0.0001 to 0.001 (***), 0.001 to 0.01 (**), 0.01 to 0.05 (*), ≥ 0.05 (ns).

The observed rate of bridging microtubule poleward flux implies that the antiparallel bridging microtubules slide apart with respect to each other at twice the rate of their poleward flux, i.e. 4.1 ± 0.2 μm/min, given that the spindle length is constant during metaphase. This rate is comparable to the sliding rate of bridging microtubules in early anaphase measured by tubulin photoactivation, which is roughly 4.5 μm/min (Vukušić et al., 2021), suggesting that the bridging microtubule sliding may be driven by a similar mechanism in metaphase and early anaphase.

To explore the relationship between the bridging and k-fiber flux under various perturbations of the spindle, I measured the flux after a set of depletions of spindle proteins given in Table 1 (see **Figure 16A–I** for depletion efficiency and **Figure 17A–M** for all speckle velocities). The level of protein depletion per treatment was not correlated with the variability in the flux velocity of k-fibers or bridging fibers (**Figure 16I**), arguing against the possibility that samples with lower total levels of depletion contained spindles in which targeted proteins

were depleted to varying degrees, which would lead to large variability in flux rates. Strikingly, the flux of bridging fibers was faster than or equal to the flux of k-fibers across the treatments, even though the relationship between these two velocities was complex (**Figure 18A,B**). Thus, the relationship between the bridging and k-fiber flux holds also in altered spindles with changed flux velocities suggesting that the bridging fiber flux drives the k-fiber flux.

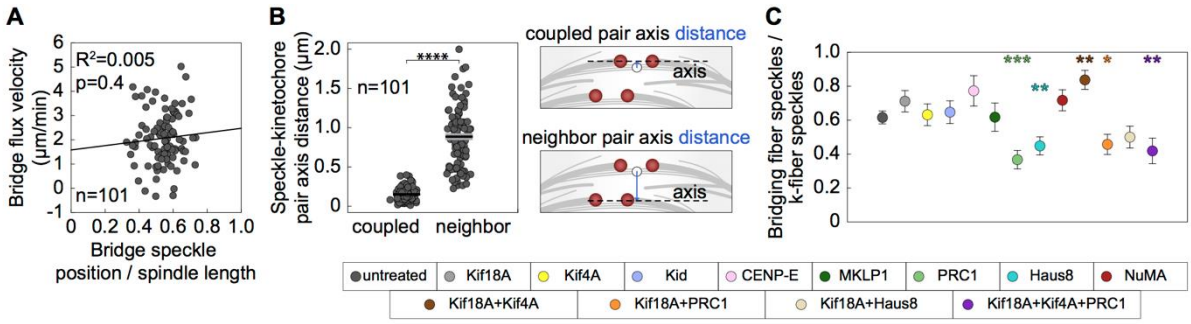


Figure 15. Validation of speckle microscopy assay for identification of speckles in the bridging fiber. (**A**) The poleward velocity of bridging fiber speckles depending on their relative starting speckle-pole distance. The starting position of all bridging fiber speckles was close to the position of the associated kinetochore pair. (**B**) Distances between tracked bridging fiber speckle and kinetochore pair they were associated to and between tracked bridging fiber speckle and their closest neighboring kinetochore pair. Schematics represent how these distances were measured. (**C**) The ratio of tracked speckles within bridging fibers and k-fibers (top) color-coded for corresponding treatments as in legend (bottom). In **C**, each treatment is compared with untreated cells. Treatments include at least three independent experiments. Statistical analysis, t-test (**B**), and two-proportions z-test (**C**). p-value legend as in **Figure 14**.

To explore whether bridging microtubules are at the origin of the differential k-fiber flux in longer and shorter k-fibers, I tested the relative flux distribution in treatments that perturb the number of microtubules in the bridging fiber. I found that k-fibers in PRC1-depleted spindles undergo similar differential flux as in untreated ones, whereas Haus8-depleted spindles showed no differential k-fiber flux rates (**Figure 19A**). This is in agreement with the fact that Haus8 depletion perturbs bridging fibers to a larger extent than PRC1 (Jagrić et al., 2021; Manenica et al., 2020).

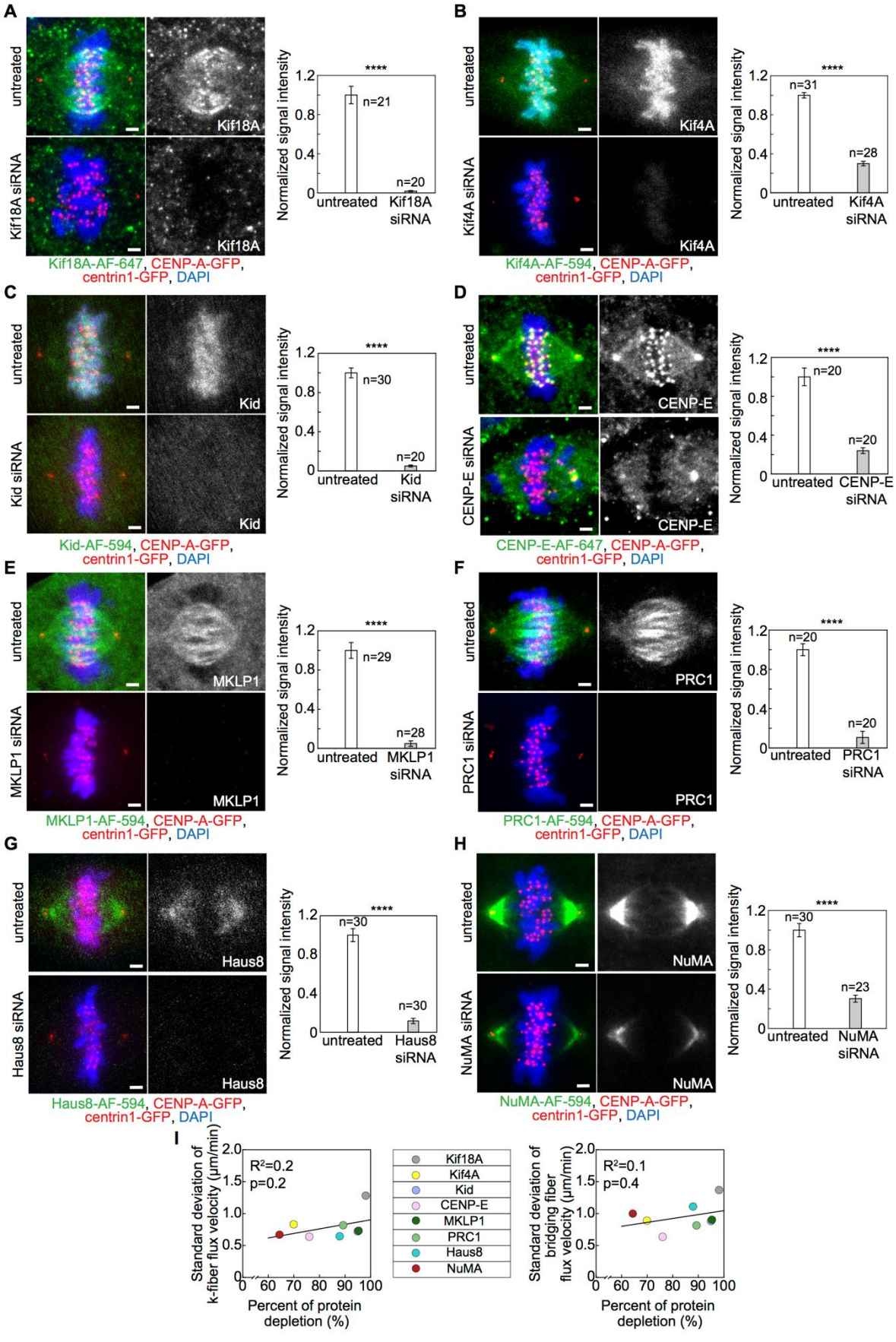

A
untreated
Kif18A siRNA
Kif18A
Kif18A
Normalized signal intensity
****
n=21
n=20
untreated
Kif18A siRNA
Kif18A-AF-647, CENP-A-GFP, centrin1-GFP, DAPI
B
Kif4A
Kif4A
n=31
n=28
Kif4A siRNA
C
Kid
Kid
n=30
n=20
Kid siRNA
Kid-AF-594, CENP-A-GFP, centrin1-GFP, DAPI
D
CENP-E
CENP-E
n=20
n=20
CENP-E siRNA
CENP-E-AF-647, CENP-A-GFP, centrin1-GFP, DAPI
E
MKLP1
MKLP1
n=29
n=28
MKLP1 siRNA
MKLP1-AF-594, CENP-A-GFP, centrin1-GFP, DAPI
F
PRC1
PRC1
n=20
n=20
PRC1 siRNA
PRC1-AF-594, CENP-A-GFP, centrin1-GFP, DAPI
G
Haus8
Haus8
n=30
n=30
Haus8 siRNA
Haus8-AF-594, CENP-A-GFP, centrin1-GFP, DAPI
H
NuMA
NuMA
n=30
n=23
NuMA siRNA
NuMA-AF-594, CENP-A-GFP, centrin1-GFP, DAPI
I
Standard deviation of k-fiber flux velocity (μm/min)
R²=0.2
p=0.2
Percent of protein depletion (%)
Kif18A
Kif4A
Kid
CENP-E
MKLP1
PRC1
Haus8
NuMA
Standard deviation of bridging fiber flux velocity (μm/min)
R²=0.1
p=0.4
Percent of protein depletion (%)

Figure 16. Depletion efficiency of siRNA treatment targeting spindle proteins. (**A**)-(**H**) Fixed spindles in RPE1 cell line stably expressing CENP-A-GFP (red) and centrin1-GFP (red) in cells immunostained for (**A**) Kif18A (AF-647, green), (**B**) Kif4A (AF-594, green), (**C**) Kid (AF-594, green), (**D**) CENP-E (AF-647, green), (**E**) MKLP1 (AF-594, green), (**F**) PRC1 (AF-594, green), (**G**) Haus8 (AF-594, green) and (**H**) NuMA (AF-594, green) in untreated (upper rows) and corresponding siRNA-treated cells (bottom rows), with DNA stained with DAPI (blue). Left: merge; right: protein of interest (grey). Graphs showing intensities of indicated proteins in untreated (white bars) and siRNA treated (grey bars) cells are given on the right. All values are normalized to the mean intensity value of untreated cells for each protein. All treatments include at least two independent experiments. n; number of cells. Scale bars; 2 μm. All images are maximum intensity projections of five z-planes smoothed with 0.5 pixel-sigma Gaussian blur. (**I**) The standard deviation of k-fiber (left) and bridging fiber (right) flux velocity with respect to the level of protein depletion in corresponding siRNA treatments (legend). Statistical analysis, t-test. p-value legend as in **Figure 14**.

To study to what extent k-fibers affect the sliding of bridging microtubules, I depleted Ndc80, the main coupler of kinetochores to microtubule ends (Cheeseman et al., 2006; Cheeseman and Desai, 2008) (**Figure 18A**, **Figure 19B**). As expected, I did not detect speckles on k-fibers, i.e. those at the pole-facing side of the kinetochore, after Ndc80 depletion (n = 8 cells). I found that the speckles that appear on one side of a pair of sister kinetochores, pass the region between them, and end up on the other side, which I interpret to be speckles on bridging microtubules, fluxed at a similar velocity as in untreated cells (**Figure 18A, Table 1**), suggesting that the sliding of bridging microtubules is largely unaffected by k-fibers and that the poleward flux is generated within the bridging fiber. Moreover, I found this velocity to be similar to microtubule poleward flux in the spindles without k-fibers and lateral kinetochore attachments to the spindle obtained by Ndc80 depletion and Aurora B inhibition by ZM447439 (**Figure 18A,C**). By perturbing a set of proteins, I was unable to increase the rate of bridging fiber flux in the spindles, which suggests that the antiparallel overlapping non-kinetochore microtubules and thus bridging microtubules flux at their maximal rate. However, in treatments where bridging fiber flux was reduced, due to Haus8, CENP-E, or MKLP1 depletion, k-fiber flux velocities were also reduced (**Figure 18A, Figure 19C, Table 1**), suggesting that these proteins affect antiparallel sliding within bridging fiber overlaps and consequently k-fiber sliding.

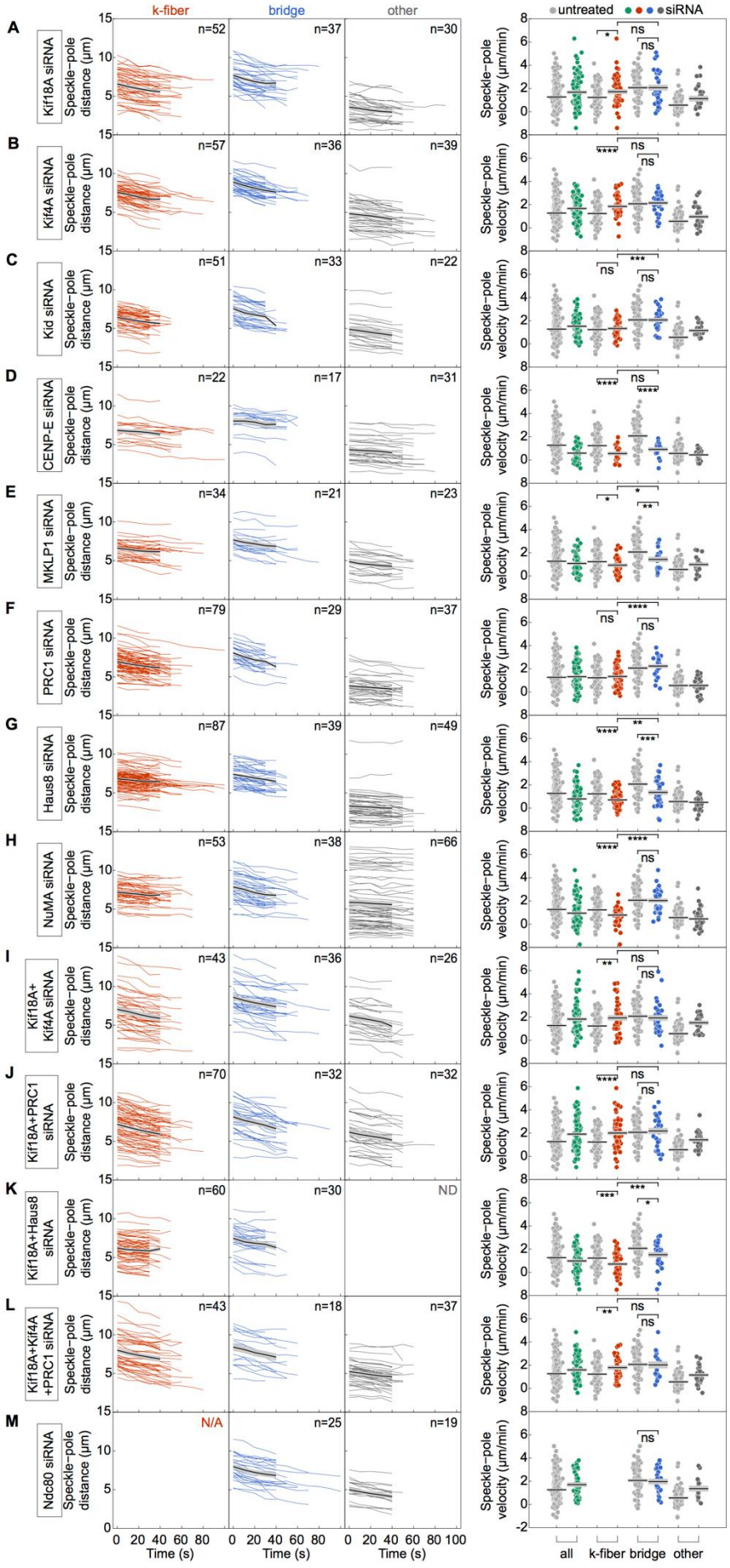

k-fiber
bridge
other
untreated
siRNA
A
Kif18A siRNA
B
Kif4A siRNA
C
Kid siRNA
D
CENP-E siRNA
E
MKLP1 siRNA
F
PRC1 siRNA
G
Haus8 siRNA
H
NuMA siRNA
I
Kif18A+ Kif4A siRNA
J
Kif18A+PRC1 siRNA
K
Kif18A+Haus8 siRNA
L
Kif18A+Kif4A +PRC1 siRNA
M
Ndc80 siRNA
Speckle–pole distance (μm)
Speckle–pole velocity (μm/min)
Time (s)
all
k-fiber
bridge
other
ND
N/A
ns

Figure 17. Speckle velocities after various siRNA treatments. Poleward flux after depletion of (**A**) Kif18A, (**B**) Kif4A, (**C**) Kid, (**D**) CENP-E, (**E**) MKLP1, (**F**) PRC1, (**G**) Haus8, (**H**) NuMA, (**I**) Kif18A+Kif4A, (**J**) Kif18A+PRC1, (**K**) Kif18A+Haus8, (**L**) Kif18A+Kif4A+PRC1 and (**M**) Ndc80. Graphs from left to right show: speckles on kinetochore microtubules, speckles on bridging microtubules, and other speckles. Colored lines show individual speckles. Black line; mean. Grey area; SEM. The poleward velocity of the speckles is shown on the right. Black line; mean. Grey area; SEM. One outlier in untreated cells is not shown. All treatments include at least three independent experiments. n; number of measurements. Statistical analysis, t-test. p-value legend as in **Figure 14**.

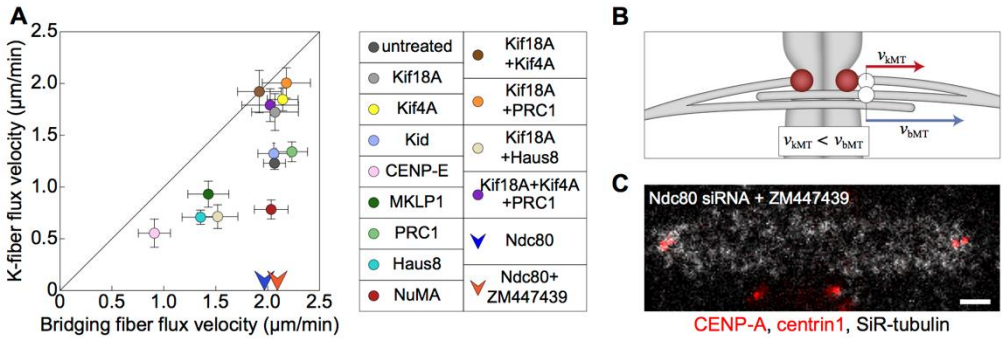


Figure 18. Bridging fibers flux at higher or equal rates with respect to the flux of k-fibers across the treatments. (**A**) The poleward velocity of the k-fiber versus the poleward velocity of the bridging fiber. Circles; mean. Error bars; SEM. Line; x = y. siRNA treatments are color-coded, see the legend. Note that Ndc80-depleted and Ndc80-depleted and ZM447439 treated cells are shown as arrows because the poleward velocity of k-fibers could not be assessed. (**B**) Scheme showing that a speckle within the bridging fiber fluxes faster than a speckle within the k-fiber. (**C**) Spindle in an RPE1 cell stably expressing CENP-A-GFP (red) and centrin1-GFP (red) stained with 1 nM SiR-tubulin dye (grey). The cell is treated with Ndc80 siRNA and ZM447439 inhibitor. Scale bar: 2 µm.

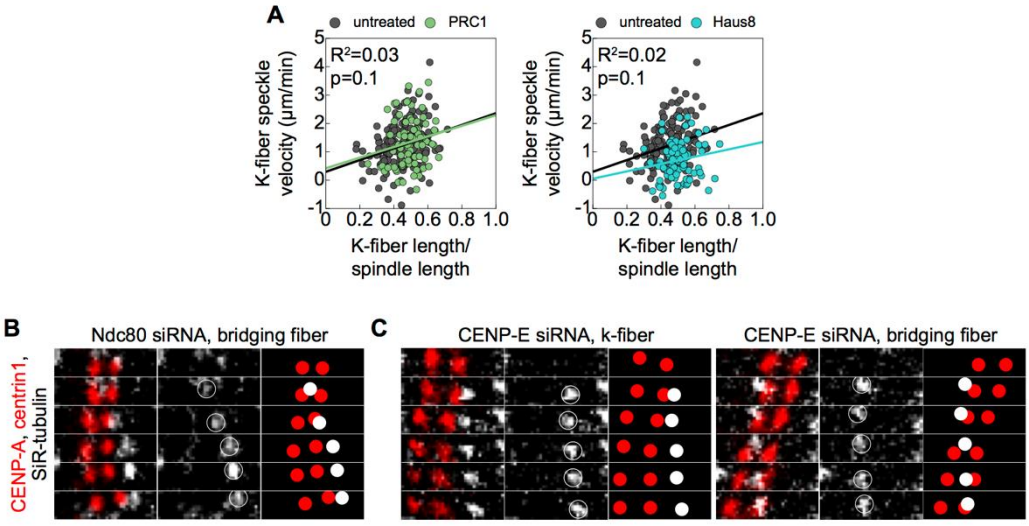


Figure 19. Bridging microtubules are at the origin of the differential k-fiber flux. (**A**) The poleward velocity of k-fiber speckles depending on their relative starting speckle-pole distance in PRC1 (left) and Haus8 (right) siRNA-treated cells. (**B**) Montage over time demonstrating the movement of a speckle belonging to the bridging fiber in Ndc80 siRNA treatment. (**C**) Montage over time demonstrating the movement of a speckle belonging to the k-fiber (left) and bridging fiber (right) in CENP-E siRNA treatment. Legend as in **Figure 10B**. The time interval between images is 10 s.

4.4. Kinetochore centering efficiency depends on the flux velocity of k-fibers

To explore whether kinetochore centering efficiency depends on the flux velocity of k-fibers, I quantified kinetochore alignment by measuring the distances of sister kinetochore midpoints from the equatorial plane of the spindle (**Figure 20A–C**) and explored how this distance depends on the ratio of the k-fiber flux and bridging fiber flux velocities across all treatments (**Figure 20D**, **Figure 21A**). The treatments with this ratio similar to or lower than that of untreated cells show efficient centering comparable to untreated cells. In contrast, treatments with a larger ratio of k-fiber and bridging fiber flux velocities show worse centering, except for Kif4A depletion which I comment on in the Discussion. Worse centering with respect to untreated cells was found only in treatments that included Kif18A depletion (**Figure 20C, Table 1**; note that Ndc80 depletion resulted in worse centering due to abolished k-fibers). As Kif18A has a major role in k-fiber plus-end dynamics and thus in kinetochore alignment (Stumpff et al., 2008), it is important to test the link between flux and kinetochore alignment

independently of Kif18A. Thus, I focus on the treatments that include Kif18A depletion to decouple the flux-driven centering mechanism from the role of Kif18A in k-fiber tip regulation. Among the five treatments where Kif18A was depleted, co-depletion of Haus8 and Kif18A resulted in the lowest ratio of the k-fiber flux to bridging fiber flux and best kinetochore alignment (**Figure 20D**). In contrast, Kif18A depletion alone and co-depletions with Kif4A, PRC1, or Kif4A and PRC1 resulted in a high flux ratio, which was not different from 1 ($p > 0.34$ for each treatment). In these four treatments with a high flux ratio, kinetochore alignment was worse than in Haus8/Kif18A co-depletion ($p < 0.02$ for each of the four treatments, Mann-Whitney test). Thus, the flux ratio is related to kinetochore alignment in the Kif18A-depleted background, suggesting that the effect of flux-driven centering can be observed in the absence of Kif18A-dependent k-fiber plus-end dynamics.

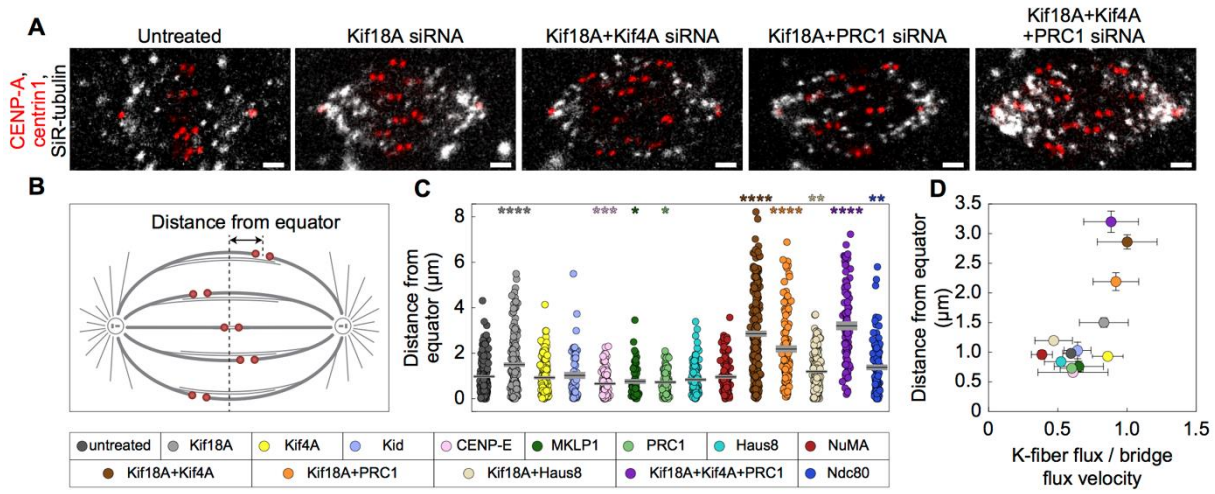


Figure 20. Kinetochore alignment depends on the ratio of k-fiber to bridging fiber flux velocity. (**A**) Spindles in RPE1 cells stably expressing CENP-A-GFP (red) and centrin1-GFP (red) stained with 1 nM SiR-tubulin dye (grey). Cells are untreated, depleted for Kif18A, Kif18A and Kif4A, Kif18A and PRC1, and Kif18A, Kif4A and PRC1 (from left to right). Scale bars: 2 μm. (**B**) The scheme shows that the distance from the equator was measured as the distance between the sister kinetochore midpoint and the equatorial plane. (**C**) Kinetochore distance from equator in untreated and siRNA-treated cells. Each treatment is compared with untreated cells. (**D**) Experimental data for the kinetochore distance from equator versus the ratio of k-fiber and bridging fiber flux velocity in untreated and siRNA-treated cells. Circles; mean. Error bars; SEM. Treatments in **C** and **D** are color-coded according to the legend at the bottom. Statistical analysis, Mann-Whitney test; p-values as in **Figure 14**.

As a control for proper attachment of misaligned kinetochores, I imaged astrin, which marks mature end-on attachments (Shrestha et al., 2017), and found it localized at all kinetochores including those that were highly off-centered (**Figure 21B**). This suggests that the reason for off-centering was not a lack of kinetochore biorientation. I also note that the observed worse centering after combined depletion of Kif18A and Kif4A in comparison with Kif18A depletion differs from a previous report (Stumpff et al., 2012). This difference is not due to the use of different cell lines as I obtained similar results on HeLa and U2OS cells as on RPE1 (**Figure 22A,B**), but likely related to a different effect of the double depletion on spindle length. Taken together, these experiments suggest that kinetochores are better centered when the k-fiber flux is markedly slower than the bridging fiber flux, allowing for sliding of k-fibers along bridging fibers and thus the movement of the center of sister k-fibers towards the spindle center.

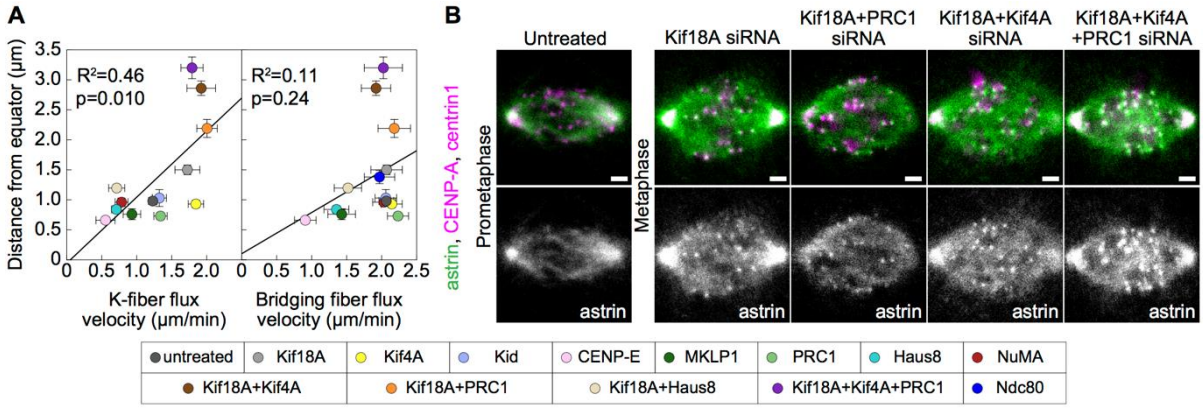


Figure 21. Off-centering of bi-oriented kinetochores is k-fiber specific. (**A**) Kinetochore distance from equator versus k-fiber (left) and bridging fiber (right) flux velocity in untreated and siRNA-treated cells. Treatments are color-coded according to the legend. (**B**) Fixed spindles in RPE1 cells stably expressing CENP-A-GFP and centrin1-GFP (magenta), immunostained for astrin (AF-594, green) in untreated and treated with Kif18A, Kif18A and PRC1, Kif18A and Kif4A, and Kif18A, Kif4A and PRC1 siRNA (left to right). Top: merge; bottom: astrin (grey). Images are sum intensity projections of five z-planes. Scale bars; 2 µm.

4.5. Longer overlaps of antiparallel microtubules lead to an increase in the k-fiber flux velocity to the bridging fiber flux velocity

Experiments have shown that an increased flux velocity of k-fibers is related to less efficient kinetochore centering. What caused this speeding up of the k-fiber flux in the treatments with

misaligned kinetochores? To explore this intriguing relationship, I measured the overlap length by measuring the length of PRC1-labeled regions in all the treatments except those where PRC1 was depleted (**Figure 23A,B**). Out of these treatments, overlaps were longer after depletion of Kif18A or Kif4A, in agreement with previous results (Jagrić et al., 2021), and after a combined depletion of Kif18A and Kif4A (**Table 1, Figure 23C**; see **Figure 22C** for HeLa and U2OS cells). These treatments specifically increased the flux velocity of k-fibers without changing the flux of bridging fibers, resulting in k-fibers fluxing at ~90% of the bridging fiber flux velocity (**Figure 24A-C, Table 1**). For comparison, in untreated cells k-fibers flux at ~60% of the bridging fiber flux velocity (**Table 1**). Thus, these experiments reveal a relationship between the overlap length and the k-fiber flux velocity, suggesting that the sliding forces generated within the bridging fiber are transferred to the k-fibers through the antiparallel overlaps between these two types of fibers.

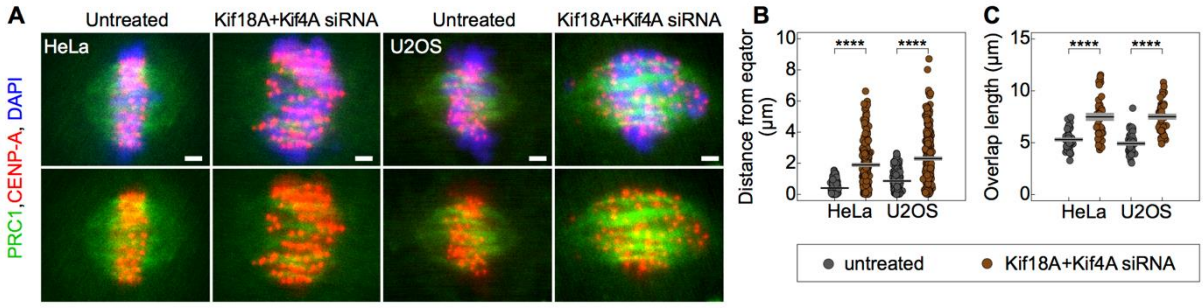


Figure 22. HeLa and U2OS cells exhibit kinetochore misalignment upon Kif18A and Kif4A co-depletion. (**A**) Fixed spindles in HeLa and U2OS cells stably expressing CENP-A-GFP (red) in untreated (left) and Kif18A and Kif4A siRNA treated cells (right), immunostained for PRC1 (AF-594, green) and stained with DAPI (blue). Upper row; merge, bottom row; GFP and AF-594. Images are maximum intensity projections of five z-planes. Scale bars; 2 µm. (**B**) Kinetochore distance from equator in untreated and Kif18A and Kif4A siRNA treated HeLa (n = 172 and n = 235 kinetochore pairs) and U2OS (n = 216 and n = 281 kinetochore pairs) cells. (**C**) Length of individual PRC1-labeled overlaps in untreated and Kif18A and Kif4A siRNA treated HeLa (n = 46 and n = 49 PRC1 bundles) and U2OS (n = 47 and n = 41 PRC1 bundles) cells. Black line; mean. Grey area; SEM. Treatments are color-coded according to the legend. Statistical analysis, Mann-Whitney test in **B**, t-test in **C**. p-value legend as in **Figure 14**.

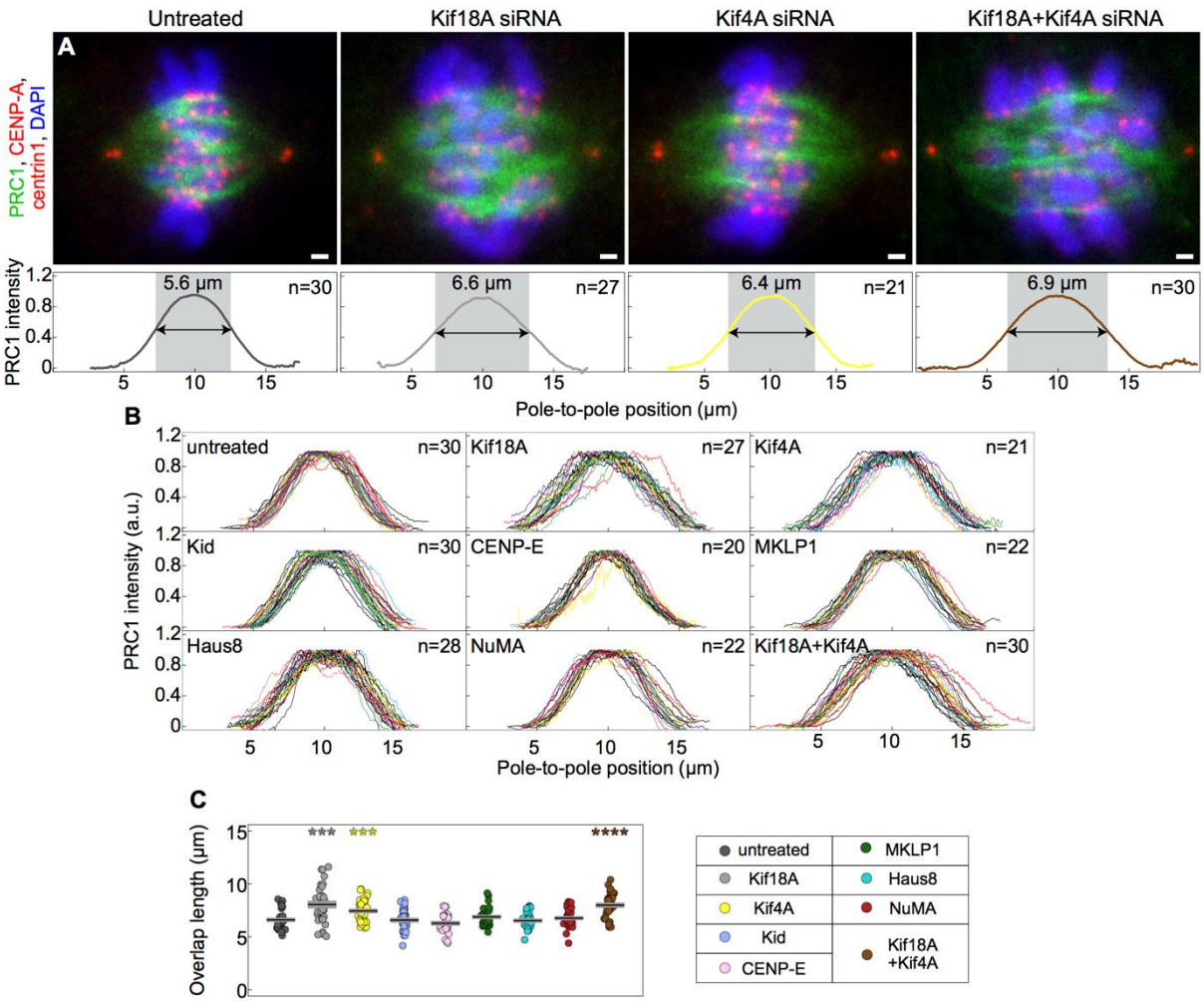


Figure 23. Kinetochore alignment correlates with overlap length across siRNA treatments. (**A**) Fixed spindles in RPE1 cells stably expressing CENP-A-GFP and centrin1-GFP (red) in untreated, Kif18A siRNA, Kif4A siRNA, and Kif18A and Kif4A siRNA treated cells (from left to right), immunostained for endogenous PRC1 (AF-594, green) and stained with DAPI (blue). Images are sum intensity projections of five z-planes. Scale bars: 1 µm. Graphs show normalized pole-to-pole PRC1 intensity profiles of complete spindles for corresponding treatments. Colored line; mean. (**B**) Normalized pole-to-pole PRC1 intensity profiles of complete spindles for given treatments. Lines correspond to individual spindles. (**C**) Length of individual PRC1-labeled overlaps. siRNA treatments in **A**, **C** are color-coded according to the legend. In **C**, each treatment is compared with untreated cells. Statistical analysis, t-test. p-value legend as in **Figure 14**.

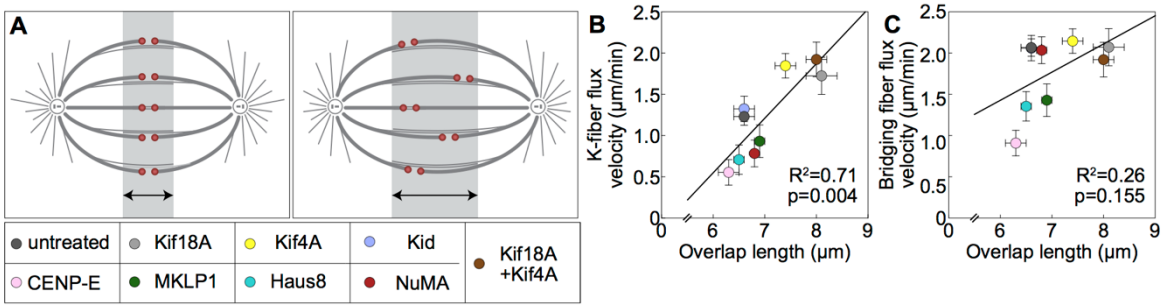


Figure 24. Overlap length dictates k-fiber flux velocity. (**A**) The scheme shows that spindles with shorter (left) and longer (right) overlap regions have better (left) and worse (right) kinetochore alignment at the spindle equator, respectively. K-fiber (**B**) and bridging fiber (**C**) flux velocity versus PRC1-labeled overlap length. Treatments are color-coded as shown in the legend below.

4.6. The difference in the flux of bridging and k-fibers increases for smaller concentrations of passive crosslinkers

The sliding forces from the bridging fiber are transmitted to the k-fibers not only through the antiparallel overlaps but also through the regions of parallel overlaps, where the bridging and kinetochore microtubules extending from the same spindle half are linked together by passive crosslinkers. Thus, reducing the number of passive crosslinkers should result in reduced force transmitted from the bridging to the k-fibers and consequently in a slower flux of k-fibers.

To explore the role of passive crosslinkers in the parallel overlaps of bridging and kinetochore microtubules, I chose NuMA as a candidate because it is required for local load-bearing in the spindle (Elting et al., 2017) (**Figure 25A**) and for synchronous microtubule flux across the spindle (Steblyanko et al., 2020). After depletion of NuMA by siRNA (Figure 23B), I found that the flux velocity of kinetochore microtubules decreased by ~40% (from 1.23 ± 0.06 in untreated cells to 0.78 ± 0.09 µm/min after NuMA depletion, **Figure 25C,D**, **Table 1**). On the contrary, the flux velocity of bridging fibers did not change significantly (**Figure 25C,D**), thus the difference compared to the k-fiber velocity increased. These results support the idea that NuMA acts as a passive crosslinker transmitting the sliding forces from the bridging fiber onto the associated k-fibers through their parallel overlaps.

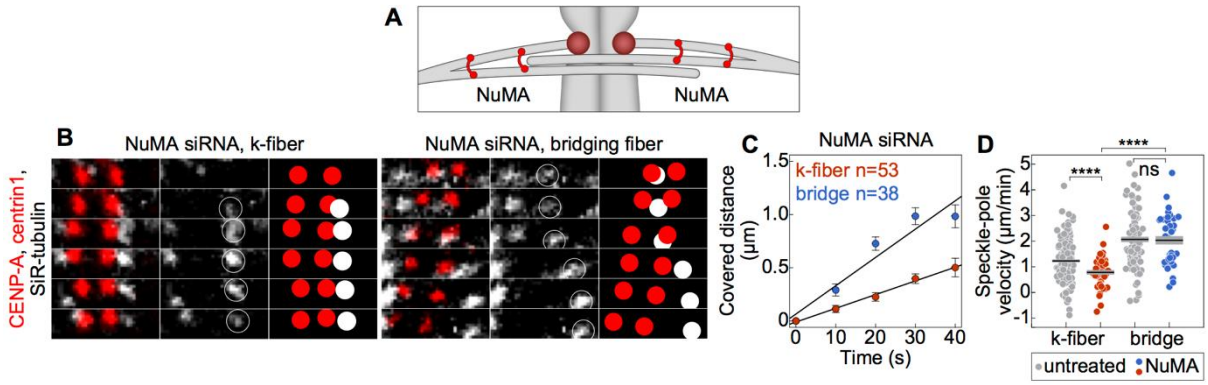


Figure 25. NuMA-mediated coupling between bridging and k-fibers controls k-fiber flux velocity. (**A**) Scheme of NuMA localization. (**B**) Montage over time from an RPE1 cell stably expressing CENP-A-GFP (red) and centrin1-GFP (red) stained with 1 nM SiR-tubulin dye (grey) demonstrating the movement of a speckle belonging to the k-fiber (left) and bridging fiber (right) in NuMA siRNA treatment. Legend as in **Figure 10B**. The time interval between images is 10 s. (**C**) Change in the speckle-pole distance over time for speckles within bridging and k-fibers in cells treated with NuMA siRNA. (**D**) The poleward velocity of the speckles in NuMA siRNA-treated (red: k-fiber, blue: bridging fiber) and untreated (grey) cells. Black line; mean. Grey area; SEM. Statistical analysis, t-test. p-value as in **Figure 14**.

4.7. Comparison with the model

To compare experimental data with theoretical predictions, theoretical curves from Risteski et al., (2021a) were used. First, it can be observed that the model prediction explains the data points with slower bridging fiber flux when the motor velocity is varied (v_0; **Figure 26A**). For the treatments that had unchanged bridging fiber flux, the theoretical curve retrieved by varying the effective friction on the kinetochore, where an increase in this friction slows down the k-fiber flux and vice versa, agrees with this subset of treatments (μ_{KC}; **Figure 26A**). Thus, experimental data together with the theoretical model developed in Risteski et al., (2021a) suggest that the used treatments can be divided roughly into two groups, in one of which the sliding velocity was altered, whereas in the other the interaction between the k-fiber and kinetochore. Because faster bridging than k-fiber flux is a signature of the flux-driven centering mechanism, experimental findings over various treatments suggest that the bridging fiber flux drives the k-fiber flux.

Moreover, predictions from the model obtained in two different ways, by varying either the effective kinetochore friction (μ_{KC}) or the motor velocity (v_0), showed a trend similar to the

experimental data, even though each experimental treatment likely altered several spindle features (**Figure 26B**). The model prediction with varying the effective kinetochore friction agrees more closely with the experimental data than the one with varying motor velocity likely because among the used treatments, many of them altered the dynamics of the k-fiber plus end, such as those that include Kif18A depletion, whereas only a few treatments changed the sliding velocity. Thus, the experiments together with theory suggest that the ratio of k-fiber flux to bridging fiber flux velocities influences chromosome alignment.

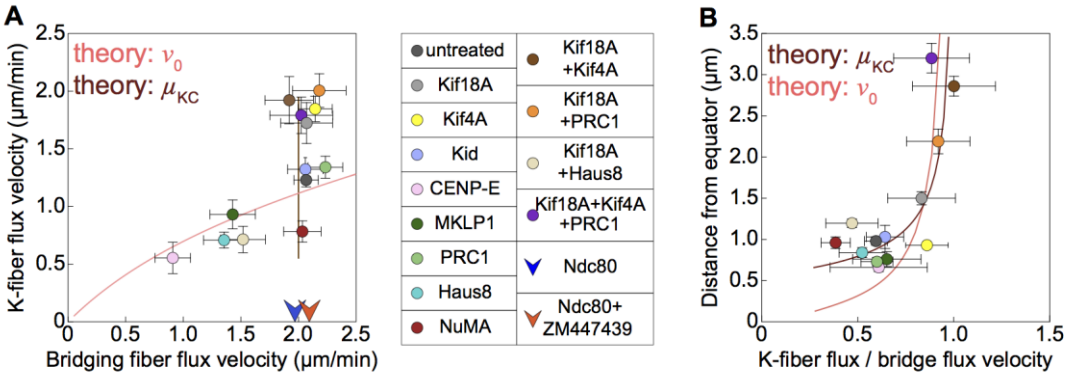


Figure 26. Predictions from the model obtained by varying either the effective kinetochore friction or the motor velocity. (**A**) The poleward velocity of the k-fiber versus the poleward velocity of the bridging fiber. Circles; mean. Error bars; SEM. siRNA treatments are color-coded, see the legend. Note that Ndc80-depleted and Ndc80-depleted and ZM447439 treated cells are shown as arrows because the poleward velocity of k-fibers could not be assessed. Theoretical predictions (lines) for v_0 = 0.1-10 μm/min (pink), and for μ_{KC} = 1-100 pNmin/μm (brown), x_{KC} = 0 μm, and other parameters are as in (Risteski et al., 2021a) (**B**) Experimental data for the kinetochore distance from equator versus the ratio of k-fiber and bridging fiber flux velocity in untreated and siRNA-treated cells. Circles; mean. Error bars; SEM. Theoretical predictions for centering efficiency, described as $\langle x^2 \rangle = 2DT$, where T is centering time and is calculated from kinetochore distance from the center and centering velocity, $T = x_{KC}/v_{KC}$, as a function of the ratio of k-fiber and bridging fiber flux velocities. D = 0.009 μm^2/min and 0.1 μm^2/min, obtained from the fit to the data by varying the model parameter motor velocity (pink curve) or the effective friction at the kinetochore (brown curve), respectively. Theoretical curves retrieved from Risteski et al., (2021a).

Table 1. Measurements of flux, spindle, and kinetochore parameters in RPE1 cells, untreated and siRNA-depleted. Values are given as mean ± sem. The numbers in brackets denote the number of measurements (number of speckles for flux measurements or number of kinetochore pairs; for spindle length, this number is not given because it is equal to the number of cells), number of cells, and p-value from a t-test or Mann-Whitney test (last column) for comparison with untreated cells. n.a., not applicable; n.d., not determined.

	Flux, all (µm/min)	Flux, k-fiber (µm/min)	Flux, bridge (µm/min)	Flux, other (µm/min)	Spindle length (µm)	Overlap length (µm)	Kinetochore distance to equatorial plane (µm)
Untreated	1.27 ± 0.05 (371, 68, n.a.)	1.23 ± 0.06 (164, 68, n.a.)	2.07 ± 0.11 (101, 68, n.a.)	0.56 ± 0.09 (106, 27, n.a.)	13.87 ± 0.23 (44, n.a.)	6.6 ± 0.2 (33, 11, n.a.)	0.98 ± 0.05 (258, 44, n.a.)
Kif18A	1.68 ± 0.12 (119, 27, 0.002)	1.72 ± 0.18 (52, 27, 0.01)	2.07 ± 0.23 (37, 27, 0.9)	1.13 ± 0.22 (30, 21, 0.02)	15.12 ± 0.33 (25, 0.003)	8.1 ± 0.3 (35, 14, 1e-04)	1.50 ± 0.08 (198, 28, 9e-6)
Kif4A	1.66 ± 0.08 (132, 30, 1e-04)	1.85 ± 0.11 (57, 30, 3e-06)	2.14 ± 0.15 (36, 30, 0.6)	0.96 ± 0.14 (39, 10, 0.01)	15.70 ± 0.28 (25, 7e-06)	7.4 ± 0.2 (39, 10, 6e-04)	0.93 ± 0.06 (165, 25, 0.4)
Kid	1.52 ± 0.08 (106, 24, 0.01)	1.32 ± 0.10 (51, 24, 0.4)	2.06 ± 0.15 (33, 24, 0.9)	1.15 ± 0.12 (22, 7, 1e-04)	13.29 ± 0.69 (10, 0.4)	6.6 ± 0.2 (33, 12, 0.9)	1.03 ± 0.14 (57, 10, 0.5)
CENP-E	0.59 ± 0.07 (70, 9, 7e-13)	0.55 ± 0.14 (22, 9, 8e-05)	0.91 ± 0.15 (17, 9, 5e-07)	0.44 ± 0.07 (31, 9, 0.2)	15.17 ± 0.23 (20, 2e-04)	6.3 ± 0.2 (28, 11, 0.17)	0.66 ± 0.05 (122, 25, 1e-04)
MKLP1	1.08 ± 0.09 (78, 13, 0.07)	0.93 ± 0.13 (34, 13, 0.03)	1.43 ± 0.20 (21, 13, 0.007)	0.99 ± 0.14 (23, 13, 0.01)	13.39 ± 0.39 (10, 0.3)	6.9 ± 0.1 (32, 14, 0.2)	0.76 ± 0.09 (57, 10, 0.02)
PRC1	1.32 ± 0.08 (145, 28, 0.5)	1.34 ± 0.10 (79, 28, 0.3)	2.23 ± 0.15 (29, 28, 0.3)	0.57 ± 0.10 (37, 11, 0.9)	13.86 ± 0.24 (15, 0.97)	n.a.	0.73 ± 0.05 (93, 15, 0.01)

Haus8	0.79 ± 0.06 (175, 34, 9e-09)	0.71 ± 0.07 (87, 34, 4e-08)	1.35 ± 0.18 (39, 34, 9e-04)	0.50 ± 0.06 (49, 14, 0.5)	13.46 ± 0.38 (23, 0.36)	6.5 ± 0.1 (30, 13, 0.7)	0.84 ± 0.06 (137, 23, 0.09)
NuMA	0.95 ± 0.08 (157, 32, 8e-04)	0.78 ± 0.09 (53, 32, 9e-05)	2.03 ± 0.16 (38, 32, 0.8)	0.45 ± 0.08 (66, 13, 0.3)	14.42 ± 0.32 (17, 0.18)	6.8 ± 0.1 (33, 10, 0.45)	0.96 ± 0.07 (130, 17, 0.7)
Kif18A + Kif4A	1.82 ± 0.12 (105, 23, 3e-05)	1.92 ± 0.20 (43, 23, 0.002)	1.92 ± 0.21 (36, 23, 0.5)	1.50 ± 0.15 (26, 23, 3e-06)	16.96 ± 0.31 (37, 1e-11)	8 ± 0.2 (35, 13, 1e-04)	2.86 ± 0.12 (235, 37, 2e-16)
Kif18A + PRC1	1.91 ± 0.10 (134, 16, 8e-08)	2.00 ± 0.15 (70, 16, 3e-06)	2.18 ± 0.23 (32, 16, 0.6)	1.42 ± 0.13 (32, 16, 5e-07)	15.41 ± 0.44 (18, 0.005)	n.a.	2.19 ± 0.15 (116, 18, 8e-15)
Kif18A + Haus8	0.98 ± 0.11 (90, 30, 0.01)	0.71 ± 0.11 (60, 30, 1e-04)	1.59 ± 0.20 (30, 30, 0.01)	n.d.	n.d.	n.d.	1.20 ± 0.05 (242, 30, 0.002)
Kif18A + Kif4A + PRC1	1.59 ± 0.10 (98, 16, 0.005)	1.79 ± 0.16 (43, 16, 0.001)	2.02 ± 0.27 (18, 16, 0.8)	1.15 ± 0.11 (37, 16, 7e-05)	17.09 ± 0.29 (20, 4e-11)	n.a.	3.20 ± 0.18 (91, 20, 2e-16)
Ndc80	1.71 ± 0.16 (44, 8, 0.01)	n.a.	1.97 ± 0.22 (25, 8, 0.6)	1.36 ± 0.22 (19, 8, 0.002)	15.09 ± 0.29 (15, 0.002)	n.d.	1.38 ± 0.11 (105, 15, 0.003)

4.8. Aneuploidy can occur due to persistent chromosome alignment defects in metaphase

To determine the relevance of chromosome alignment for chromosome segregation fidelity in untreated, physiological conditions, I used non-transformed and cancer cells to investigate whether chromosomes with underlying alignment defects are more prone to end up in wrong daughter nuclei. For non-transformed cells, I used RPE1 cell line, whilst U2OS (osteosarcoma) and HeLa (cervical adenocarcinoma) cell lines were used as cancer cells. For assessment of chromosome segregation error types and frequencies of their occurrence in anaphase, cells were classified as having lagging chromosomes, chromosome bridges, or persistent alignment defects (**Figure 26A**). If one stretched kinetochore was found to lag behind separating chromosome masses in the central part of the spindle, the kinetochore was categorized as having

merotelic attachment and being associated with a lagging chromosome (**Figure 26B**). Furthermore, if a pair of non-stretched kinetochores was found to lag behind separating chromosome masses on a line parallel to the pole-to-pole axis, those kinetochores were associated with chromosome bridges (**Figure 26C**). Moreover, if a pair of sister kinetochores remained outside of the metaphase plate throughout mitosis, I classified it as being associated with a persistent alignment defect (**Figure 26D**). This identification assay allowed me to assess the occurrence of each type of chromosome segregation error across inspected cell lines.

By using quantitative analyses of the kinetochore positions in anaphase, I calculated the fraction of chromosome segregation error types in RPE1, U2OS, and HeLa cells. Here, more than 90% of RPE1 cells exhibited no chromosome segregation error, which validates the use of applied imaging settings for error assessment since this rate agrees with previous reports on RPE1 cells (Janssen et al., 2011; Worrall et al., 2018). Upon inspection, the most numerous chromosome segregation errors were microtubule-independent errors, i.e. chromosome bridges that arise due to chromosome end-to-end fusions, DNA catenation, or replication stress (Levine and Holland, 2018). Anaphase chromosome bridges occurred in 5%, 8%, and 19% of RPE1, U2OS, and HeLa cells, respectively (**Figure 27A,B**). These rates may be overestimated as some errors categorized as chromosome bridges could be double merotelics where both kinetochores are attached to both spindle poles. Furthermore, lagging chromosomes were observed in 1.9%, 6.4%, and 8% of RPE1, U2OS, and HeLa cells, respectively (**Figure 27A,B**). These rates may be overestimated as not all kinetochores found in the spindle midzone during anaphase are associated with lagging chromosomes, and could correspond to lazy kinetochores which are rapidly corrected in anaphase (Sen et al., 2021). However, due to a 1-min time-frame interval, these types could not be discerned. Apart from the elevated occurrence of chromosome bridges in HeLa cells, observed rates of chromosome segregation errors were similar to previous studies (Janssen et al., 2011; Bakhoum et al., 2014). Strikingly, I found 3.5 ± 1.3% of U2OS and 3.0 ± 1.7% of HeLa cells with unaligned chromosomes that persist in anaphase (**Figure 27A,B**). Unaligned chromosomes were not observed in RPE1 cells at the anaphase onset. Unlike lagging chromosomes which mostly segregate to the correct daughter cell (Thompson and Compton, 2011), unaligned chromosomes that persist in anaphase caused monosomy and trisomy in all observed cases. Thus, aneuploidy can occur due to persistent chromosome alignment defects in cancer cells.

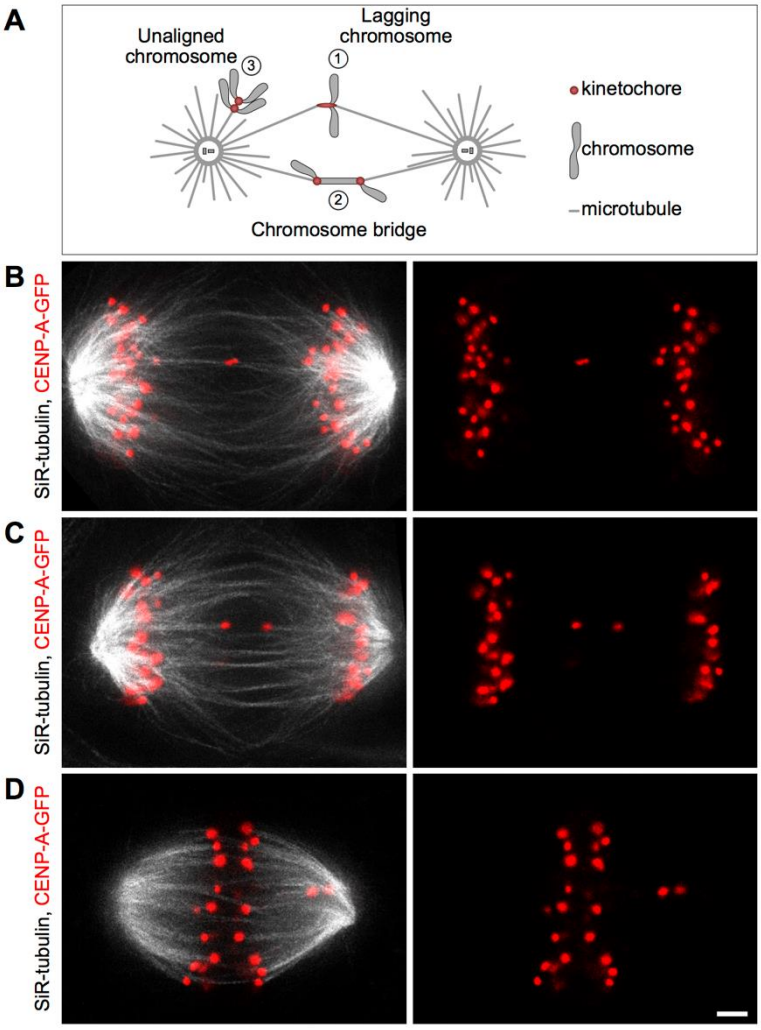


Figure 26. Chromosome segregation error classification. (**A**) Schematic representation of the criteria for the classification of chromosome segregation errors in anaphase. Identified chromosome defects were classified as lagging chromosomes, chromosome bridges, and unaligned chromosomes according to the position of their kinetochores during anaphase. (**B**) Super-resolution STED image of U2OS cell stably expressing CENP-A-GFP (red) and stained with SiR-tubulin dye (grey), which exhibits lagging kinetochore in anaphase. STED was done only for the SiR-tubulin channel. Left, merge; right, CENP-A-GFP. (**C**) U2OS cell with chromosome bridge in anaphase. Legend as in **B**. (**D**) U2OS cell with unaligned kinetochores that persist in anaphase. Legend as in **B**. Scale bar, 2 μm.

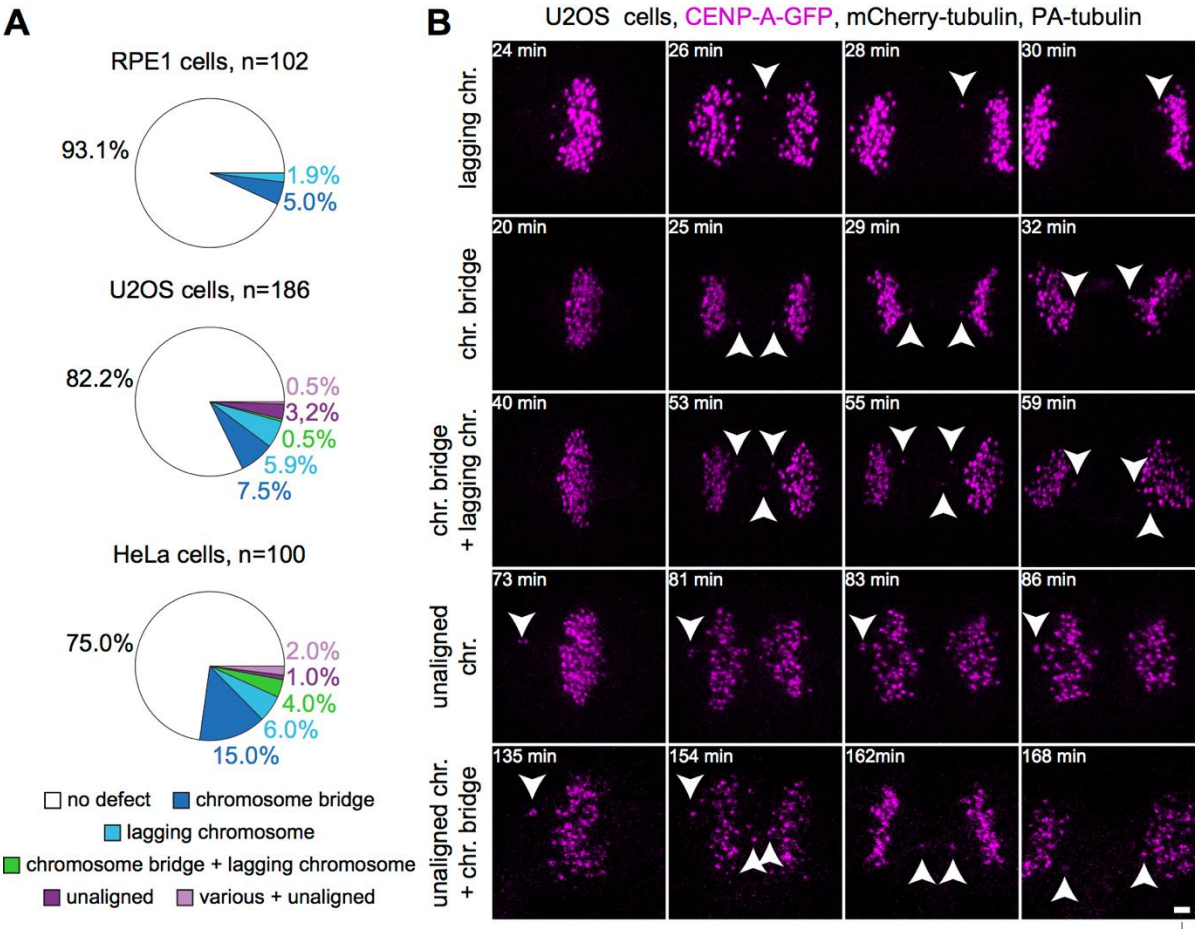


Figure 27. Frequency of chromosome segregation errors in non-transformed and cancer cell lines. (**A**) Fractions of cells with chromosome segregation errors in anaphase. RPE1 cells, top; U2OS cells, middle; HeLa cells, bottom. Chromosome segregation errors are color-coded according to the legend at the bottom. (**B**) Time-lapse images of U2OS cells with stable expression of CENP-A-GFP (magenta), mCherry-α-tubulin, and PA-GFP-α-tubulin. Arrows point to kinetochores associated with chromosome segregation errors. Scale bar, 2 μm.

To explore whether observed persistent chromosome alignment defects are caused by premature anaphase entry due to spindle assembly checkpoint deficiency (Lara-Gonzalez et al., 2021), I analyzed the duration of metaphase in each cell line. The duration of metaphase was defined as the time upon alignment of the majority of chromosomes until anaphase onset. The calculated time until anaphase onset shows that cancer cells spend more time in metaphase with respect to RPE1 cells (**Figure 28A**). Specifically, the duration of metaphase was ~2x and ~3x longer in HeLa and U2OS cells, respectively. This result suggests that HeLa and U2OS cells are spindle assembly checkpoint-proficient and that presence of unaligned chromosomes in anaphase is not due to premature anaphase entry, which is in agreement with spindle assembly checkpoint-related deficiencies being infrequent in human cancers (Levine and Holland, 2018;

Gordon et al., 2012). Interestingly, the prolonged duration of metaphase was associated with the occurrence of chromosome alignment defects during metaphase (**Figure 28B**). Here, both cells that experience chromosome alignment defects during metaphase but align all chromosomes before anaphase onset, and cells that enter anaphase with unaligned chromosomes exhibit anaphase delay (**Figure 28B**). Additionally, the presence of unaligned chromosomes per cell line correlates with the average duration of their metaphase. Similar to previous results (Gregan et al., 2011; Finardi et al., 2020), chromosome bridges and lagging chromosomes do not delay anaphase entry. Thus, chromosome alignment defects, and not the occurrence of chromosome bridges and lagging chromosomes, account for prolonged metaphase in spindle assembly checkpoint-proficient cells. Moreover, this suggests that aneuploidy caused by persistent chromosome alignment defect is spindle assembly checkpoint-deficiency independent.

By quantitatively assessing chromosome segregation errors in non-transformed cells and cancer cells, I observed that cancer cells undergo cell divisions with multiple errors of the same type (**Figure 29A,B**). To estimate how likely is for multiple same-type errors to occur in the cell, I explored the chance of getting more than one error from the Poisson distribution. The sum of probabilities of multiple same-type errors occurring in cells was less than 0.05, both in U2OS and HeLa cells. Specifically, multiple lagging chromosomes in U2OS ($p=0.003$) and HeLa cells ($p=0.004$), multiple persistently unaligned chromosomes in U2OS cells (0.001) or chromosome bridges in U2OS ($p= 0.003$) and HeLa cells (0.01) suggest that it is not reasonable to get more than one same-type error from the Poisson distribution with observed means from the experiments. As observed events do not follow the expected distribution, multiple chromosome segregation errors are not random events. This suggests that multiple chromosome segregation errors per cell are improbable to occur due to the stochasticity of the events but are likely caused by some defects in the mitotic machinery.

A recent breakthrough study revealed a role for tissue architecture in enhancing chromosome segregation fidelity. By showing that cells in 2D cultures are more prone to acquire chromosome segregation errors with respect to 3D cultures, it is speculated that tissue architecture promotes proper microtubule-kinetochore attachments (Knouse et al., 2018). To test whether observed error rates in cancer cells can be decreased by tissue-like conditions, I used cell-micropatterning to confine U2OS cell growth and division in an environment that promotes cell-cell interactions. Once imaged, micropatterned cells were defined as isolated if no surrounding cell was observed (**Figure 30A**), typically on a 20-μm micropatterned islet, and defined as surrounded if displayed 100% of contact with other cells around them (**Figure 30A**).

Here, an assessment of chromosome segregation errors in isolated and surrounded cells showed that both groups exhibit similar error rates (**Figure 30B**). Thus, I speculate that observed chromosome segregation errors are environment-independent.

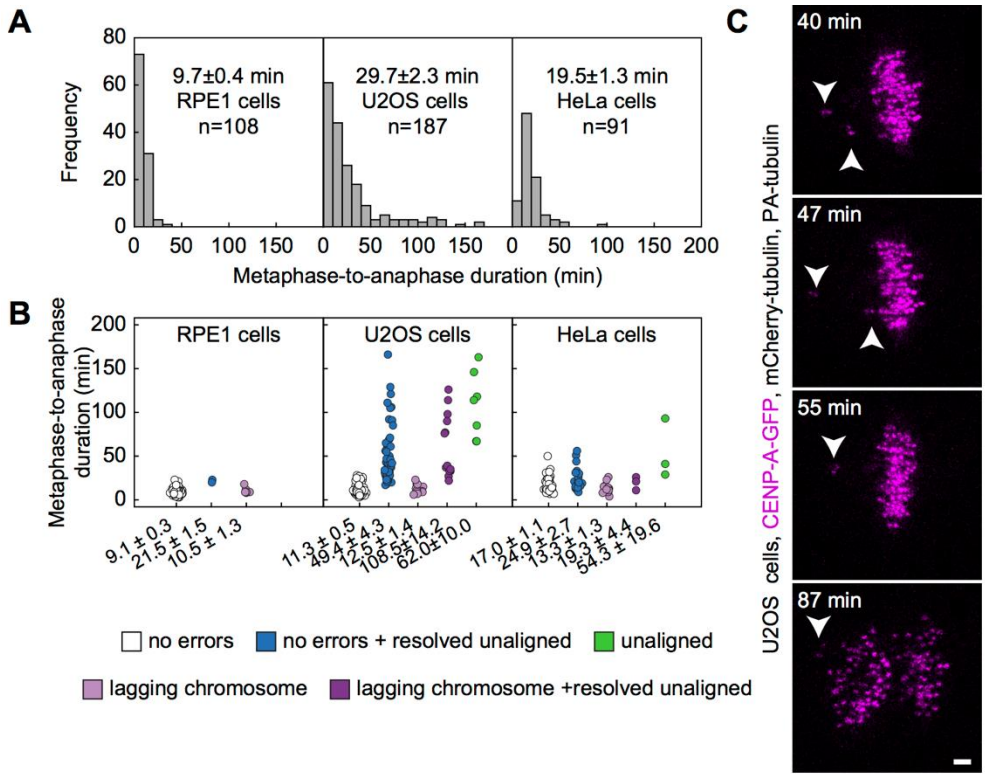


Figure 28. Cells with chromosome alignment defects exhibit prolonged metaphase duration. (**A**) Metaphase-to-anaphase duration in RPE1, U2OS, and HeLa cells (from left to right). (**B**) Metaphase-to-anaphase duration with respect to underlying chromosome segregation error in RPE1, U2OS, and HeLa cells (from left to right). Chromosome segregation errors are color-coded according to the legend at the bottom. Note that resolved unaligned category is defined as unaligned chromosomes in metaphase that become aligned, i.e. resolved, before anaphase. (**C**) Time-lapse images of U2OS cells with stable expression of CENP-A-GFP, mCherry-α-tubulin, and PA-GFP-α-tubulin. Arrows point to misaligned kinetochores that are either aligned, i.e. resolved, before anaphase onset or persist through anaphase. Scale bar, 2 μm.

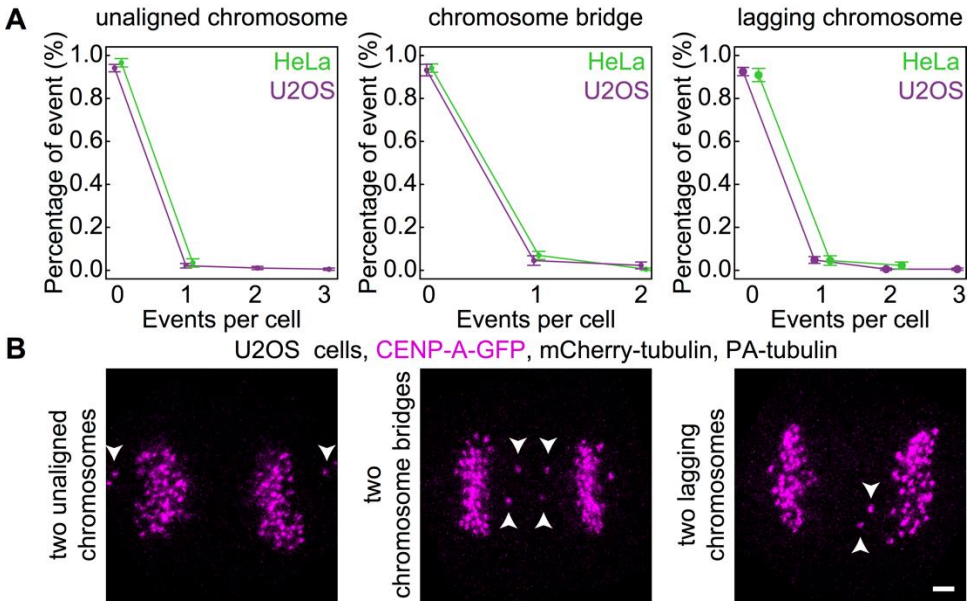


Figure 29. Multiple same-type errors can occur in individual cells. (**A**) Percentage of chromosome segregation errors as events occurring in U2OS and HeLa cells. Graphs show unaligned chromosomes, chromosome bridges, and lagging chromosomes (from left to right). (**B**) Stills from U2OS cells with stable expression of CENP-A-GFP, mCherry-α-tubulin, and PA-GFP-α-tubulin. Arrows point to two sets of misaligned sister kinetochores (left), two sets of kinetochore pairs associated with chromosome bridges (middle), and two lagging kinetochores associated with lagging chromosomes (right). Scale bar, 2 µm.

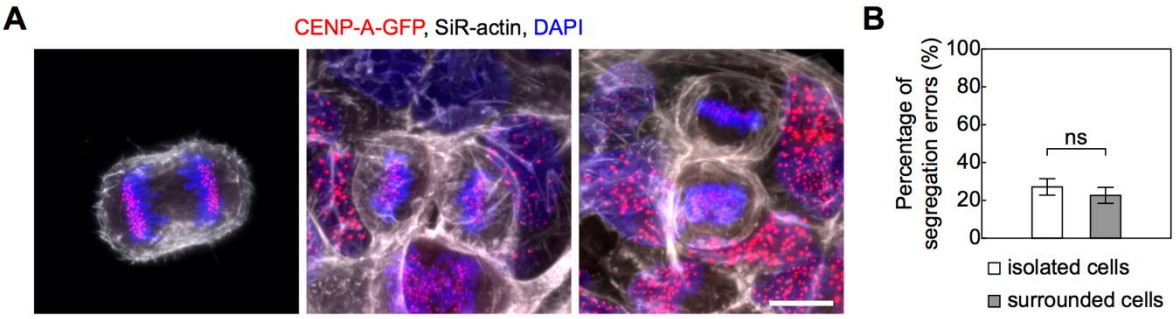


Figure 30. Chromosome segregation errors in isolated and surrounded cells. (**A**) U2OS cells with stable expression of CENP-A-GFP (red) micropatterned on islets of different sizes. Cells are dyed with SiR-actin (grey) and DAPI (blue) and labelled with tubulin-AF-594 (not shown). Cells were categorized as isolated (left) if no other cell was in proximity, and surrounded if exhibited 100% of contact. Scale bar, 10 µm. (**B**) Percentage of chromosome segregation errors assessed in anaphases of isolated and surrounded cells.

5. DISCUSSION

5.1. Flux-driven centering model explains kinetochore alignment at the equatorial plane

Based on results from speckle microscopy that allowed me to measure the relative movements of kinetochore and bridging microtubules, I propose that microtubule poleward flux promotes kinetochore centering. Motor proteins within the overlaps of k-fibers and bridging microtubules generate sliding forces proportional to the overlap length, which drive the poleward flux of the k-fiber. Thus, the flux of a longer sister k-fiber is faster than the flux of the shorter one, resulting in a tug-of-war in which the longer k-fiber wins and the kinetochores move towards the spindle center (**Figure 31A**). This key feature of the centering mechanism was indeed observed in experiments where I tracked speckles on k-fibers of different lengths.

The flux-driven centering mechanism proposed here and the previously introduced centering forces based on length-dependent suppression of k-fiber dynamics (Gardner et al., 2008; Mary et al., 2015; Gergely et al., 2016; Klemm et al., 2018) as well as on polar ejection forces (Joglekar and Hunt, 2002; Civelekoglu-Scholey et al., 2006, 2013; Armond et al., 2015) are conceptually independent. Yet, proteins such as Kif18A and Kif4A may be involved in more than one mechanism: in addition to their role in regulating bridging microtubule overlap, Kif18A regulates k-fiber dynamics (Stumpff et al., 2008) and Kif4A is a chromokinesin that affects the flux by pushing on chromosome arms (Steblyanko et al., 2020). Diverse centering mechanisms may work together but with different efficiency depending on the cell type and the stage of spindle assembly. Due to the complexity of the spindle, it is hard to dissect the contribution of different mechanisms by using only experimental approaches (Tolić and Pavin, 2021), but future theoretical studies that would include multiple microtubules, regulation of their plus-end dynamics, microtubule nucleation along pre-existing microtubules, and polar ejection forces should help to identify the role of each mechanism.

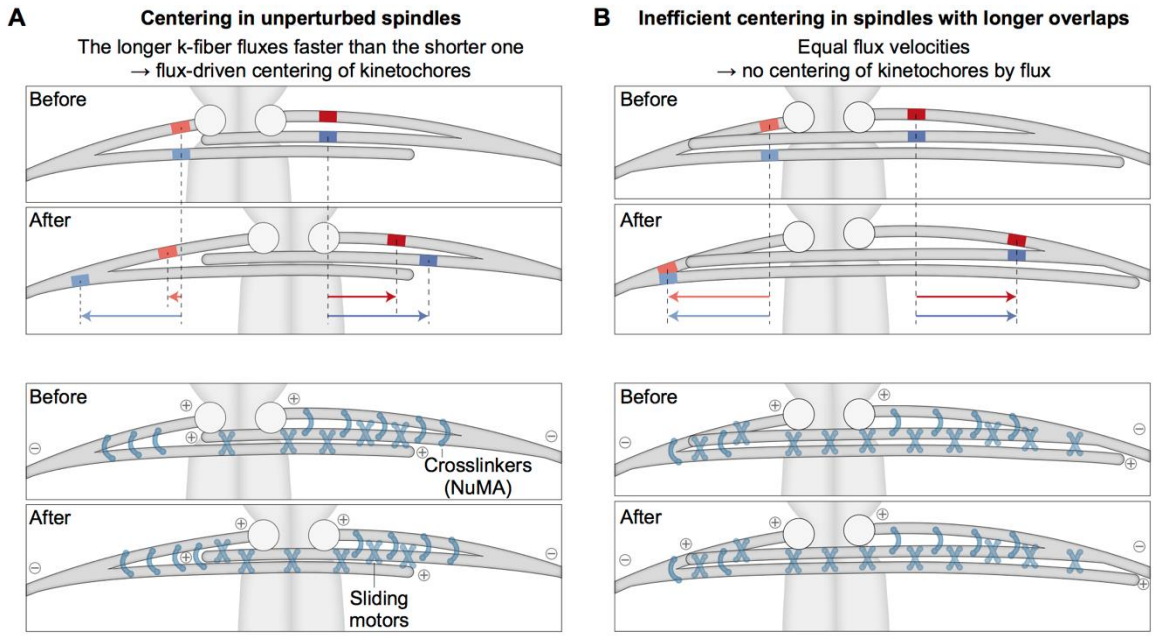


Figure 31. The mechanism by which poleward flux promotes kinetochore centering. (**A**) A pair of kinetochores (circles) is displaced towards the left (top; before). To visualize the relative movements of the microtubules, four marks are shown (red and blue). Over time (top; after), the marks on the bridging microtubules move poleward by a similar distance (arrows), whereas the marks on the k-fibers move more slowly due to imperfect coupling between the bridging and k-fibers. Importantly, the longer k-fiber on the right side (bottom; before) has a longer overlap with the bridging fiber and thus the coupling is stronger, leading to a higher flux velocity of this fiber in comparison with the shorter k-fiber, which in turn results in the movement of the kinetochores towards the spindle center (bottom; after). (**B**) If the coupling between the k-fibers and the bridging fiber is too strong, such as in cases when the antiparallel overlaps are excessively long, the k-fibers flux velocity becomes similar to the velocity of the bridging fiber. Thus, k-fibers do not slide with respect to the bridging fiber, resulting in chromosome misalignment.

5.2. Kinetochore fiber flux is driven by interactions with the bridging fiber

By developing a speckle microscopy assay based on low doses of SiR-tubulin to distinguish kinetochore and bridging microtubules, this work demonstrated that bridging microtubules undergo poleward flux and this flux is faster than that of kinetochore microtubules. In contrast to metaphase, k-fibers and bridging fibers slide together at a similar rate in early anaphase (Vukušić et al., 2017). This difference is most likely due to the tension between sister

kinetochores, which is present in metaphase when sister kinetochores are linked by chromatin, but not in anaphase when this link vanishes. By using various siRNA-mediated protein depletions, I was able to increase or decrease the difference in the metaphase flux velocities, but the k-fiber flux remained slower or equal to the bridging fiber flux, suggesting that motor proteins and crosslinkers regulate the relationship between these two velocities. Interestingly, a slower flux of kinetochore microtubules than adjacent non-kinetochore ones was observed in *Xenopus* egg extracts (Maddox et al., 2003; Yang et al., 2008) and crane-fly spermatocytes (LaFountain et al., 2004), indicating that the relationship between the flux of these two sets of microtubules is conserved across organisms whose spindles undergo flux. As the flux-driven centering mechanism relies on this difference, I propose that flux could promote chromosome centering in a variety of organisms.

Two flux velocities have been observed also in human U2OS cells, where the subset of microtubules fluxing faster than kinetochore microtubules was associated with the γ-tubulin ring complex (γTuRC) (Lecland and Lüders, 2014). γTuRC is recruited to microtubules by the augmin complex to nucleate new microtubules (Kamasaki et al., 2013; Uehara et al., 2009; David et al., 2019; Goshima et al., 2008), including nucleation of bridging microtubules along k-fibers (Manenica et al., 2020; O'Toole et al., 2020). Thus, the fast flux of bridging microtubules in comparison with k-fibers measured here likely corresponds to the fast γTuRC-nucleated microtubule fraction. My observation that the flux of bridging microtubules slowed down after depletion of the augmin subunit Haus8 supports this conclusion.

In spindles without k-fibers, i.e, after Ndc80 depletion, or with chromosomes completely detached from the spindle, i.e., after Ndc80 depletion and Aurora B inhibition, the flux velocity of antiparallel overlapping non-kinetochore microtubules, which I interpret to be speckles on bridging microtubules, was similar to that of bridging fibers in untreated cells, showing that bridging fiber flux is largely unaffected by k-fibers. This result, together with the faster flux of bridging fibers in comparison with k-fibers across treatments, suggests that bridging fibers drive the poleward flux of k-fibers. The forces driving poleward flux have been debated, where the dominant forces are thought to be either at the spindle pole (Rogers et al., 2004; Ganem et al., 2005) or within interpolar microtubules (Miyamoto et al., 2004; Brust-Mascher et al., 2009; Matos et al., 2009). Thus, my experiments are in agreement with the latter possibility and support the assumption that the leading forces are generated within antiparallel overlaps.

In this model, sliding may be coupled to depolymerization at spindle poles, as it was previously suggested by Miyamoto et al., (2004) and Brust-Mascher et al., (2009).

Depolymerization of bridging and kinetochore microtubules at the poles would then maintain a constant spindle length. The maintenance of constant spindle length is thought to be disrupted by the termination of depolymerization of interpolar microtubules at spindle poles which then because of the lack of depolymerization at minus ends starts anaphase spindle elongation (Cheerambathur et al., 2007). Given that bridging microtubules flux at faster rates than kinetochore microtubules, it would be important to test at what positions and rates depolymerization of bridging microtubule minus ends occurs with respect to kinetochore microtubules.

I found that the depletion of NuMA, a passive crosslinker of microtubules (Elting et al., 2017), decreases the poleward flux of kinetochore microtubules without affecting the flux of bridging microtubules. As the model developed in Risteski et al., (2021a) predicts slower k-fiber flux for decreased amount of passive crosslinkers, my experiments together with the model suggest that NuMA transmits the force from the bridging onto the k-fibers. Interestingly, NuMA depletion was shown to cause asynchrony of microtubule poleward flux (Steblyanko et al., 2020), implying that NuMA crosslinks neighboring k-fibers and synchronizes their flux. I suggest that the synchrony in the poleward flux of neighboring k-fibers is reflected in the correlated movement of neighboring kinetochore pairs (Vladimirou et al., 2013). In addition to NuMA, bridging microtubules may promote synchrony in k-fiber flux as bridging microtubules were shown to fan out at their ends and interact with neighboring k-fibers (O'Toole et al., 2020).

Depletion of PRC1 did not change the flux velocity of bridging or kinetochore microtubules, in agreement with a previous study (Steblyanko et al., 2020). Similarly, PRC1 depletion does not affect the sliding of bridging microtubules and spindle elongation in anaphase (Vukušić et al., 2021). As PRC1 depletion leads to a ~50% decrease in the number of microtubules in the bridging fiber in metaphase (Jagrić et al., 2021), my result suggests that the remaining bridging microtubules are sufficient to generate flux. In contrast to PRC1, depletion of augmin, which decreases the number of bridging microtubules to a larger extent than PRC1 (Manenica et al., 2020), led to slower bridging fiber flux. This was accompanied by the slower k-fiber flux in agreement with the model prediction for slower sliding velocity of bridging microtubules. Beside augmin, MKLP1 depletion led to a decrease in k-fiber and bridging fiber flux velocities. Given that MKLP1 localizes to the bridging fibers in metaphase and anaphase and is involved in anaphase spindle elongation (Jagrić et al., 2021; Vukušić et al., 2021), this motor may contribute to antiparallel sliding within bridging fiber overlaps. Additionally, CENP-E siRNA-depletion reduced poleward flux rates, likely due to the role of CENP-E in targeting CLASPs, which promote flux, to kinetochores (Maiato et al., 2005; Maffini et al.,

2009; Girão et al., 2020). Even though in the theoretical model (Risteski et al., 2021a) the sliding of antiparallel microtubules is driven by motor proteins with the same physical properties, previous work (Steblyanko et al., 2020) and my experiments suggest that multiple different motor proteins contribute to sliding in real spindles. These motors may have different physical properties and thus bring new phenomena to the flux-driven centering mechanism by affecting sliding forces.

5.3. Chromosome alignment depends on the overlap length of bridging microtubules

In the proposed mechanism, the length of antiparallel overlaps determines the flux velocity of k-fibers and kinetochore centering. If overlaps are longer, the coupling between bridging and k-fibers increases, leading to an increase in the k-fiber flux velocity to the bridging fiber flux velocity. This prevents the sliding of k-fibers along the bridging fiber and results in worse kinetochore centering (**Figure 31B**).

My experiments with depletions of spindle proteins revealed a trend where kinetochores are misaligned when overlaps are longer and k-fiber flux is faster. For example, depletion of Kif18A resulted in extended overlaps, faster k-fiber flux, and misaligned chromosomes. I propose that Kif18A regulates chromosome alignment by the flux-driven centering mechanism, where this motor protein controls k-fiber flux through the regulation of the length of antiparallel overlaps between bridging and k-fibers. Previous work showing that Kif18A is localized within bridging fibers in addition to k-fibers (Jagrić et al., 2021) supports this possibility. This mechanism may work together with the known mechanism where Kif18A suppresses the dynamics of longer k-fibers at their plus ends (Stumpff et al., 2012; Du et al., 2010) (Stumpff et al., 2012; Du et al., 2010). To understand the roles of the Kif18A motors localized within bridging fibers versus those on k-fibers in chromosome alignment, it will be crucial to develop approaches based on separation-of-function experiments.

In contrast to depletions of Kif18A alone or in combination with Kif4A and PRC1, depletion of Kif4A alone showed no effect on chromosome alignment even though the overlaps of bridging microtubules were extended, and the k-fiber flux was faster. On the other hand, the elimination of microtubule poleward flux by co-depletion of Kif2A and MCAK was shown not to hinder chromosome alignment in U2OS cells (Ganem et al., 2005). These results are possible due to the activity of Kif18A at the k-fiber tips. Yet, it is important to test the effect of Kif2A and MCAK on poleward flux and chromosome alignment in RPE1 cells. Additionally, the degree of kinetochore centering was not perturbed upon depletion of a fiber coupler, i.e. NuMA.

In the presented mechanism, this is achieved by motors in antiparallel regions which are, unlike parallel crosslinks between bridging and k-fiber, not eliminated.

Whereas in the theoretical model the relationship between k-fiber flux and kinetochore centering was observed by varying a single parameter (Risteski et al., 2021a), experimental perturbations relied on the depletion of motor proteins, which have multiple functions within the spindle. Thus, the interpretation in light of the model is not always straightforward. For example, a closer comparison between experiments and the model could be achieved by extending the model to include the regulation of the length of bridging and kinetochore microtubules by Kif18A, as in this case, one could explore the resulting overlap length and kinetochore positions after changing Kif18A concentration in the model.

5.4. Chromosome alignment defect leads to aneuploidy

Based on the assessment of chromosome segregation errors after live imaging of human cells, I found that cells with chromosome alignment defects, in which chromosomes are unaligned at the anaphase onset, are prone to undergo nondisjunction events. Here, both chromosomes of the pair passed to the same cell, which gave rise to aneuploid daughters. These experimental data are direct evidence that chromosome alignment is necessary for chromosome segregation fidelity. Similarly, a recent study has shown that chromosome alignment ensures mitotic fidelity as the loss of chromosome alignment leads to inter-chromosomal compaction defects during anaphase, abnormal organization of chromosomes into a single nucleus, and the formation of micronuclei (Fonseca et al., 2019).

By inspecting a non-transformed, i.e. RPE1, and two cancer cell lines, i.e. U2OS and HeLa, I observed that RPE1 cells do not acquire an aneuploid state due to persistently unaligned chromosomes. This could be due to chromosome missegregation being a rare event in non-transformed human cells as pre-anaphase error correction infrequently fails (Thompson and Compton, 2008; Bakhoum et al., 2009b; a), thus making persistently unaligned chromosomes difficult to detect. In agreement with this, it was proposed that cells with normal tubulin dynamics and a functional spindle assembly checkpoint have a very low chromosome missegregation rate (Schukken et al., 2020). Moreover, the same study proposed that altered microtubule dynamics and spindle assembly checkpoint increase the number of unaligned chromosomes that are not signaled by the spindle assembly checkpoint, leading to increased rates of chromosome missegregation (Schukken et al., 2020). However, my experimental data on both U2OS and HeLa cells show that these cells are spindle assembly checkpoint-proficient,

as the presence of unaligned kinetochores delays anaphase onset. Thus, I speculate that aneuploidy due to persistently unaligned chromosomes in prolonged metaphases occurs eventually due to spindle assembly checkpoint override. Similarly, a recent study showed that misaligned chromosomes may become ensheathed by endomembranes which may delay mitosis in a spindle assembly checkpoint–dependent manner, and if the checkpoint is extinguished in the absence of congression it leads to chromosome missegregation (Ferrandiz et al., 2022).

Across the siRNA treatments that perturb microtubule poleward flux in the spindles, it was found that the spindle length was also altered. For example, in spindles where spindle length is increased, the k-fiber flux increases, or vice versa (Steblyanko et al., 2020). This could be due to increased microtubule dynamics, as microtubule growth rate was shown to control spindle length (Lacroix et al., 2018). This is in line with measured spindle and overlap lengths in RPE1, U2OS, and HeLa cells, as non-transformed cells exhibit larger lengths than cancer cells (**Table 1**) (Jagrić et al., 2021). Interestingly, it was observed that, unlike non-transformed cells, cancer cells exhibit altered chromosome dynamics at the spindle equator. The difference between non-transformed and cancer cell lines was even more pronounced for those cancer cell lines which are categorized as undergoing chromosomal instability (Iemura et al., 2021). Furthermore, RPE1 cells exhibit higher microtubule poleward flux rates with respect to previously reported rates in HeLa and U2OS cells (Ganem et al., 2005; Steblyanko et al., 2020; Ma et al., 2010). Therefore, is altered chromosome dynamics, as a property of cancer cell lines, a consequence of altered microtubule poleward flux? Surprisingly, the ratio of previously reported k-fiber flux to the fast flux of γTuRC-nucleated microtubule fraction in U2OS cells (Lecland and Lüders, 2014), which I presume are bridging microtubules, was much lower than one measured here in RPE1 cells. This suggests that cancer cells have altered microtubule dynamics compared to non-transformed cells, and that underlying flux-driven centering could be perturbed. Indeed, it was shown that cancer cells that have whole genome doubling, often have Kif18A overexpression (Quinton et al., 2021). As Kif18A is a motor protein that affects chromosome alignment and microtubule poleward flux, I speculate that cancer cells have enhanced chromosome missegregations due to chromosome alignment defects driven by a perturbed flux-dependent centering mechanism.

6. CONCLUSION

My work suggests a new mechanism of kinetochore alignment where lateral length-dependent sliding forces that the bridging fiber exerts onto k-fibers promote the movement of kinetochores towards the spindle center. In this mechanism, bridging microtubules slide apart and this sliding is transmitted to kinetochore microtubules. The longer the overlaps between kinetochore and bridging microtubules, the larger the forces, resulting in a net force towards the spindle center. I propose that this mechanism based on length-dependent relative sliding of kinetochore along bridging microtubules works together with the length-dependent regulation of microtubule dynamics and polar ejection forces to ensure alignment of kinetochores at the equatorial plane of the spindle in metaphase. The centering mechanism based on sliding opens an attractive new avenue of research on the molecular players involved in the sliding of bridging fibers, regulation of their plus and minus ends, and their coupling with k-fibers. Whereas this study was focused on kinetochore alignment during metaphase, the same mechanism may also reinforce spindle assembly in prometaphase by supporting chromosome congression to the metaphase plate. Given that spindles in prometaphase undergo poleward flux (Steblyanko et al., 2020), future experiments will reveal whether and how it contributes to chromosome congression.

The physiological importance of chromosome alignment is in preventing unaligned chromosomes-driven aneuploidy, as shown here, but also lagging chromosomes and the appearance of micronuclei, thereby promoting proper nuclear reformation and karyotype stability (Fonseca et al., 2019; Maiato et al., 2017). It will be interesting to explore the robustness of the flux-driven chromosome alignment and the resulting segregation fidelity in healthy cells. Even more importantly, as my results demonstrate that unaligned chromosomes can lead to aneuploidy, future work should reveal what aberrations in this mechanism lead to errors in chromosome segregation in cells with unstable karyotypes in which misaligned chromosomes appear.

7. REFERENCES

Akhmanova, A., and M.O. Steinmetz. 2019. Microtubule minus-end regulation at a glance. *J. Cell Sci.* 132. doi:10.1242/jcs.227850.

Al-Bassam, J., and F. Chang. 2011. Regulation of microtubule dynamics by TOG-domain proteins XMAP215/Dis1 and CLASP. *Trends Cell Biol.* 21:604–614. doi:10.1016/j.tcb.2011.06.007.

Al-Bassam, J., H. Kim, G. Brouhard, A. van Oijen, S.C. Harrison, and F. Chang. 2010. CLASP promotes microtubule rescue by recruiting tubulin dimers to the microtubule. *Dev. Cell*. 19:245–258. doi:10.1016/j.devcel.2010.07.016.

Alberts, B., A. Johnson, J. Lewis, M. Raff, K. Roberts, and P. Walter. 2002. Molecular Biology of the Cell. Garland Science, New York.

Antonio, C., I. Ferby, H. Wilhelm, M. Jones, E. Karsenti, A.R. Nebreda, and I. Vernos. 2000. Xkid, a chromokinesin required for chromosome alignment on the metaphase plate. *Cell*. 102:425–435. doi:10.1016/s0092-8674(00)00048-9.

Armond, J.W., E.F. Harry, A.D. McAinsh, and N.J. Burroughs. 2015. Inferring the forces controlling metaphase kinetochore oscillations by reverse engineering system dynamics. *PLoS Comput. Biol.* 11:1–26. doi:10.1371/journal.pcbi.1004607.

Ault, J.G., A.J. DeMarco, E.D. Salmon, and C.L. Rieder. 1991. Studies on the ejection properties of asters: astral microtubule turnover influences the oscillatory behavior and positioning of mono-oriented chromosomes. *J. Cell Sci.* 99:701–710. doi:10.1242/jcs.99.4.701.

Ault, J.G., and R.B. Nicklas. 1989. Tension, microtubule rearrangements, and the proper distribution of chromosomes in mitosis. *Chromosoma*. 98:33–39. doi:10.1007/BF00293332.

Azioune, A., N. Carpi, Q. Tseng, M. Théry, and M. Piel. 2010. Protein micropatterns: A direct printing protocol using deep UVs. *Methods Cell Biol.* 97:133–146. doi:10.1016/S0091-679X(10)97008-8.

Bajer, A.S., C. Cypher, J. Molè-Bajer, and H.M. Howard. 1982. Taxol-induced anaphase reversal: evidence that elongating microtubules can exert a pushing force in living cells. *Proc. Natl. Acad. Sci. U. S. A.* 79:6569–6573. doi:10.1073/pnas.79.21.6569.

Bakhoum, S.F., G. Genovese, and D.A. Compton. 2009a. Deviant kinetochore microtubule dynamics underlie chromosomal instability. *Curr. Biol.* 19:1937–1942. doi:10.1016/j.cub.2009.09.055.

Bakhoum, S.F., L. Kabeche, J.P. Murnane, B.I. Zaki, and D.A. Compton. 2014. DNA-damage response during mitosis induces whole-chromosome missegregation. *Cancer Discov.* 4:1281–1289. doi:10.1158/2159-8290.CD-14-0403.

Bakhoum, S.F., S.L. Thompson, A.L. Manning, and D.A. Compton. 2009b. Genome stability is ensured by temporal control of kinetochore-microtubule dynamics. *Nat. Cell Biol.* 11:27–35. doi:10.1038/ncb1809.

Barber, T.D., K. McManus, K.W.Y. Yuen, M. Reis, G. Parmigiani, D. Shen, I. Barrett, Y. Nouhi, F. Spencer, S. Markowitz, V.E. Velculescu, K.W. Kinzler, B. Vogelstein, C. Lengauer, and P. Hieter. 2008. Chromatid cohesion defects may underlie chromosome instability in human colorectal cancers. *Proc. Natl. Acad. Sci. U. S. A.* 105:3443–3448. doi:10.1073/pnas.0712384105.

Barisic, M., P. Aguiar, S. Geley, and H. Maiato. 2014. Kinetochore motors drive congression of peripheral polar chromosomes by overcoming random arm-ejection forces. *Nat. Cell Biol.* 16:1249–1256. doi:10.1038/ncb3060.

Barisic, M., R. Silva e Sousa, S.K. Tripathy, M.M. Magiera, A. V Zaytsev, A.L. Pereira, C. Janke, E.L. Grishchuk, and H. Maiato. 2015. Mitosis. Microtubule detyrosination guides chromosomes during mitosis. *Science*. 348:799–803. doi:10.1126/science.aaa5175.

Ben-David, U., and A. Amon. 2020. Context is everything: aneuploidy in cancer. *Nat. Rev. Genet.* 21:44–62. doi:10.1038/s41576-019-0171-x.

Bieling, P., I.A. Telley, and T. Surrey. 2010. A minimal midzone protein module controls formation and length of antiparallel microtubule overlaps. *Cell*. 142:420–432. doi:10.1016/j.cell.2010.06.033.

Birchler, J.A., and R.A. Veitia. 2012. Gene balance hypothesis: connecting issues of dosage sensitivity across biological disciplines. *Proc. Natl. Acad. Sci. U. S. A.* 109:14746–14753. doi:10.1073/pnas.1207726109.

Brouhard, G.J., and A.J. Hunt. 2005. Microtubule movements on the arms of mitotic chromosomes: polar ejection forces quantified in vitro. *Proc. Natl. Acad. Sci. U. S. A.* 102:13903–13908. doi:10.1073/pnas.0506017102.

Brust-Mascher, I., P. Sommi, D.K. Cheerambathur, and J.M. Scholey. 2009. Kinesin-5-dependent poleward flux and spindle length control in *Drosophila* embryo mitosis. *Mol. Biol. Cell*. 20:1749–1762. doi:10.1091/mbc.e08-10-1033.

Buđa, R., K. Vukušić, and I.M. Tolić. 2017. Dissection and characterization of microtubule bundles in the mitotic spindle using femtosecond laser ablation. *Methods Cell Biol.* 139:81–101. doi:10.1016/bs.mcb.2016.11.007.

Cameron, L.A., G. Yang, D. Cimini, J.C. Canman, O. Kisurina-Evgenieva, A. Khodjakov, G. Danuser, and E.D. Salmon. 2006. Kinesin 5-independent poleward flux of kinetochore microtubules in PtK1 cells. *J. Cell Biol.* 173:173–179. doi:10.1083/jcb.200601075.

Campàs, O., and P. Sens. 2006. Chromosome oscillations in mitosis. *Phys. Rev. Lett.* 97:128102. doi:10.1103/PhysRevLett.97.128102.

Cane, S., A.A. Ye, S.J. Luks-Morgan, and T.J. Maresca. 2013. Elevated polar ejection forces

stabilize kinetochore-microtubule attachments. *J. Cell Biol.* 200:203–218. doi:10.1083/jcb.201211119.

Catalán, J., G.C.-M. Falck, and H. Norppa. 2000. The X chromosome frequently lags behind in female lymphocyte anaphase. *Am. J. Hum. Genet.* 66:687–691. doi:10.1086/302769.

Cerami, E., J. Gao, U. Dogrusoz, B.E. Gross, S.O. Sumer, B.A. Aksoy, A. Jacobsen, C.J. Byrne, M.L. Heuer, E. Larsson, Y. Antipin, B. Reva, A.P. Goldberg, C. Sander, and N. Schultz. 2012. The cBio cancer genomics portal: an open platform for exploring multidimensional cancer genomics data. *Cancer Discov.* 2:401–404. doi:10.1158/2159-8290.CD-12-0095.

Cheerambathur, D.K., G. Civelekoglu-Scholey, I. Brust-Mascher, P. Sommi, A. Mogilner, and J.M. Scholey. 2007. Quantitative analysis of an anaphase B switch: predicted role for a microtubule catastrophe gradient. *J. Cell Biol.* 177:995–1004. doi:10.1083/jcb.200611113.

Cheeseman, I.M., J.S. Chappie, E.M. Wilson-Kubalek, and A. Desai. 2006. The conserved KMN network constitutes the core microtubule-binding site of the kinetochore. *Cell*. 127:983–997. doi:10.1016/j.cell.2006.09.039.

Cheeseman, I.M., and A. Desai. 2008. Molecular architecture of the kinetochore-microtubule interface. *Nat. Rev. Mol. Cell Biol.* 9:33–46. doi:10.1038/nrm2310.

Chen, G., W.A. Mulla, A. Kucharavy, H.-J. Tsai, B. Rubinstein, J. Conkright, S. McCroskey, W.D. Bradford, L. Weems, J.S. Haug, C.W. Seidel, J. Berman, and R. Li. 2015. Targeting the adaptability of heterogeneous aneuploids. *Cell*. 160:771–784. doi:10.1016/j.cell.2015.01.026.

Chen, G., B. Rubinstein, and R. Li. 2012. Whole chromosome aneuploidy: big mutations drive adaptation by phenotypic leap. *Bioessays*. 34:893–900. doi:10.1002/bies.201200069.

Cimini, D. 2003. Merotelic kinetochore orientation occurs frequently during early mitosis in mammalian tissue cells and error correction is achieved by two different mechanisms. *J. Cell Sci.* 116:4213–4225. doi:10.1242/jcs.00716.

Cimini, D., L.A. Cameron, and E.D. Salmon. 2004. Anaphase spindle mechanics prevent mis-segregation of merotelically oriented chromosomes. *Curr. Biol.* 14:2149–2155. doi:10.1016/j.cub.2004.11.029.

Cimini, D., and F. Degrassi. 2005. Aneuploidy: A matter of bad connections. *Trends Cell Biol.* 15:442–451. doi:10.1016/j.tcb.2005.06.008.

Cimini, D., D. Fioravanti, E.D. Salmon, and F. Degrassi. 2002. Merotelic kinetochore orientation versus chromosome mono-orientation in the origin of lagging chromosomes in human primary cells. *J. Cell Sci.* 115:507–15. doi:10.1007/s00120-014-3434-3.

Cimini, D., B. Howell, P. Maddox, A. Khodjakov, F. Degrassi, and E.D. Salmon. 2001. Merotelic kinetochore orientation is a major mechanism of aneuploidy in mitotic mammalian tissue cells. *J. Cell Biol.* 152:517–527. doi:10.1083/jcb.153.3.517.

Civelekoglu-Scholey, G., B. He, M. Shen, X. Wan, E. Roscioli, B. Bowden, and D. Cimini. 2013. Dynamic bonds and polar ejection force distribution explain kinetochore oscillations in PtK1 cells. *J. Cell Biol.* 201:577–593. doi:10.1083/jcb.201301022.

Civelekoglu-Scholey, G., D.J. Sharp, A. Mogilner, and J.M. Scholey. 2006. Model of chromosome motility in *Drosophila* embryos: Adaptation of a general mechanism for rapid mitosis. *Biophys. J.* 90:3966–3982. doi:10.1529/biophysj.105.078691.

Claussen, U., A. Mazur, and N. Rubtsov. 1994. Chromosomes are highly elastic and can be stretched. *Cytogenet. Cell Genet.* 66:120–125. doi:10.1159/000133681.

Cortés-Ciriano, I., J.J.-K. Lee, R. Xi, D. Jain, Y.L. Jung, L. Yang, D. Gordenin, L.J. Klimczak, C.-Z. Zhang, D.S. Pellman, and P.J. Park. 2020. Comprehensive analysis of chromothripsis in 2,658 human cancers using whole-genome sequencing. *Nat. Genet.* 52:331–341. doi:10.1038/s41588-019-0576-7.

Crasta, K., N.J. Ganem, R. Dagher, A.B. Lantermann, E. V Ivanova, Y. Pan, L. Nezi, A. Protopopov, D. Chowdhury, and D. Pellman. 2012. DNA breaks and chromosome pulverization from errors in mitosis. *Nature*. 482:53–58. doi:10.1038/nature10802.

Czaban, B.B., A. Forer, and A.S. Bajer. 1993. Ultraviolet microbeam irradiation of chromosomal spindle fibres in *Haemanthus katherinae* endosperm. I. Behaviour of the irradiated region. *J. Cell Sci.* 105:571–578. doi:10.1242/jcs.105.2.571.

Darlington, C.D. 1937. Recent advances in cytology. P. Blakiston's Son & Co., Inc., Philadelphia.

David, A.F., P. Roudot, W.R. Legant, E. Betzig, G. Danuser, and D.W. Gerlich. 2019. Augmin accumulation on long-lived microtubules drives amplification and kinetochore-directed growth. *J. Cell Biol.* 218:2150–2168. doi:10.1083/jcb.201805044.

Dephoure, N., S. Hwang, C. O'Sullivan, S.E. Dodgson, S.P. Gygi, A. Amon, and E.M. Torres. 2014. Quantitative proteomic analysis reveals posttranslational responses to aneuploidy in yeast. *Elife*. 3:e03023. doi:10.7554/eLife.03023.

Desai, A., and T.J. Mitchison. 1997. Microtubule polymerization dynamics. *Annu. Rev. Cell Dev. Biol.* 13:83–117. doi:10.1146/annurev.cellbio.13.1.83.

Dogterom, M., and S. Leibler. 1993. Physical aspects of the growth and regulation of microtubule structures. *Phys. Rev. Lett.* 70:1347–1350. doi:10.1103/PhysRevLett.70.1347.

Dogterom, M., and B. Yurke. 1997. Measurement of the force-velocity relation for growing microtubules. *Science*. 278:856–860. doi:10.1126/science.278.5339.856.

Du, Y., C.A. English, and R. Ohi. 2010. The kinesin-8 Kif18A dampens microtubule plus-end dynamics. *Curr. Biol.* 20:374–380. doi:10.1016/j.cub.2009.12.049.

Dudka, D., A. Noatynska, C.A. Smith, N. Liaudet, A.D. McAinsh, and P. Meraldi. 2018.

Complete microtubule-kinetochore occupancy favours the segregation of merotelic attachments. *Nat. Commun.* 9:2042. doi:10.1038/s41467-018-04427-x.

Elting, M.W., M. Prakash, D.B. Udy, and S. Dumont. 2017. Mapping load-bearing in the mammalian spindle reveals local kinetochore fiber anchorage that provides mechanical isolation and redundancy. *Curr. Biol.* 27:2112-2122.e5. doi:10.1016/j.cub.2017.06.018.

Endesfelder, D., R. Burrell, N. Kanu, N. McGranahan, M. Howell, P.J. Parker, J. Downward, C. Swanton, and M. Kschischo. 2014. Chromosomal instability selects gene copy-number variants encoding core regulators of proliferation in ER+ breast cancer. *Cancer Res.* 74:4853–4863. doi:10.1158/0008-5472.CAN-13-2664.

Ertych, N., A. Stolz, A. Stenzinger, W. Weichert, S. Kaulfuß, P. Burfeind, A. Aigner, L. Wordeman, and H. Bastians. 2014. Increased microtubule assembly rates influence chromosomal instability in colorectal cancer cells. *Nat. Cell Biol.* 16:779–791. doi:10.1038/ncb2994.

Ferrandiz, N., L. Downie, G.P. Starling, and S.J. Royle. 2022. Endomembranes promote chromosome missegregation by ensheathing misaligned chromosomes. *J. Cell Biol.* 221:e202203021. doi:10.1083/jcb.202203021.

Finardi, A., L.F. Massari, and R. Visintin. 2020. Anaphase bridges: Not all natural fibers are healthy. *Genes (Basel).* 11:902. doi:10.3390/genes11080902.

Foley, E.A., and T.M. Kapoor. 2013. Microtubule attachment and spindle assembly checkpoint signalling at the kinetochore. *Nat. Rev. Mol. Cell Biol.* 14:25–37. doi:10.1038/nrm3494.

Fonseca, C.L., H.L.H. Malaby, L.A. Sepaniac, W. Martin, C. Byers, A. Czechanski, D. Messinger, M. Tang, R. Ohi, L.G. Reinholdt, and J. Stumpff. 2019. Mitotic chromosome alignment ensures mitotic fidelity by promoting interchromosomal compaction during anaphase. *J. Cell Biol.* 218:1148–1163. doi:10.1083/jcb.201807228.

Ford, J.H., C.J. Schultz, and A.T. Correll. 1988. Chromosome Elimination in Micronuclei: A Common Cause of Hypoploidy. *Am. J. Hum. Genet*. 43:733–740.

Forer, A. 1965. Local reduction of spindle fiber birefringence in living *Nephrotoma suturalis* (Loew) spermatocytes induced by ultraviolet microbeam irradiation. *J. Cell Biol*. 25:95–117. doi:10.1083/jcb.25.1.95.

Funabiki, H., and A.W. Murray. 2000. The *Xenopus* chromokinesin Xkid is essential for metaphase chromosome alignment and must be degraded to allow anaphase chromosome movement. *Cell*. 102:411–424. doi:10.1016/s0092-8674(00)00047-7.

Gandhi, R., S. Bonaccorsi, D. Wentworth, S. Doxsey, M. Gatti, and A. Pereira. 2004. The *Drosophila* kinesin-like protein KLP67A is essential for mitotic and male meiotic spindle assembly. *Mol. Biol. Cell*. 15:121–131. doi:10.1091/mbc.e03-05-0342.

Ganem, N.J., K. Upton, and D.A. Compton. 2005. Efficient mitosis in human cells lacking poleward microtubule flux. *Curr. Biol.* 15:1827–1832. doi:10.1016/j.cub.2005.08.065.

Gao, H., X. Chen, Q. Cai, Z. Shang, and Y. Niu. 2018. Increased KIF4A expression is a potential prognostic factor in prostate cancer. *Oncol. Lett.* 15:7941–7947. doi:10.3892/ol.2018.8322.

Gao, J., B.A. Aksoy, U. Dogrusoz, G. Dresdner, B. Gross, S.O. Sumer, Y. Sun, A. Jacobsen, R. Sinha, E. Larsson, E. Cerami, C. Sander, and N. Schultz. 2013. Integrative analysis of complex cancer genomics and clinical profiles using the cBioPortal. *Sci. Signal.* 6:pl1. doi:10.1126/scisignal.2004088.

Garcia, M.A., N. Koonrugsa, and T. Toda. 2002. Two kinesin-like Kin I family proteins in fission yeast regulate the establishment of metaphase and the onset of anaphase A. *Curr. Biol.* 12:610–621. doi:10.1016/s0960-9822(02)00761-3.

Gardner, M.K., D.C. Bouck, L. V Paliulis, J.B. Meehl, E.T. O'Toole, J. Haase, A. Soubry, A.P. Joglekar, M. Winey, E.D. Salmon, K. Bloom, and D.J. Odde. 2008. Chromosome congression by Kinesin-5 motor-mediated disassembly of longer kinetochore microtubules. *Cell*. 135:894–906. doi:10.1016/j.cell.2008.09.046.

Gayek, A.S., and R. Ohi. 2014. Kinetochore-microtubule stability governs the metaphase requirement for Eg5. *Mol. Biol. Cell*. 25:2051–2060. doi:10.1091/mbc.E14-03-0785.

Gergely, Z.R., A. Crapo, L.E. Hough, J. Richard McIntosh, and M.D. Betterton. 2016. Kinesin-8 effects on mitotic microtubule dynamics contribute to spindle function in fission yeast. *Mol. Biol. Cell*. 27:3490–3514. doi:10.1091/mbc.E15-07-0505.

Girão, H., N. Okada, T.A. Rodrigues, A.O. Silva, A.C. Figueiredo, Z. Garcia, T. Moutinho-Santos, I. Hayashi, J.E. Azevedo, S. Macedo-Ribeiro, and H. Maiato. 2020. CLASP2 binding to curved microtubule tips promotes flux and stabilizes kinetochore attachments. *J. Cell Biol.* 219:1-20. doi:10.1083/jcb.201905080.

Godinho, S.A., and D. Pellman. 2014. Causes and consequences of centrosome abnormalities in cancer. *Philos. Trans. R. Soc. London. Ser. B, Biol. Sci.* 369:20130467. doi:10.1098/rstb.2013.0467.

Gordon, D.J., B. Resio, and D. Pellman. 2012. Causes and consequences of aneuploidy in cancer. *Nat. Rev. Genet.* 13:189–203. doi:10.1038/nrg3123.

Goshima, G., M. Mayer, N. Zhang, N. Stuurman, and R.D. Vale. 2008. Augmin: a protein complex required for centrosome-independent microtubule generation within the spindle. *J. Cell Biol.* 181:421–429. doi:10.1083/jcb.200711053.

Goshima, G., and R.D. Vale. 2003. The roles of microtubule-based motor proteins in mitosis: comprehensive RNAi analysis in the *Drosophila* S2 cell line. *J. Cell Biol.* 162:1003–1016. doi:10.1083/jcb.200303022.

Gregan, J., S. Polakova, L. Zhang, I.M. Tolić-Nørrelykke, and D. Cimini. 2011. Merotelic kinetochore attachment: Causes and effects. *Trends Cell Biol.* 21:374–381. doi:10.1016/j.tcb.2011.01.003.

Grishchuk, E.L., M.I. Molodtsov, F.I. Ataullakhanov, and J.R. McIntosh. 2005. Force production by disassembling microtubules. *Nature*. 438:384–388. doi:10.1038/nature04132.

Gupta, M.L.J., P. Carvalho, D.M. Roof, and D. Pellman. 2006. Plus end-specific depolymerase activity of Kip3, a kinesin-8 protein, explains its role in positioning the yeast mitotic spindle. *Nat. Cell Biol.* 8:913–923. doi:10.1038/ncb1457.

Hamaguchi, Y., M. Toriyama, H. Sakai, and Y. Hiramoto. 1987. Redistribution of fluorescently labeled tubulin in the mitotic apparatus of sand dollar eggs and the effects of Taxol. *Cell Struct. Funct.* 12:43–52. doi:10.1247/csf.12.43.

Hassold, T., and P. Hunt. 2001. To err (meiotically) is human: the genesis of human aneuploidy. *Nat. Rev. Genet.* 2:280–291. doi:10.1038/35066065.

Hayden, J.H., S.S. Bowser, and C.L. Rieder. 1990. Kinetochores capture astral microtubules during chromosome attachment to the mitotic spindle: direct visualization in live newt lung cells. *J. Cell Biol.* 111:1039–1045. doi:10.1083/jcb.111.3.1039.

Hays, T.S., and E.D. Salmon. 1990. Poleward force at the kinetochore in metaphase depends on the number of kinetochore microtubules. *J. Cell Biol.* 110:391–404. doi:10.1083/jcb.110.2.391.

Hays, T.S., D. Wise, and E.D. Salmon. 1982. Traction force on a kinetochore at metaphase acts as a linear function of kinetochore fiber length. *J. Cell Biol.* 93:374–389. doi:10.1083/jcb.93.2.374.

Helenius, J., G. Brouhard, Y. Kalaidzidis, S. Diez, and J. Howard. 2006. The depolymerizing kinesin MCAK uses lattice diffusion to rapidly target microtubule ends. *Nature*. 441:115–119. doi:10.1038/nature04736.

Hiramoto, Y., and K. Izutsu. 1977. Poleward movement of “markers” existing in mitotic spindles of grasshopper spermatocytes. *Cell Struct. Funct.* 2:257–259. doi:10.1247/csf.2.257.

Holland, A.J., and D.W. Cleveland. 2012. Losing balance: the origin and impact of aneuploidy in cancer. *EMBO Rep.* 13:501–514. doi:10.1038/embor.2012.55.

Hou, G., C. Dong, Z. Dong, G. Liu, H. Xu, L. Chen, L. Liu, H. Wang, and W. Zhou. 2017. Upregulate KIF4A enhances proliferation, invasion of hepatocellular carcinoma and indicates poor prognosis across human cancer types. *Sci. Rep.* 7:4148. doi:10.1038/s41598-017-04176-9.

Hou, J., X. Shi, C. Chen, M.S. Islam, A.F. Johnson, T. Kanno, B. Huettel, M.-R. Yen, F.-M. Hsu, T. Ji, P.-Y. Chen, M. Matzke, A.J.M. Matzke, J. Cheng, and J.A. Birchler. 2018. Global impacts of chromosomal imbalance on gene expression in *Arabidopsis* and other taxa. *Proc. Natl. Acad. Sci. U. S. A.* 115:E11321–E11330. doi:10.1073/pnas.1807796115.

Howard, J. 2001. Mechanics of motor proteins and the cytoskeleton. Sinauer Associates,

Sunderland.

Howard, J., and A.A. Hyman. 2003. Dynamics and mechanics of the microtubule plus end. *Nature*. 422:753–758. doi:10.1038/nature01600.

Hughes, T.R., C.J. Roberts, H. Dai, A.R. Jones, M.R. Meyer, D. Slade, J. Burchard, S. Dow, T.R. Ward, M.J. Kidd, S.H. Friend, and M.J. Marton. 2000. Widespread aneuploidy revealed by DNA microarray expression profiling. *Nat. Genet.* 25:333–337. doi:10.1038/77116.

Hunter, A.W., M. Caplow, D.L. Coy, W.O. Hancock, S. Diez, L. Wordeman, and J. Howard. 2003. The kinesin-related protein MCAK is a microtubule depolymerase that forms an ATP-hydrolyzing complex at microtubule ends. *Mol. Cell*. 11:445–457. doi:10.1016/S1097-2765(03)00049-2.

Hwang, S., P. Cavaliere, R. Li, L.J. Zhu, N. Dephoure, and E.M. Torres. 2021. Consequences of aneuploidy in human fibroblasts with trisomy 21. *Proc. Natl. Acad. Sci. U. S. A.* 118:e2014723118. doi:10.1073/pnas.2014723118.

ICGC/TCGA Pan-Cancer Analysis of Whole Genomes Consortium. 2020. Pan-cancer analysis of whole genomes. *Nature*. 578:82–93. doi:10.1038/s41586-020-1969-6.

Iemura, K., T. Natsume, K. Maehara, M.T. Kanemaki, and K. Tanaka. 2021. Chromosome oscillation promotes Aurora A-dependent Hec1 phosphorylation and mitotic fidelity. *J. Cell Biol.* 220. doi:10.1083/jcb.202006116.

Ippolito, M.R., V. Martis, S. Martin, A.E. Tijhuis, C. Hong, R. Wardenaar, M. Dumont, J. Zerbib, D.C.J. Spierings, D. Fachinetti, U. Ben-David, F. Foijer, and S. Santaguida. 2021. Gene copy-number changes and chromosomal instability induced by aneuploidy confer resistance to chemotherapy. *Dev. Cell*. 56:2440-2454.e6. doi:10.1016/j.devcel.2021.07.006.

Jagrić, M., P. Risteski, J. Martinčić, A. Milas, and I.M. Tolić. 2021. Optogenetic control of PRC1 reveals its role in chromosome alignment on the spindle by overlap length-dependent forces. *Elife*. 10:e61170. doi:10.7554/eLife.61170.

Janicke, M.A., L. Lasko, R. Oldenbourg, and J.R.J. LaFountain. 2007. Chromosome malorientations after meiosis II arrest cause nondisjunction. *Mol. Biol. Cell*. 18:1645–1656. doi:10.1091/mbc.e06-10-0963.

Janssen, A., M. van der Burg, K. Szuhai, G.J.P.L. Kops, and R.H. Medema. 2011. Chromosome segregation errors as a cause of DNA damage and structural chromosome aberrations. *Science*. 333:1895–1898. doi:10.1126/science.1210214.

Janssen, A., G.J.P.L. Kops, and R.H. Medema. 2009. Elevating the frequency of chromosome mis-segregation as a strategy to kill tumor cells. *Proc. Natl. Acad. Sci.* 106:19108–19113. doi:10.1073/pnas.0904343106.

Janssen, L.M.E., T. V. Averink, V.A. Blomen, T.R. Brummelkamp, R.H. Medema, and J.A.

Raaijmakers. 2018. Loss of Kif18A results in spindle assembly checkpoint activation at microtubule-attached kinetochores. *Curr. Biol.* 28:2685-2696.e4. doi:10.1016/j.cub.2018.06.026.

Jaqaman, K., E.M. King, A.C. Amaro, J.R. Winter, J.F. Dorn, H.L. Elliott, N. McHedlishvili, S.E. McClelland, I.M. Porter, M. Posch, A. Toso, G. Danuser, A.D. McAinsh, P. Meraldi, and J.R. Swedlow. 2010. Kinetochore alignment within the metaphase plate is regulated by centromere stiffness and microtubule depolymerases. *J. Cell Biol.* 188:665–679. doi:10.1083/jcb.200909005.

Joglekar, A.P., and A.J. Hunt. 2002. A simple, mechanistic model for directional instability during mitotic chromosome movements. *Biophys. J.* 83:42–58. doi:10.1016/S0006-3495(02)75148-5.

Kajtez, J., A. Solomatina, M. Novak, B. Polak, K. Vukušić, J. Rüdiger, G. Cojoc, A. Milas, I. Šumanovac Šestak, P. Risteski, F. Tavano, A.H. Klemm, E. Roscioli, J. Welburn, D. Cimini, M. Glunčić, N. Pavin, and I.M. Tolić. 2016. Overlap microtubules link sister k-fibres and balance the forces on bi-oriented kinetochores. *Nat. Commun.* 7:10298. doi:10.1038/ncomms10298.

Kamasaki, T., E. O'Toole, S. Kita, M. Osumi, J. Usukura, J.R. McIntosh, and G. Goshima. 2013. Augmin-dependent microtubule nucleation at microtubule walls in the spindle. *J. Cell Biol.* 202:25–33. doi:10.1083/jcb.201304031.

Kapoor, T.M., M.A. Lampson, P. Hergert, L. Cameron, D. Cimini, E.D. Salmon, B.F. McEwen, and A. Khodjakov. 2006. Chromosomes can congress to the metaphase plate before biorientation. *Science*. 311:388–391. doi:10.1126/science.1122142.

Ke, K., J. Cheng, and A.J. Hunt. 2009. The distribution of polar ejection forces determines the amplitude of chromosome directional instability. *Curr. Biol.* 19:807–815. doi:10.1016/j.cub.2009.04.036.

Khodjakov, A., R.W. Cole, B.F. McEwen, K.F. Buttle, and C.L. Rieder. 1997. Chromosome fragments possessing only one kinetochore can congress to the spindle equator. *J. Cell Biol.* 136:229–240. doi:10.1083/jcb.136.2.229.

Khodjakov, A., and C.L. Rieder. 1996. Kinetochores moving away from their associated pole do not exert a significant pushing force on the chromosome. *J. Cell Biol.* 135:315–327. doi:10.1083/jcb.135.2.315.

Klemm, A.H., A. Bosilj, M. Glunčic, N. Pavin, and I.M. Tolic. 2018. Metaphase kinetochore movements are regulated by kinesin-8 motors and microtubule dynamic instability. *Mol. Biol. Cell*. 29:1332–1345. doi:10.1091/mbc.E17-11-0667.

Kline-Smith, S.L., A. Khodjakov, P. Hergert, and C.E. Walczak. 2004. Depletion of centromeric MCAK leads to chromosome congression and segregation defects due to improper kinetochore attachments. *Mol. Biol. Cell*. 15:1146–1159. doi:10.1091/mbc.e03-08-0581.

Knouse, K.A., K.E. Lopez, M. Bachofner, and A. Amon. 2018. Chromosome segregation fidelity in epithelia requires tissue architecture. *Cell*. 175:200-211.e13. doi:10.1016/j.cell.2018.07.042.

Koshland, D.E., T.J. Mitchison, and M.W. Kirschner. 1988. Polewards chromosome movement driven by microtubule depolymerization *in vitro*. *Nature*. 331:499–504. doi:10.1038/331499a0.

Kung, P.-P., R. Martinez, Z. Zhu, M. Zager, A. Blasina, I. Rymer, J. Hallin, M. Xu, C. Carroll, J. Chionis, P. Wells, K. Kozminski, J. Fan, O. Guicherit, B. Huang, M. Cui, C. Liu, Z. Huang, A. Sistla, J. Yang, and B.W. Murray. 2014. Chemogenetic evaluation of the mitotic kinesin CENP-E reveals a critical role in triple-negative breast cancer. *Mol. Cancer Ther.* 13:2104–2115. doi:10.1158/1535-7163.MCT-14-0083-T.

Kuniyasu, K., K. Iemura, and K. Tanaka. 2018. Delayed chromosome alignment to the spindle equator increases the rate of chromosome missegregation in cancer cell lines. *Biomolecules*. 9. doi:10.3390/biom9010010.

Lacroix, B., G. Letort, L. Pitayu, J. Sallé, M. Stefanutti, G. Maton, A.-M. Ladouceur, J.C. Canman, P.S. Maddox, A.S. Maddox, N. Minc, F. Nédélec, and J. Dumont. 2018. Microtubule dynamics scale with cell size to set spindle length and assembly timing. *Dev. Cell*. 45:496-511.e6. doi:10.1016/j.devcel.2018.04.022.

LaFountain, J.R.J., C.S. Cohan, A.J. Siegel, and D.J. LaFountain. 2004. Direct visualization of microtubule flux during metaphase and anaphase in crane-fly spermatocytes. *Mol. Biol. Cell*. 15:5724–5732. doi:10.1091/mbc.e04-08-0750.

Lampson, M.A., K. Renduchitala, A. Khodjakov, and T.M. Kapoor. 2004. Correcting improper chromosomes-spindle attachments during cell division. *Nat. Cell Biol.* 6:232–237. doi:10.1038/ncb1102.

Lara-Gonzalez, P., J. Pines, and A. Desai. 2021. Spindle assembly checkpoint activation and silencing at kinetochores. *Semin. Cell Dev. Biol.* 117:86–98. doi:10.1016/j.semcdb.2021.06.009.

Lecland, N., and J. Lüders. 2014. The dynamics of microtubule minus ends in the human mitotic spindle. *Nat. Cell Biol.* 16:770–778. doi:10.1038/ncb2996.

Levesque, A.A., and D.A. Compton. 2001. The chromokinesin Kid is necessary for chromosome arm orientation and oscillation, but not congression, on mitotic spindles. *J. Cell Biol.* 154:1135–1146. doi:10.1083/jcb.200106093.

Levine, M.S., and A.J. Holland. 2018. The impact of mitotic errors on cell proliferation and tumorigenesis. *Genes Dev.* 32:620–638. doi:10.1101/gad.314351.118.

Liu, S., M. Kwon, M. Mannino, N. Yang, F. Renda, A. Khodjakov, and D. Pellman. 2018. Nuclear envelope assembly defects link mitotic errors to chromothripsis. *Nature*. 561:551–555. doi:10.1038/s41586-018-0534-z.

Liu, Z., K. Ling, X. Wu, J. Cao, B. Liu, S. Li, Q. Si, Y. Cai, C. Yan, Y. Zhang, and Y. Weng. 2009. Reduced expression of cenp-e in human hepatocellular carcinoma. *J. Exp. Clin. Cancer Res.* 28:156. doi:10.1186/1756-9966-28-156.

Loncarek, J., O. Kisurina-Evgenieva, T. Vinogradova, P. Hergert, S. La Terra, T.M. Kapoor, and A. Khodjakov. 2007. The centromere geometry essential for keeping mitosis error free is controlled by spindle forces. *Nature*. 450:745–749. doi:10.1038/nature06344.

Lukinavičius, G., L. Reymond, E. D'Este, A. Masharina, F. Göttfert, H. Ta, A. Güther, M. Fournier, S. Rizzo, H. Waldmann, C. Blaukopf, C. Sommer, D.W. Gerlich, H.-D. Arndt, S.W. Hell, and K. Johnsson. 2014. Fluorogenic probes for live-cell imaging of the cytoskeleton. *Nat. Methods*. 11:731–733. doi:10.1038/nmeth.2972.

Lukow, D.A., E.L. Sausville, P. Suri, N.K. Chunduri, A. Wieland, J. Leu, J.C. Smith, V. Girish, A.A. Kumar, J. Kendall, Z. Wang, Z. Storchova, and J.M. Sheltzer. 2021. Chromosomal instability accelerates the evolution of resistance to anti-cancer therapies. *Dev. Cell*. 56:2427-2439.e4. doi:10.1016/j.devcel.2021.07.009.

Ma, N., U.S. Tulu, N.P. Ferenz, C. Fagerstrom, A. Wilde, and P. Wadsworth. 2010. Poleward transport of TPX2 in the mammalian mitotic spindle requires dynein, Eg5, and microtubule flux. *Mol. Biol. Cell*. 21:979–988. doi:10.1091/mbc.e09-07-0601.

Maddox, P., A. Straight, P. Coughlin, T.J. Mitchison, and E.D. Salmon. 2003. Direct observation of microtubule dynamics at kinetochores in *Xenopus* extract spindles: implications for spindle mechanics. *J. Cell Biol.* 162:377–382. doi:10.1083/jcb.200301088.

Maffini, S., A.R.R. Maia, A.L. Manning, Z. Maliga, A.L. Pereira, M. Junqueira, A. Shevchenko, A. Hyman, J.R. 3rd Yates, N. Galjart, D.A. Compton, and H. Maiato. 2009. Motor-independent targeting of CLASPs to kinetochores by CENP-E promotes microtubule turnover and poleward flux. *Curr. Biol.* 19:1566–1572. doi:10.1016/j.cub.2009.07.059.

Magidson, V., C.B. O'Connell, J. Lončarek, R. Paul, A. Mogilner, and A. Khodjakov. 2011. The spatial arrangement of chromosomes during prometaphase facilitates spindle assembly. *Cell*. 146:555–567. doi:10.1016/j.cell.2011.07.012.

Maiato, H., E.A.L. Fairley, C.L. Rieder, J.R. Swedlow, C.E. Sunkel, and W.C. Earnshaw. 2003. Human CLASP1 is an outer kinetochore component that regulates spindle microtubule dynamics. *Cell*. 113:891–904. doi:10.1016/s0092-8674(03)00465-3.

Maiato, H., A. Gomes, F. Sousa, and M. Barisic. 2017. Mechanisms of Chromosome Congression during Mitosis. *Biology (Basel).* 6:13. doi:10.3390/biology6010013.

Maiato, H., A. Khodjakov, and C.L. Rieder. 2005. *Drosophila* CLASP is required for the incorporation of microtubule subunits into fluxing kinetochore fibres. *Nat. Cell Biol.* 7:42–47. doi:10.1038/ncb1207.

Manenica, M., V. Štimac, I. Koprivec, J. Simunić, and I.M. Tolić. 2020. Augmin regulates kinetochore tension and spatial arrangement of spindle microtubules by nucleating bridging fibers. *bioRxiv*. doi:10.1101/2020.09.10.291740.

Mann, B.J., and P. Wadsworth. 2018. Distribution of Eg5 and TPX2 in mitosis: Insight from CRISPR tagged cells. *Cytoskeleton*. 75:508–521. doi:10.1002/cm.21486.

Marshall, W.F., J.F. Marko, D.A. Agard, and J.W. Sedat. 2001. Chromosome elasticity and mitotic polar ejection force measured in living *Drosophila* embryos by four-dimensional microscopy-based motion analysis. *Curr. Biol.* 11:569–578. doi:10.1016/s0960-9822(01)00180-4.

Mary, H., J. Fouchard, G. Gay, C. Reyes, T. Gauthier, C. Gruget, J. Pécréaux, S. Tournier, and Y. Gachet. 2015. Fission yeast kinesin-8 controls chromosome congression independently of oscillations. *J. Cell Sci.* 128:3720–3730. doi:10.1242/jcs.160465.

Mastronarde, D.N., K.L. McDonald, R. Ding, and J.R. McIntosh. 1993. Interpolar spindle microtubules in PTK cells. *J. Cell Biol.* 123:1475–1489. doi:10.1083/jcb.123.6.1475.

Matos, I., A.J. Pereira, M. Lince-Faria, L.A. Cameron, E.D. Salmon, and H. Maiato. 2009. Synchronizing chromosome segregation by flux-dependent force equalization at kinetochores. *J. Cell Biol.* 186:11–26. doi:10.1083/jcb.200904153.

Mayr, M.I., S. Hümmer, J. Bormann, T. Grüner, S. Adio, G. Woehlke, and T.U. Mayer. 2007. The human kinesin Kif18A is a motile microtubule depolymerase essential for chromosome congression. *Curr. Biol.* 17:488–498. doi:10.1016/j.cub.2007.02.036.

Mazumdar, M., J.-H. Lee, K. Sengupta, T. Ried, S. Rane, and T. Misteli. 2006. Tumor formation via loss of a molecular motor protein. *Curr. Biol.* 16:1559–1564. doi:10.1016/j.cub.2006.06.029.

McDonald, K.L., E.T. O'Toole, D.N. Mastronarde, and J.R. McIntosh. 1992. Kinetochore microtubules in PTK cells. *J. Cell Biol.* 118:369–383. doi:10.1083/jcb.118.2.369.

McIntosh, J.R., E.L. Grishchuk, and R.R. West. 2002. Chromosome-microtubule interactions during mitosis. *Annu. Rev. Cell Dev. Biol.* 18:193–219. doi:10.1146/annurev.cellbio.18.032002.132412.

McNeill, P.A., and M.W. Berns. 1981. Chromosome behavior after laser microirradiation of a single kinetochore in mitotic PtK2 cells. *J. Cell Biol.* 88:543–553. doi:10.1083/jcb.88.3.543.

Mimori-Kiyosue, Y., I. Grigoriev, H. Sasaki, C. Matsui, A. Akhmanova, S. Tsukita, and I. Vorobjev. 2006. Mammalian CLASPs are required for mitotic spindle organization and kinetochore alignment. *Genes Cells*. 11:845–857. doi:10.1111/j.1365-2443.2006.00990.x.

Mitchison, T., L. Evans, E. Schulze, and M. Kirschner. 1986. Sites of microtubule assembly and disassembly in the mitotic spindle. *Cell*. 45:515–527. doi:10.1016/0092-8674(86)90283-7.

Mitchison, T., and M. Kirschner. 1984. Dynamic instability of microtubule growth. *Nature*. 312:237–242. doi:10.1038/312237a0.

Mitchison, T.J. 1989. Polewards microtubule flux in the mitotic spindle: evidence from photoactivation of fluorescence. *J. Cell Biol.* 109:637–652. doi:10.1083/jcb.109.2.637.

Mitchison, T.J. 2005. Mechanism and function of poleward flux in *Xenopus* extract meiotic spindles. *Philos. Trans. R. Soc. London. Ser. B, Biol. Sci.* 360:623–629. doi:10.1098/rstb.2004.1616.

Mitchison, T.J., and E.D. Salmon. 1992. Poleward kinetochore fiber movement occurs during both metaphase and anaphase-A in newt lung cell mitosis. *J. Cell Biol.* 119:569–582. doi:10.1083/jcb.119.3.569.

Miyamoto, D.T., Z.E. Perlman, K.S. Burbank, A.C. Groen, and T.J. Mitchison. 2004. The kinesin Eg5 drives poleward microtubule flux in *Xenopus laevis* egg extract spindles. *J. Cell Biol.* 167:813–818. doi:10.1083/jcb.200407126.

Nagahara, M., N. Nishida, M. Iwatsuki, S. Ishimaru, K. Mimori, F. Tanaka, T. Nakagawa, T. Sato, K. Sugihara, D.S.B. Hoon, and M. Mori. 2011. Kinesin 18A expression: clinical relevance to colorectal cancer progression. *Int. J. cancer*. 129:2543–2552. doi:10.1002/ijc.25916.

Nicklas, R.B., D.F. Kubai, and T.S. Hays. 1982. Spindle microtubules and their mechanical associations after micromanipulation in anaphase. *J. Cell Biol.* 95:91–104. doi:10.1083/jcb.95.1.91.

Nixon, F.M., T.R. Honnor, N.I. Clarke, G.P. Starling, A.J. Beckett, A.M. Johansen, J.A. Brettschneider, I.A. Prior, and S.J. Royle. 2017. Microtubule organization within mitotic spindles revealed by serial block face scanning electron microscopy and image analysis. *J. Cell Sci.* 130:1845–1855. doi:10.1242/jcs.203877.

O'Toole, E., M. Morphew, and J.R. McIntosh. 2020. Electron tomography reveals aspects of spindle structure important for mechanical stability at metaphase. *Mol. Biol. Cell*. 31:184–195. doi:10.1091/mbc.E19-07-0405.

Ohi, R., M.L. Coughlin, W.S. Lane, and T.J. Mitchison. 2003. An inner centromere protein that stimulates the microtubule depolymerizing activity of a KinI kinesin. *Dev. Cell*. 5:309–321. doi:10.1016/s1534-5807(03)00229-6.

Östergren, G. 1950. Considerations on some elementary features of mitosis. *Hereditas*. 36:1–18.

Paul, R., R. Wollman, W.T. Silkworth, I.K. Nardi, D. Cimini, and A. Mogilner. 2009. Computer simulations predict that chromosome movements and rotations accelerate mitotic spindle assembly without compromising accuracy. *Proc. Natl. Acad. Sci. U. S. A.* 106:15708–15713. doi:10.1073/pnas.0908261106.

Pavelka, N., G. Rancati, J. Zhu, W.D. Bradford, A. Saraf, L. Florens, B.W. Sanderson, G.L.

Hattem, and R. Li. 2010. Aneuploidy confers quantitative proteome changes and phenotypic variation in budding yeast. *Nature*. 468:321–325. doi:10.1038/nature09529.

Pavin, N., and I.M. Tolić. 2016. Self-Organization and Forces in the Mitotic Spindle. *Annu. Rev. Biophys.* 45:279–298. doi:10.1146/annurev-biophys-062215-010934.

Pereira, A.J., and H. Maiato. 2012. Maturation of the kinetochore-microtubule interface and the meaning of metaphase. *Chromosome Res.* 20:563–577. doi:10.1007/s10577-012-9298-8.

Pereira, A.L., A.J. Pereira, A.R.R. Maia, K. Drabek, C.L. Sayas, P.J. Hergert, M. Lince-Faria, I. Matos, C. Duque, T. Stepanova, C.L. Rieder, W.C. Earnshaw, N. Galjart, and H. Maiato. 2006. Mammalian CLASP1 and CLASP2 cooperate to ensure mitotic fidelity by regulating spindle and kinetochore function. *Mol. Biol. Cell*. 17:4526–4542. doi:10.1091/mbc.e06-07-0579.

Petry, S. 2016. Mechanisms of mitotic spindle assembly. *Annu. Rev. Biochem.* 85:659–683. doi:10.1146/annurev-biochem-060815-014528.

Pfau, S.J., and A. Amon. 2012. Chromosomal instability and aneuploidy in cancer: from yeast to man. *EMBO Rep.* 13:515–527. doi:10.1038/embor.2012.65.

Pickett-Heaps, J.D., D.H. Tippit, and K.R. Porter. 1982. Rethinking mitosis. *Cell*. 29:729–744. doi:10.1016/0092-8674(82)90435-4.

Polak, B., P. Risteski, S. Lesjak, and I.M. Tolić. 2017. PRC1-labeled microtubule bundles and kinetochore pairs show one-to-one association in metaphase. *EMBO Rep.* 18:217–230. doi:10.15252/embr.201642650.

Ponjavić, I., K. Vukušić, and I.M. Tolić. 2021. Expansion microscopy of the mitotic spindle. *Methods Cell Biol.* 161:247–274. doi:10.1016/bs.mcb.2020.04.014.

Prosser, S.L., and L. Pelletier. 2017. Mitotic spindle assembly in animal cells: a fine balancing act. *Nat. Rev. Mol. Cell Biol.* 18:187–201. doi:10.1038/nrm.2016.162.

Quinton, R.J., A. DiDomizio, M.A. Vittoria, K. Kotýnková, C.J. Ticas, S. Patel, Y. Koga, J. Vakhshoorzadeh, N. Hermance, T.S. Kuroda, N. Parulekar, A.M. Taylor, A.L. Manning, J.D. Campbell, and N.J. Ganem. 2021. Whole-genome doubling confers unique genetic vulnerabilities on tumour cells. *Nature*. 590:492–497. doi:10.1038/s41586-020-03133-3.

Rancati, G., N. Pavelka, B. Fleharty, A. Noll, R. Trimble, K. Walton, A. Perera, K. Staehling-Hampton, C.W. Seidel, and R. Li. 2008. Aneuploidy underlies rapid adaptive evolution of yeast cells deprived of a conserved cytokinesis motor. *Cell*. 135:879–893. doi:10.1016/j.cell.2008.09.039.

Redemann, S., J. Baumgart, N. Lindow, M. Shelley, E. Nazockdast, A. Kratz, S. Prohaska, J. Brugués, S. Fürthauer, and T. Müller-Reichert. 2017. *C. elegans* chromosomes connect to centrosomes by anchoring into the spindle network. *Nat. Commun.* 8:15288. doi:10.1038/ncomms15288.

Rieder, C.L., and S.P. Alexander. 1990. Kinetochores are transported poleward along a single astral microtubule during chromosome attachment to the spindle in newt lung cells. *J. Cell Biol.* 110:81–95. doi:10.1083/jcb.110.1.81.

Rieder, C.L., R.W. Cole, A. Khodjakov, and G. Sluder. 1995. The checkpoint delaying anaphase in response to chromosome monoorientation is mediated by an inhibitory signal produced by unattached kinetochores. *J. Cell Biol.* 130:941–948. doi:10.1083/jcb.130.4.941.

Rieder, C.L., E.A. Davison, L.C. Jensen, L. Cassimeris, and E.D. Salmon. 1986. Oscillatory movements of monooriented chromosomes and their position relative to the spindle pole result from the ejection properties of the aster and half-spindle. *J. Cell Biol.* 103:581–591. doi:10.1083/jcb.103.2.581.

Rieder, C.L., and H. Maiato. 2004. Stuck in division or passing through: what happens when cells cannot satisfy the spindle assembly checkpoint. *Dev. Cell*. 7:637–651. doi:10.1016/j.devcel.2004.09.002.

Rieder, C.L., and E.D. Salmon. 1994. Motile kinetochores and polar ejection forces dictate chromosome position on the vertebrate mitotic spindle. *J. Cell Biol.* 124:223–233. doi:10.1083/jcb.124.3.223

Rieder, C.L., and E.D. Salmon. 1998. The vertebrate cell kinetochore and its roles during mitosis. *Trends Cell Biol.* 8:310–318. doi:10.1016/s0962-8924(98)01299-9.

Rieder, C.L., A. Schultz, R. Cole, and G. Sluder. 1994. Anaphase onset in vertebrate somatic cells is controlled by a checkpoint that monitors sister kinetochore attachment to the spindle. *J. Cell Biol.* 127:1301–1310. doi:10.1083/jcb.127.5.1301.

Risteski, P., D. Božan, M. Jagrić, A. Bosilj, N. Pavin, and I.M. Tolić. 2021a. Coordinated poleward flux of sister kinetochore fibers drives chromosome alignment. *bioRxiv*. doi:10.1101/2020.12.30.424837.

Risteski, P., M. Jagrić, N. Pavin, and I.M. Tolić. 2021b. Biomechanics of chromosome alignment at the spindle midplane. *Curr. Biol.* 31:R574–R585. doi:10.1016/j.cub.2021.03.082.

Rizzoni, M., C. Tanzarella, B. Gustavino, F. Degrassi, A. Guarino, and E. Vitagliano. 1989. Indirect mitotic nondisjunction in *Vicia faba* and Chinese hamster cells. *Chromosoma*. 97:339–346. doi:10.1007/BF00371976.

Rogers, G.C., S.L. Rogers, T.A. Schwimmer, S.C. Ems-McClung, C.E. Walczak, R.D. Vale, J.M. Scholey, and D.J. Sharp. 2004. Two mitotic kinesins cooperate to drive sister chromatid separation during anaphase. *Nature*. 427:364–370. doi:10.1038/nature02256.

Roos, U.P. 1976. Light and electron microscopy of rat kangaroo cells in mitosis. III. Patterns of chromosome behavior during prometaphase. *Chromosoma*. 54:363–385. doi:10.1007/BF00292816.

Rosenkrantz, J.L., and L. Carbone. 2017. Investigating somatic aneuploidy in the brain: why we need a new model. *Chromosoma*. 126:337–350. doi:10.1007/s00412-016-0615-4.

Rowald, K., M. Mantovan, J. Passos, C. Buccitelli, B.R. Mardin, J.O. Korbel, M. Jechlinger, and R. Sotillo. 2016. Negative selection and chromosome instability induced by Mad2 overexpression delay breast cancer but dacilitate oncogene-independent outgrowth. *Cell Rep.* 15:2679–2691. doi:10.1016/j.celrep.2016.05.048.

Sacristan, C., and G.J.P.L. Kops. 2015. Joined at the hip: kinetochores, microtubules, and spindle assembly checkpoint signaling. *Trends Cell Biol.* 25:21–28. doi:10.1016/j.tcb.2014.08.006.

Santaguida, S., and A. Amon. 2015. Short- and long-term effects of chromosome mis-segregation and aneuploidy. *Nat. Rev. Mol. Cell Biol.* 16:473–485. doi:10.1038/nrm4025.

Sauer, G., R. Körner, A. Hanisch, A. Ries, E.A. Nigg, and H.H.W. Silljé. 2005. Proteome analysis of the human mitotic spindle. *Mol. Cell. Proteomics*. 4:35–43. doi:10.1074/mcp.M400158-MCP200.

Schukken, K.M., Y.-C. Lin, P.L. Bakker, M. Schubert, S.F. Preuss, J.E. Simon, H. van den Bos, Z. Storchova, M. Colomé-Tatché, H. Bastians, D.C. Spierings, and F. Foijer. 2020. Altering microtubule dynamics is synergistically toxic with spindle assembly checkpoint inhibition. *Life Sci. Alliance*. 3:e201900499. doi:10.26508/lsa.201900499.

Sen, O., J.U. Harrison, N.J. Burroughs, and A.D. McAinsh. 2021. Kinetochore life histories reveal an Aurora-B-dependent error correction mechanism in anaphase. *Dev. Cell*. 56:3082-3099.e5. doi:10.1016/j.devcel.2021.10.007.

Shan, L., M. Zhao, Y. Lu, H. Ning, S. Yang, Y. Song, W. Chai, and X. Shi. 2019. CENPE promotes lung adenocarcinoma proliferation and is directly regulated by FOXM1. *Int. J. Oncol.* 55:257–266. doi:10.3892/ijo.2019.4805.

Shrestha, R.L., D. Conti, N. Tamura, D. Braun, R.A. Ramalingam, K. Cieslinski, J. Ries, and V.M. Draviam. 2017. Aurora-B kinase pathway controls the lateral to end-on conversion of kinetochore-microtubule attachments in human cells. *Nat. Commun.* 8:150. doi:10.1038/s41467-017-00209-z.

Skibbens, R. V, V.P. Skeen, and E.D. Salmon. 1993. Directional instability of kinetochore motility during chromosome congression and segregation in mitotic newt lung cells: a push-pull mechanism. *J. Cell Biol.* 122:859–875. doi:10.1083/jcb.122.4.859.

Soto, M., I. García-Santisteban, L. Krenning, R.H. Medema, and J.A. Raaijmakers. 2018. Chromosomes trapped in micronuclei are liable to segregation errors. *J. Cell Sci.* 131. doi:10.1242/jcs.214742.

Steblyanko, Y., G. Rajendraprasad, M. Osswald, S. Eibes, A. Jacome, S. Geley, A.J. Pereira, H. Maiato, and M. Barisic. 2020. Microtubule poleward flux in human cells is driven by the coordinated action of four kinesins. *EMBO J.* 39:e105432.

doi:10.15252/embj.2020105432.

Stingele, S., G. Stoehr, K. Peplowska, J. Cox, M. Mann, and Z. Storchova. 2012. Global analysis of genome, transcriptome and proteome reveals the response to aneuploidy in human cells. *Mol. Syst. Biol.* 8:608. doi:10.1038/msb.2012.40.

Stumpff, J., G. von Dassow, M. Wagenbach, C. Asbury, and L. Wordeman. 2008. The kinesin-8 motor Kif18A suppresses kinetochore movements to control mitotic chromosome alignment. *Dev. Cell*. 14:252–262. doi:10.1016/j.devcel.2007.11.014.

Stumpff, J., M. Wagenbach, A. Franck, C.L. Asbury, and L. Wordeman. 2012. Kif18A and chromokinesins confine centromere movements via microtubule growth suppression and spatial control of kinetochore tension. *Dev. Cell*. 22:1017–1029. doi:10.1016/j.devcel.2012.02.013.

Suresh, P., A.F. Long, and S. Dumont. 2020. Microneedle manipulation of the mammalian spindle reveals specialized, short-lived reinforcement near chromosomes. *Elife*. 9:e53807. doi:10.7554/eLife.53807.

Tamura, N., N. Shaikh, D. Muliaditan, T.N. Soliman, J.R. McGuinness, E. Maniati, D. Moralli, M.-A. Durin, C.M. Green, F.R. Balkwill, J. Wang, K. Curtius, and S.E. McClelland. 2020. Specific mechanisms of chromosomal instability indicate therapeutic sensitivities in high-grade serous ovarian carcinoma. *Cancer Res.* 80:4946–4959. doi:10.1158/0008-5472.CAN-19-0852.

Terradas, M., M. Martín, and A. Genescà. 2016. Impaired nuclear functions in micronuclei results in genome instability and chromothripsis. *Arch. Toxicol.* 90:2657–2667. doi:10.1007/s00204-016-1818-4.

Thompson, S.L., S.F. Bakhoum, and D.A. Compton. 2010. Mechanisms of chromosomal instability. *Curr. Biol.* 20:R285-295. doi:10.1016/j.cub.2010.01.034.

Thompson, S.L., and D.A. Compton. 2008. Examining the link between chromosomal instability and aneuploidy in human cells. *J. Cell Biol.* 180:665–672. doi:10.1083/jcb.200712029.

Thompson, S.L., and D.A. Compton. 2011. Chromosome missegregation in human cells arises through specific types of kinetochore-microtubule attachment errors. *Proc. Natl. Acad. Sci. U. S. A.* 108:17974–17978. doi:10.1073/pnas.1109720108.

Tischer, C., D. Brunner, and M. Dogterom. 2009. Force- and kinesin-8-dependent effects in the spatial regulation of fission yeast microtubule dynamics. *Mol. Syst. Biol.* 5:250. doi:10.1038/msb.2009.5.

Tolić-Nørrelykke, I.M. 2008. Push-me-pull-you: how microtubules organize the cell interior. *Eur. Biophys. J.* 37:1271–1278. doi:10.1007/s00249-008-0321-0.

Tolić, I.M. 2018. Mitotic spindle: kinetochore fibers hold on tight to interpolar bundles. *Eur. Biophys. J.* 47:191–203. doi:10.1007/s00249-017-1244-4.

Tolić, I.M., and N. Pavin. 2021. Mitotic spindle: lessons from theoretical modeling. *Mol. Biol. Cell*. 32:218–222. doi:10.1091/mbc.E20-05-0335.

Torosantucci, L., M. De Santis Puzzonia, C. Cenciarelli, W. Rens, and F. Degrassi. 2009. Aneuploidy in mitosis of PtK1 cells is generated by random loss and nondisjunction of individual chromosomes. *J. Cell Sci.* 122:3455–3461. doi:10.1242/jcs.047944.

Torres, E.M., T. Sokolsky, C.M. Tucker, L.Y. Chan, M. Boselli, M.J. Dunham, and A. Amon. 2007. Effects of aneuploidy on cellular physiology and cell division in haploid yeast. *Science*. 317:916–924. doi:10.1126/science.1142210.

Uehara, R., R. Nozawa, A. Tomioka, S. Petry, R.D. Vale, C. Obuse, and G. Goshima. 2009. The augmin complex plays a critical role in spindle microtubule generation for mitotic progression and cytokinesis in human cells. *Proc. Natl. Acad. Sci.* 106:6998–7003. doi:10.1073/pnas.0901587106.

Varga, V., J. Helenius, K. Tanaka, A.A. Hyman, T.U. Tanaka, and J. Howard. 2006. Yeast kinesin-8 depolymerizes microtubules in a length-dependent manner. *Nat. Cell Biol.* 8:957–962. doi:10.1038/ncb1462.

Varga, V., C. Leduc, V. Bormuth, S. Diez, and J. Howard. 2009. Kinesin-8 motors act cooperatively to mediate length-dependent microtubule depolymerization. *Cell*. 138:1174–1183. doi:10.1016/j.cell.2009.07.032.

Vladimirou, E., N. Mchedlishvili, I. Gasic, J.W. Armond, C.P. Samora, P. Meraldi, and A.D. McAinsh. 2013. Nonautonomous movement of chromosomes in mitosis. *Dev. Cell*. 27:60–71. doi:10.1016/j.devcel.2013.08.004.

Vukušić, K., R. Buđa, A. Bosilj, A. Milas, N. Pavin, and I.M. Tolić. 2017. Microtubule sliding within the bridging fiber pushes kinetochore fibers apart to segregate chromosomes. *Dev. Cell*. 43:11-23.e6. doi:10.1016/j.devcel.2017.09.010.

Vukušić, K., I. Ponjavić, R. Buđa, P. Risteski, and I.M. Tolić. 2021. Microtubule-sliding modules based on kinesins EG5 and PRC1-dependent KIF4A drive human spindle elongation. *Dev. Cell*. 56:1253-1267.e10. doi:10.1016/j.devcel.2021.04.005.

Walczak, C.E., S. Cai, and A. Khodjakov. 2010. Mechanisms of chromosome behaviour during mitosis. *Nat. Rev. Mol. Cell Biol.* 11:91–102. doi:10.1038/nrm2832.

Wandke, C., M. Barisic, R. Sigl, V. Rauch, F. Wolf, A.C. Amaro, C.H. Tan, A.J. Pereira, U. Kutay, H. Maiato, P. Meraldi, and S. Geley. 2012. Human chromokinesins promote chromosome congression and spindle microtubule dynamics during mitosis. *J. Cell Biol.* 198:847–863. doi:10.1083/jcb.201110060.

Wargacki, M.M., J.C. Tay, E.G. Muller, C.L. Asbury, and T.N. Davis. 2010. Kip3, the yeast kinesin-8, is required for clustering of kinetochores at metaphase. *Cell Cycle*. 9:2581–2588. doi:10.4161/cc.9.13.12076.

Waterman-Storer, C.M., A. Desai, J.C. Bulinski, and E.D. Salmon. 1998. Fluorescent speckle

microscopy, a method to visualize the dynamics of protein assemblies in living cells. *Curr. Biol.* 8:1227–1230. doi:10.1016/s0960-9822(07)00515-5.

Waterman-Storer, C.M., and E.D. Salmon. 1998. How microtubules get fluorescent speckles. *Biophys. J.* 75:2059–2069. doi:10.1016/S0006-3495(98)77648-9.

Waters, J.C., R.H. Chen, A.W. Murray, and E.D. Salmon. 1998. Localization of Mad2 to kinetochores depends on microtubule attachment, not tension. *J. Cell Biol.* 141:1181–1191. doi:10.1083/jcb.141.5.1181.

Waters, J.C., R. V Skibbens, and E.D. Salmon. 1996. Oscillating mitotic newt lung cell kinetochores are, on average, under tension and rarely push. *J. Cell Sci.* 109:2823–2831. doi:10.1242/jcs.109.12.2823.

Weaver, B.A.A., Z.Q. Bonday, F.R. Putkey, G.J.P.L. Kops, A.D. Silk, and D.W. Cleveland. 2003. Centromere-associated protein-E is essential for the mammalian mitotic checkpoint to prevent aneuploidy due to single chromosome loss. *J. Cell Biol.* 162:551–563. doi:10.1083/jcb.200303167.

West, R.R., T. Malmstrom, and J.R. McIntosh. 2002. Kinesins klp5+ and klp6+ are required for normal chromosome movement in mitosis. *J. Cell Sci.* 115:931–940. doi:10.1242/jcs.115.5.931.

West, R.R., T. Malmstrom, C.L. Troxell, and J.R. McIntosh. 2001. Two related kinesins, klp5+ and klp6+, foster microtubule disassembly and are required for meiosis in fission yeast. *Mol. Biol. Cell*. 12:3919–3932. doi:10.1091/mbc.12.12.3919.

Williams, B.R., V.R. Prabhu, K.E. Hunter, C.M. Glazier, C.A. Whittaker, D.E. Housman, and A. Amon. 2008. Aneuploidy affects proliferation and spontaneous immortalization in mammalian cells. *Science*. 322:703–709. doi:10.1126/science.1160058.

Wordeman, L., and T.J. Mitchison. 1995. Identification and partial characterization of mitotic centromere- associated kinesin, a kinesin-related protein that associates with centromeres during mitosis. *J. Cell Biol.* 128:95–105. doi:10.1083/jcb.128.1.95.

Wordeman, L., M. Wagenbach, and G. von Dassow. 2007. MCAK facilitates chromosome movement by promoting kinetochore microtubule turnover. *J. Cell Biol.* 179:869–879. doi:10.1083/jcb.200707120.

Worrall, J.T., N. Tamura, A. Mazzagatti, N. Shaikh, T. van Lingen, B. Bakker, D.C.J. Spierings, E. Vladimirou, F. Foijer, and S.E. McClelland. 2018. Non-random mis-segregation of human chromosomes. *Cell Rep.* 23:3366–3380. doi:10.1016/j.celrep.2018.05.047.

Yang, G., L.A. Cameron, P.S. Maddox, E.D. Salmon, and G. Danuser. 2008. Regional variation of microtubule flux reveals microtubule organization in the metaphase meiotic spindle. *J. Cell Biol.* 182:631–639. doi:10.1083/jcb.200801105.

Yu, C.-H., S. Redemann, H.-Y. Wu, R. Kiewisz, T.Y. Yoo, W. Conway, R. Farhadifar, T. Müller-Reichert, and D. Needleman. 2019. Central-spindle microtubules are strongly

coupled to chromosomes during both anaphase A and anaphase B. *Mol. Biol. Cell*. 30:2503–2514. doi:10.1091/mbc.E19-01-0074.

Zhai, Y., P.J. Kronebusch, and G.G. Borisy. 1995. Kinetochore microtubule dynamics and the metaphase-anaphase transition. *J. Cell Biol.* 131:721–734. doi:10.1083/jcb.131.3.721.

Zhang, C.-Z., A. Spektor, H. Cornils, J.M. Francis, E.K. Jackson, S. Liu, M. Meyerson, and D. Pellman. 2015. Chromothripsis from DNA damage in micronuclei. *Nature*. 522:179–184. doi:10.1038/nature14493.

Zhang, C., C. Zhu, H. Chen, L. Li, L. Guo, W. Jiang, and S.H. Lu. 2010. Kif18A is involved in human breast carcinogenesis. *Carcinogenesis*. 31:1676–1684. doi:10.1093/carcin/bgq134.

Zhong, Y., L. Jiang, H. Lin, X. Li, X. Long, Y. Zhou, B. Li, and Z. Li. 2019. Overexpression of KIF18A promotes cell proliferation, inhibits apoptosis, and independently predicts unfavorable prognosis in lung adenocarcinoma. *IUBMB Life*. 71:942–955. doi:10.1002/iub.2030.

Zhou, J., D. Panda, J.W. Landen, L. Wilson, and H.C. Joshi. 2002. Minor alteration of microtubule dynamics causes loss of tension across kinetochore pairs and activates the spindle checkpoint. *J. Biol. Chem.* 277:17200–17208. doi:10.1074/jbc.M110369200.

Zhu, C., J. Zhao, M. Bibikova, J.D. Leverson, E. Bossy-Wetzel, J.-B. Fan, R.T. Abraham, and W. Jiang. 2005. Functional analysis of human microtubule-based motor proteins, the kinesins and dyneins, in mitosis/cytokinesis using RNA interference. *Mol. Biol. Cell*. 16:3187–3199. doi:10.1091/mbc.e05-02-0167.

8. AUTHOR BIOGRAPHY

Patrik Risteski received MSc and BSc degrees in Molecular Biology at the Department of Biology, Faculty of Science, the University of Zagreb in 2017 and 2015, respectively. Before starting his PhD research under the supervision of Prof Iva M Tolić at the Laboratory of Cell Biophysics, Division of Molecular Biology, Ruđer Bošković Institute, Patrik was a research intern in the same lab. For his work as a research intern, Patrik was awarded Rector's (University of Zagreb) Acknowledgement for Scientific Achievements. During his research career, Patrik published four first/co-first authored papers (Polak et al., *EMBO Rep* 2017; Jagrić et al., *eLife* 2021; Risteski et al., *Curr Biol* 2021; Risteski et al., *Cell Rep* 2022) and three co-authored papers (Kajtez et al., *Nat Commun* 2016; Vukušić et al., *Dev Cell* 2021; Klaassen et al., *Nature* 2022). He presented his results at eleven international scientific conferences and workshops, among which five of them were talks (eg. EMBO Meeting 2015, ASCB | EMBO Meeting 2017, 2021), and was part of the organizing committee for Mitotic Spindle: From Living and Synthetic Systems to Theory 2017. Patrik was awarded Director's (Ruđer Bošković Institute) Fellowship for Young Scientists for his collaborative visit to Ludwig Maximilian University (Munich, DE) and The Company of Biologists' Travelling Fellowship for his collaborative visit to Gulbenkian Science Institute (Oeiras, PT).